공학박사 학위논문

# Continuum Robot for Non-Vascular Intervention

## 비혈관 중재시술을 위한 연속체 로봇

2019 년 2 월

서울대학교 대학원

기계항공공학부

최 준 명

# Continuum Robot for Non-Vascular Intervention

## 비혈관 중재시술을 위한 연속체 로봇

지도교수 조 규 진

이 논문을 공학박사 학위논문으로 제출함

2018 년 10 월

서울대학교 대학원

기계항공공학부

최 준 명

최준명의 공학박사 학위논문을 인준함

2018 년 12 월

위 원 장 _____ 김 종 원 _____ (인)

부위원장 _____ 조 규 진 _____ (인)

위 원 _____ 김 도 년 _____ (인)

위 원 _____ 박 정 훈 _____ (인)

위 원 _____ 김 천 우 _____ (인)

# Abstract

Stent placement in gastrointestinal (GI) tract has emerged as an effective therapy for intestinal obstruction due to the advantages such as quick relief, non-invasiveness, and regional anesthesia. A stent refers to a medical device that can be placed in and expand a stenosed lumen permanently.

Stent placement for non-vascular organ is performed through the interventional procedure. In GI intervention, the tube for stent delivery is inserted through the natural orifice (mouth and anus), and the soft tissue is easily deformed by the inserted tube. Therefore, there are several issues such as loop formation of an inserted tube, abdominal pain, ulceration or minor bleeding during the GI intervention. All these difficulties are caused by flexural rigidity difference between the soft tissue and inserted tubes. For this reason, the flexural rigidity of the interventional device should not be designed too high or too low compared to the organ stiffness. To overcome the flexural rigidity difference limitation between the tubes and the soft tissue, the additional tubes with various stiffness are inserted by trial and errors. However, the use of various tubes in the interventional procedure increases procedure time. Increased procedure time affects not only fatigue to clinicians, but also the increase of radiation exposure to the clinicians and the patients because the interventional procedure requires fluoroscopic guidance. Consequently, shortening procedure time is important to both patients and clinicians. However, the current procedure time is dependent on skills and experiences of the clinicians. Moreover, the design principle and selection criteria for the interventional devices have never been quantified systematically yet in terms of engineering.

In this study, a new design principle of interventional devices which is based on the conformability model was proposed. The proposed model was built in order to extract the essence of the interactions between the soft tissue and the medical tubes during the GI intervention. As a result, a soft manipulator with variable stiffness was designed and fabricated on the basis of consideration of those conformabilities. The soft manipulator can play a role as an overtube which can maintain a high conformability during GI intervention.

In the proposed conformability model, the complexity of multi-body contact behavior between the soft tissue and the medical tube was simplified to the variables: flexural rigidity, curvature, and effective length of the curved space. Conformability in various combinations of conventional GI interventional devices was evaluated in order to design an optimized tube that can be used in GI stenting procedure.

Through the proposed conformability model, the requirements on a device for the safe GI intervention were defined. A soft manipulator with steering capability was designed and fabricated based on the conformability model. The manipulator was made of a flexible material of a size that can safely pass through the organ in consideration of the size and stiffness of the conventional medical tubes and the anatomy of the upper GI tract. The soft manipulator adopted a wire-driven mechanism with antagonistic pairs to achieve two degrees of freedom steering in the thin-walled tubular continuum structure. The soft manipulator maintained high conformability during tube insertion into the GI tract, however, it was difficult to suppress a straightening moment by the steering force during the stent introducer passing. To solve this issue, partial replacement in the soft manipulator was done by shape memory

polymer (SMP). The improved soft manipulator with SMP can maintain the acute curve configuration during the stent introducer passing without size change. Since the variable stiffness characteristic through the phase transition of the SMP, the stent introducer can be inserted along the desired trajectory. A steering handle was designed and fabricated to improve the usability of the soft manipulator. Also, the phantom simulator was made of flexible materials based on the CT data of the upper gastrointestinal tract of a patient and conducted feasibility tests. In addition, a device for measuring the stiffness of the GI tract in an in-vivo environment was developed and an animal experiment was conducted.

The conformability model is expected to be an index for predicting and evaluating interactions between a new interventional device and the soft tissue in various procedures including vascular and non-vascular interventions.

**Keywords**: Non-vascular intervention, Stent placement, Conformability model, Soft manipulator, Variable stiffness, Gastrointestinal tract

**Student Number**: 2014-31041

# Contents

# List of Tables

# List of Figures

# Nomenclature

| | |
|---|---|
| $k_s$ | Spring constant of soft tissue |
| $F$ | Exerted force |
| $F_r$ | Reaction force |
| $\alpha$ | Angle between horizontal line and deformed line |
| $d$ | Tissue deflection |
| $L$ | Horizontal length in deflection range |
| $F_{rv}$ | Vertical deflection of stomach |
| $F_{rh}$ | Horizontal deflection of stomach |
| $E_s$ | Young's modulus of stomach wall |
| $I_s$ | Area moment of inertia of stomach wall |
| $U$ | Strain energy per unit of reference volume |
| $C_{10}$ | 1st Neo-Hookean material parameter |
| $D_1$ | 2nd Neo-Hookean material parameter |
| $\overline{I}_1$ | First deviatoric strain invariant |
| $g_R$ | Dimensionless shear relaxation modulus |
| $J$ | Determinant of elastic deformation gradient |
| $G(t)$ | Time dependent shear modulus |
| $g_i$ | Normalized shear modulus in Prony series |
| $k_i$ | Normalized bulk modulus in Prony series |
| $\tau_i$ | Relaxation time in Prony series |
| $\mu_s$ | Shear modulus |
| $\kappa_s$ | Bulk modulus |
| $R$ | Radius of curvature |
| $m$ | Factor accounting for end conditions |
| $E_{GW}$ | Young's modulus of soft guidewire |
| $I_{GW}$ | Area of moment of inertia of soft guidewire |
| $P_{cr}$ | Critical buckling load |
| $L_{GW}$ | Maximum distance from the EG junction to the greater curvature |
| $F_x$ | Horizontal force of guidewire tip |
| $F_y$ | Vertical force of guidewire tip |
| $F_{rx}$ | Horizontal reaction force of stomach wall |
| $F_{ry}$ | Vertical reaction force of stomach wall |
| $\delta$ | Maximum horizontal deflection at stomach wall |
| $\mu$ | Coefficient of static friction |
| $N$ | Normal force to stomach wall |
| $M_t$ | Straightening moment by beam deflection |
| $k_t$ | Torsional spring constant of curved guidewire |
| $E$ | Young's modulus |
| $I$ | Area of moment of inertia |

| | |
|---|---|
| $K$ | Flexural rigidity |
| $C$ | Conformability factor |
| $E_s$ | Young’s modulus of stomach wall |
| $I_s$ | Area moment of inertia of stomach wall |
| $a$ | Width of stomach model |
| $b$ | Effective length of contact area in stomach model |
| $C_{s-GW}$ | Conformability factor in guidewire in stomach |
| $C_{SI-SGW,s}$ | Conformability factor in stent introducer in stiff guidewire and stomach |
| $C^{'}$ | Modified conformability factor |
| $L_t$ | Effective length in conformability model |
| $T_{cr}$ | Buckling load of tube tip |
| $P$ | Arbitrarily determined lateral component of tension |
| $x$ | Longitudinal displacement of tube |
| $dx$ | Infinitesimal longitudinal displacement |
| $\theta$ | Deflection angle |
| $y$ | Lateral deflection |
| $EI_{SMP\_G}$ | Flexural rigidity of SMP tube in glassy state |
| $EI_{SMP\_R}$ | Flexural rigidity of SMP tube in rubbery state |

# Chapter 1. Introduction

## 1.1 Motivation

### 1.1.1 Interventional Procedure and Stent Placement in GI Tract

Interventional radiology therapies are widely used for the various treatments such as for benign/malignant tumor, drug delivery, percutaneous abscess drainage procedure, gastroenteric tube feeding, thermotherapy, and stent placement. The basic concept behind interventional radiology is based on demands of diagnosis and treatment with a minimally invasive technique. Fluoroscopic images are used to direct interventional procedures, which are usually done with needles and narrow tubes called catheters (see Figure 1.1(a)). The fluoroscopic images provide road maps that allow the interventional radiologist to guide these instruments through the body to the areas containing disease (see Figure 1.1(b)). Due to the minimized physical trauma to the patient, the interventional procedure can reduce infection rates and recovery time as well as shorten hospital stays [1].

Stent placement through the interventional procedure is one of the common options that treat a malignant stricture in a stenosed lumen. A stent is a metallic or plastic tube inserted into the lumen of an anatomic vessel or duct to keep the passageway open (see Figure 1.2(a)). There is a wide variety of stents used for different purposes, from expandable coronary, vascular and biliary stents, to simple plastic stents used to allow the flow of urine between kidney and bladder. A stent is also used as a verb to describe the placement of such a device, particularly when a disease such as atherosclerosis has pathologically narrowed a structure such as an artery, biliary

tract, urinary tract and gastrointestinal (GI) tract [2]. Stent placement in GI tract usually requires both fluoroscopic and endoscopic guidance but can be done with either modality safely [3]. Owing to recent technological advances in endoscopic devices and the introduction of novel stent materials, the endoscopic approach has become the popular in GI intervention [4]. However, the fluoroscopic approach is still being widely used owing to its high feasibility under mild sedation.

(a)

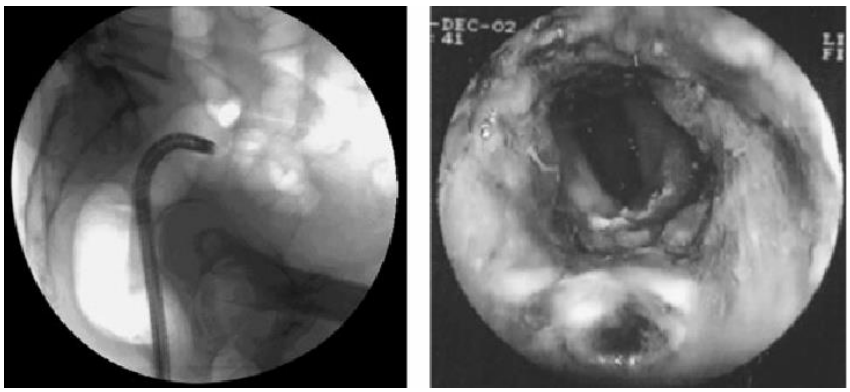

(b)

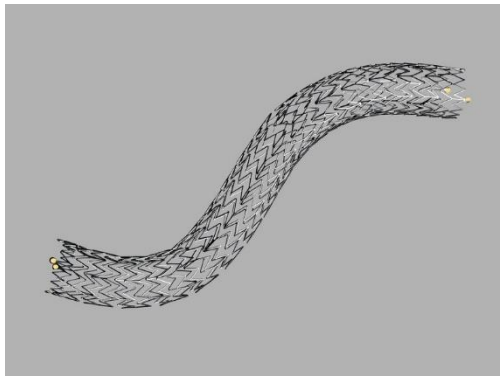

(c)

Figure 1.1: Interventional procedure. (a) Catheterization [5]
(b) Fluoroscopic-guided catheterization [6]
(c) Metallic stent (Cook Medical, Inc.)

### 1.1.2 Gastrointestinal Obstruction and Stent Therapy

GI obstruction is a significant mechanical impairment or complete arrest of the passage of contents through the intestine due to pathology that causes blockage of the bowel. The treatment of mechanical obstruction is commonly fluid resuscitation and nasogastric suction, and in most cases of treatment for a complete obstruction is surgery. Mechanical obstruction is divided into obstruction of the small bowel and obstruction of the large bowel. About 85% of partial small-bowel obstructions resolve with non-operative treatment, whereas about 85% of complete small-bowel obstructions require surgery [4]. Historically, patients with malignant gastroduodenal obstruction have been treated by a variety of open surgical interventions intended to restore continuity and function of the tract. Nevertheless, some patients are not candidates for open surgical treatment, either because surgery would not be curative for their disease or because their overall physical status prohibits such an invasive procedure [7].

Esophageal and duodenal stents were introduced as an endoscopic palliative therapy in the 1990s and have been described as a safe, minimally invasive, and cost-effective option for palliative treatment [8] (see Figure 1.2(a)). Because patients with malignant GI obstruction are generally older, may have several contraindications to invasive procedures, and may have a relatively short anticipated life expectancy (typically estimated to be 6 months), stent placement may be preferable to open surgical intervention. Further, stent placement allows faster resumption of food intake and a shorter hospitalization compared with surgical gastrojejunostomy (open or laparoscopic) [9, 10]. Therefore, stent placement is the first-line treatment for malignant gastric outlet obstruction in

patients with a single, localized distal gastric and/or small-bowel stricture. In recently published reports, technical success rates of endoscopic stent placement for malignant obstruction range from approximately 92% to 100%, whereas clinical success rates are lower and range from approximately 80% to 91% [11-14]. Stent placement is the most frequently used treatment modality for palliating dysphagia from esophageal or gastric cardia cancer. The esophageal-duodenal stents have various length and expansion diameter for an appropriate expansion force by the indications (see **Figure 1.2(a)**). The new types of esophageal stents have been introduced to reduce recurrent dysphagia owing to migration or non-tumoral or tumor overgrowth recently (see **Figure 1.2(b)**). Furthermore, duodenal stents have been used as an alternative to a stomach bypass operation (see **Figure 1.2(c)**).

(a)

(b) (c)

Figure 1.2: Stenting in GI tract. (a) GI stents (Provided by Asan Medical Center) (b) Stent in esophagus (c) Stent in duodenal bulb (Cook Medical, Inc.)

### 1.1.3 GI Stent Delivery System

In GI tract, a Self-Expandable Metallic Stent (SEMS) is inserted by endoscopy (see Figure 1.3(a)), wherein a fiber optic camera is inserted either through the mouth or retrograde through the colon, in order to reach an area of narrowing. SEMS can also be inserted using fluoroscopy where an X-ray image is used to guide insertion, or used as an adjunct to endoscopy (see Figure 1.3(b)) [15]. Fluoroscopically guided peroral placement of gastroduodenal metallic stents is widely used to manage malignant gastroduodenal obstructions [16-18]. In both methods, a dedicated Stent Delivery System (SDS) that consists of a supporting tube and a pushing structure to compress a stent in small diameter and deliver into the target site in the tract. The typical stent introducer consists of a flexible sheath, a peek tube, a pusher hub and a sheath hub (see see Figure 1.4).

Endoscopic-guided stent placement is performed through its working channel (smaller than 3.5 mm in diameter) of the flexible endoscope. First, the flexible endoscope is inserted through the patient's mouth. Local anesthesia around the patient's throat reduces a discomfort and a pain during the procedure. As same in a diagnostic procedure, the endoscopic image provides the information of a tip position and surrounding tissue in the endoscopic insertion. After the endoscopic tip is positioned nearby a stricture, a stent introducer with compressed SEMS is passed through the working channel. In stent placement, the clinician pushes a compressed stent using a pusher. The compressed stent is pushed out and the shape is recovered from a narrow shaft to an expanded structure.

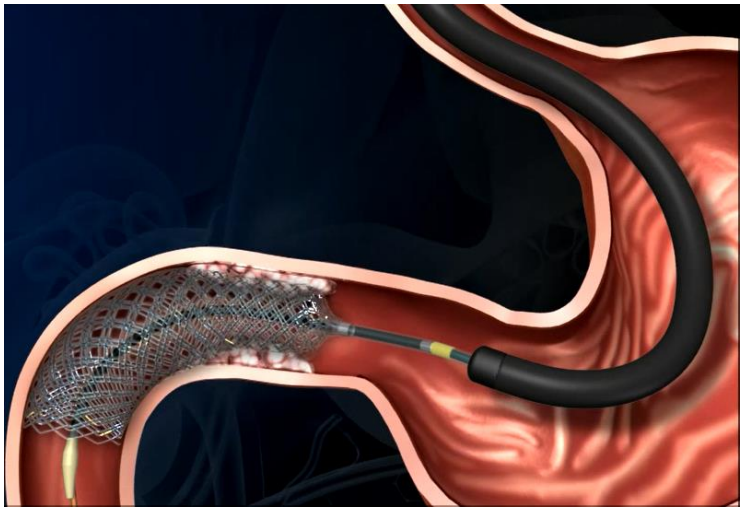

(a)

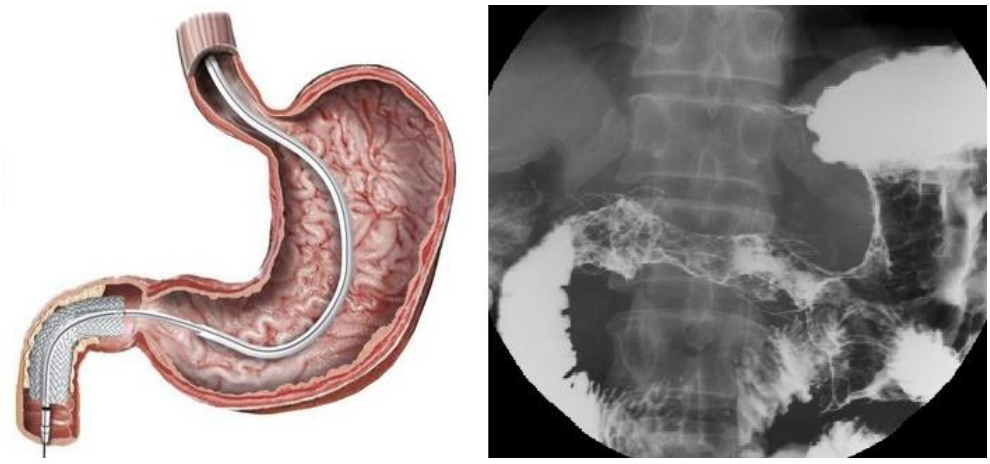

(b)

Figure 1.3: Approaches for GI tract stenting (S&G Biotech, Inc.). (a) Endoscopic-guided stenting (b) Fluoroscopic-guided stenting

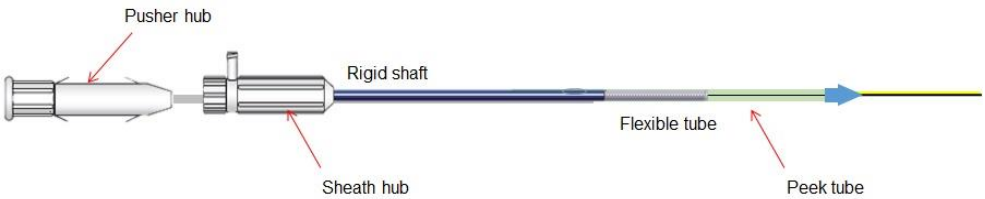


Figure 1.4: Stent introducer in endoscopic/fluoroscopic-guided intervention

(a)

(b)

(c)

(d)

Figure 1.5: Devices for fluoroscopic-guided stent placement.
(a) Guidewire (TERUMO, Inc.) (b) Coil catheter (S&G Biotech, Inc.)
(c) Super-stiff guidewire (Amplatz, Boston Scientific, Inc.)
(d) Pre-curved guiding sheath (S&G Biotech, Inc.)

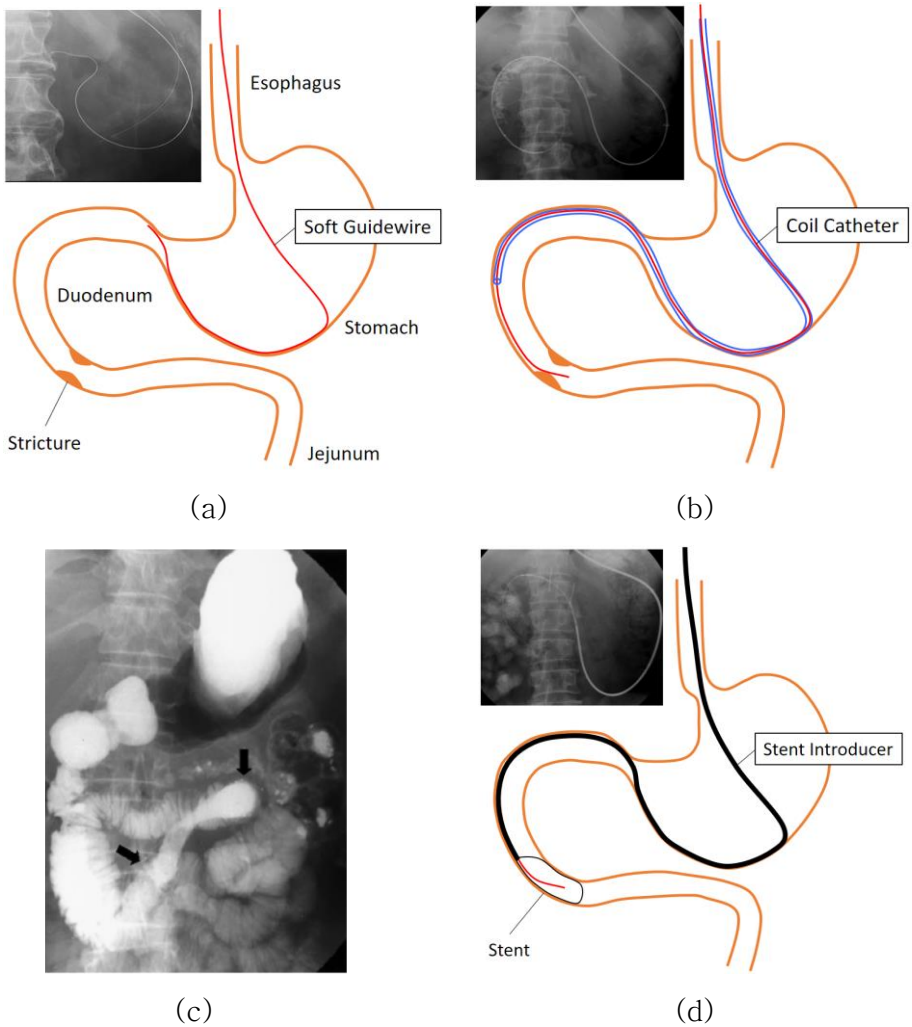


Figure 1.6: Fluoroscopic-guided stent placement process [22].
(a) Soft guidewire is inserted (b) Coil catheter is inserted
(c) Opacified organ by contrast medium [62]
(d) Stent introducer is inserted for stent placement

Fluoroscopic-guided stent placement requires additional devices compared to the endoscopic approach (see **Figure 1.5**). In fluoroscopy, the fluoroscopic imaging device provides an X-ray image during the procedure. Clinicians insert a flexible guidewire with radiopaque tip through the patient's mouth (see **Figure 1.6(a)**). When the guidewire tip contacts a stenosed lumen, the clinician feels

a reaction force in their hand. To obtain an image that can show the geometrical relationship between the guidewire and surrounding tissue, a coil catheter (see Figure 1.5(a)) is overlapped on the guidewire and inserted to follow the guidewire's trajectory (see Figure 1.6(b)). After the insertion of the coil catheter, water-soluble contrast medium is injected to opacify the area of interest (see Figure 1.6(c)). To select an appropriate stent, the stricture length is measured using the gold markers on the catheter surface after the contrast medium injection. After the catheter is completely removed, the stent introducer with a compressed stent is overlapped on the inserted guidewire and inserted to follow the guidewire's trajectory (see Figure 1.6(d)).

## 1.2 Challenges in GI Stent Placement

Placement of self-expandable metallic stents for the gastric outlet and the duodenum has been considered to be technically extremely difficult because of the anatomic angulation of the gastroduodenal lumen and the loop formation of the delivery system in the stomach. A lot of researchers have experienced difficulties in negotiating a guidewire and the SDS through strictures, especially due to guidewire buckling or a loop formation of the SDS in the dilated stomach and gastroduodenal tract [18, 19]. In patients with marked dilation of the gastric fundus, the tip of a guide wire turns upward and backward along the gastric fundus, which makes it difficult for the stent delivery set to make its way to the gastric antrum or duodenum. In order to facilitate guidewire and SDS introductions, the use of alternative methods such as the percutaneous approach and endoscopic guidance have been considered [20]. Of these methods, endoscopy has often been referred in order to help movement of a

guidewire through the working channel of the endoscope, eliminating the possibility that the guidewire becomes trapped in the gastroduodenal tract [21, 22]. However, the method has some limitations, in particular the discomfort caused by the endoscopy and an inability of the currently available large diameter SDSs, which are designed for covered stents, to pass via the working channel [20, 23]. Further study about usefulness of the guiding sheath in GI stent placement was reported as a long-term retrospective study [24]. The guiding sheath had been developed as an overtube for GI stent placement (see **Figure 1.5(d)**). The guiding sheath has a pre-curved tip to guide a stent introducer or guidewire into a direction of the distal side of the stomach. Due to the relatively high flexural rigidity compared to the guidewire, the guiding sheath plays a role as a supporting structure in the stomach (see **Figure 1.7(a)**). In addition, a soft guidewire is replaced by a stiff guidewire to facilitate smooth stent introducer passing in the curved portion. Replacing a guidewire is performed using a lumen of the inserted coil catheter and an overlapped guiding sheath. Insertion and removal of the interventional devices is a time-consuming process, and radiation exposure by the fluoroscopic imaging device increases. For this reason, the increase of the additional devices for stent placement is not desirable. Furthermore, even if with such a guiding sheath or a super-stiff guidewire, distal jejunum is still difficult to access with stent introducer because of the high stiffness of the loaded stent and stent introducer itself generate a huge straightening torque at the curved portion in the stomach (see **Figure 1.7(c)**). Excessive pressure on the stomach results in tissue distension. Tissue distension is a cause of the patient's discomfort and perforation of the organ. Consequently, to overcome the various tortuosity in GI

intervention, various stiffness range in the device or active steering tip with multiple degrees of freedom is required at the curved pathway. For this reason, overcoming the anatomical tortuosities in distal GI tract such as the 3rd and 4th portion of a duodenum is limited.

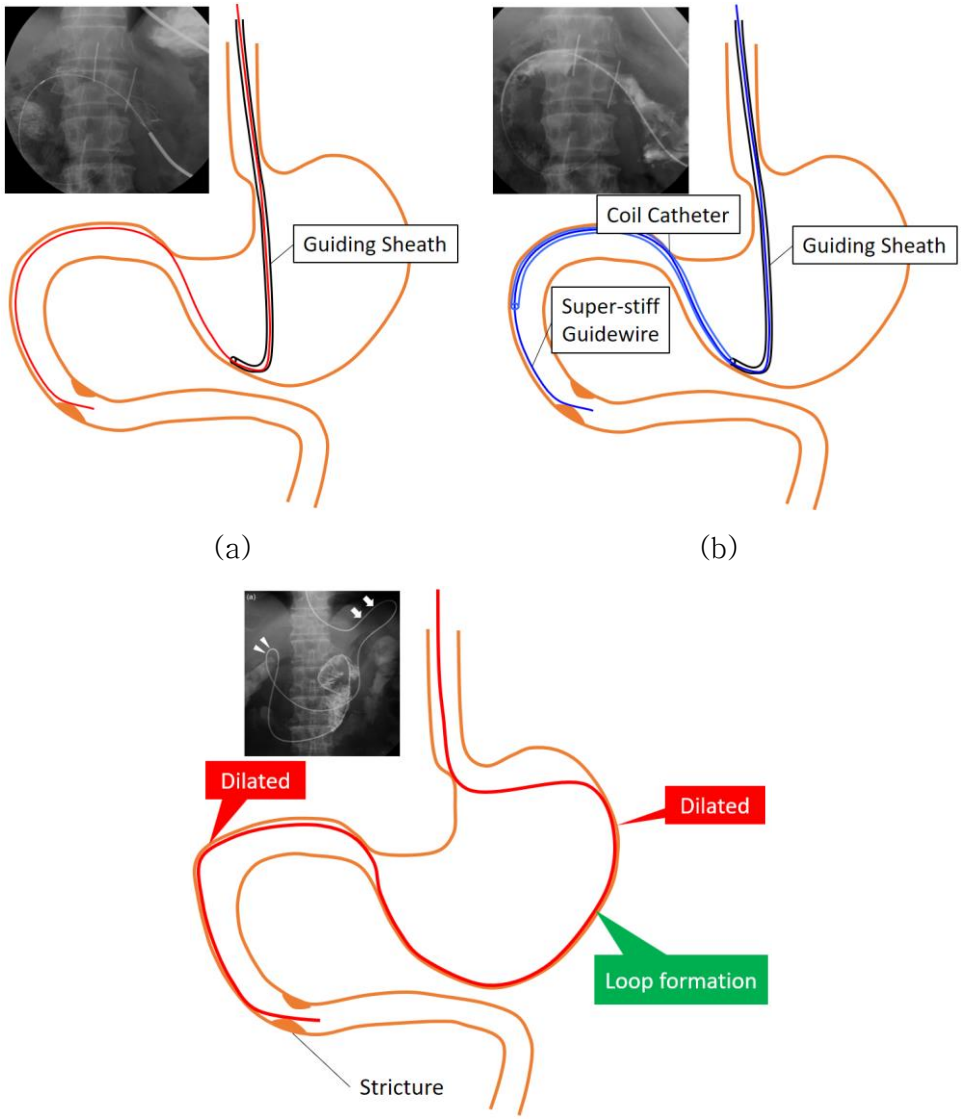


Figure 1.7: Additional devices for GI stent placement.

(a) Guiding sheath is overlapped on guidewire

(b) Guiding sheath and super-stiff guidewire in GI tract

(c) Tissue distension and loop formation during guidewire insertion

## 1.3 Objective and Contribution

In this study, a new design principle of interventional devices which is based on the conformability model was proposed. The proposed model was built in order to extract the essence of the interactions between the soft tissue and the medical tubes during the GI intervention. As a result, a soft manipulator with variable stiffness was designed and fabricated on the basis of consideration of those conformabilities. The soft manipulator can play a role as an overtube which can maintain a high conformability during GI intervention.

In the proposed conformability model, the complexity of multi-body contact behavior between the soft tissue and the medical tube was simplified to the variables: flexural rigidity, curvature, and effective length of the curved space. Conformability in various combinations of conventional GI interventional devices was evaluated in order to design an optimized tube that can be used in GI stenting procedure.

## 1.4. Thesis Organization

The thesis chapters are organized as follows:

Chapter 2: This chapter presents a new model-based method for determining flexural rigidity and length that affect conformability in tube insertion into GI tract. A numerical simulation of mechanical behavior in the interaction between the inserted structure and the soft tissue is described. For simpler expression of the multi-body contact behavior, conformability factor based modeling is defined to generalize a condition of path-following in soft tissue environment. The conformability model describes the limitation and an allowable design range for interventional devices for

stent placement in GI tract.

**Chapter 3**: This chapter describes a design principle and an actuation mechanism of the steerable soft manipulator. The design of the soft manipulator is established on the basis of the form factor analysis and compatibility with the conventional devices in GI intervention. The actuation mechanism of the continuum tubular structure which is made of a soft material is proposed. A prototype of the proposed device is presented with a description including the assembly process and the materials.

**Chapter 4**: In this chapter, the variable stiffness tube for GI intervention is described. To overcome the design limitation due to the trade-off relationship between path-following capability and shape-locking capability in terms of bending stiffness, the necessity of reconfigurable stiffness change during the procedure is described. The device prototype, experimental methods are presented

**Chapter 5**: This chapter details an experimental methods and results to verify the stiffness requirements in GI intervention.

**Chapter 6**: Thesis contributions and limitations are summarized, and the scope for future work is discussed.

# Chapter 2. Modeling of Soft Interaction in GI Tract

## 2.1 Passive Steering in GI Tract

### 2.1.1 Deformation of Soft Tissue

The fluoroscopic and endoscopic insertion techniques require the skillful clinicians due to the flexibility of the human organ. In those insertion procedures, clinicians insert long and flexible devices such as a guidewire, a catheter, and an endoscope through the natural orifices (mouth and anus). During the tube insertion, the human organ that is curved configuration is easily deformed by the relatively stiff tube. For this reason, deformation of the soft tissue should be predicted and suppressed with the use of the less stiff tube. However, the selection of the appropriate tube for each patient is done by trial and error.

In upper GI tract, the esophagus is the first gateway into the stomach. It is commonly known as the food pipe or gullet, is an organ in vertebrates through which food passes, aided by peristaltic contractions, from the pharynx to the stomach. The esophagus is a fibromuscular tube, about $25 - 30\,\mathrm{cm}$ long in adults, which travels behind the trachea and heart, passes through the diaphragm and empties into the uppermost region of the stomach (see Figure 2.1(a)). During swallowing, the epiglottis tilts backward to prevent food from going down the larynx and lungs [25].

In upper GI tract intervention, the clinician continuously pushes a tube from the proximal side to insert a tube into the stomach. When the distal tip collides with the stomach wall beyond an esophagus, the stomach is distended by the applied pushing force on the tube structure due to the high flexibility of the organs. The organs have a distension limit which is determined by the surrounding tissue and

the ligaments as shown in **Figure 2.1(b)**. By the pushing force increases, the wall distension stops and the distal tip bends at the stomach wall. If the strictures exist in duodenum or jejunum, the distal tip of a medical tube should be inserted into the duodenum. To advance a tube into the deeper side, for example, duodenum, the distal tip should bend in the curvature to conform to the duodenal bulb shape. However, the achievement of two different curve configurations in a single continuum structure requires passive bending characteristics in the GI tract (in this paper, this characteristic is called passive bending). In order to overcome an anatomical tortuosity in GI tract, a tube must not be too stiffer than the stomach wall. If the tube is too stiff compared to the soft tissue, pushing force on the tube for insertion will result in tissue distension (see **Figure 2.2(b)**). By contrast, a soft tube can follow the organ wall with minimum tissue distension (see **Figure 2.2(c)**).

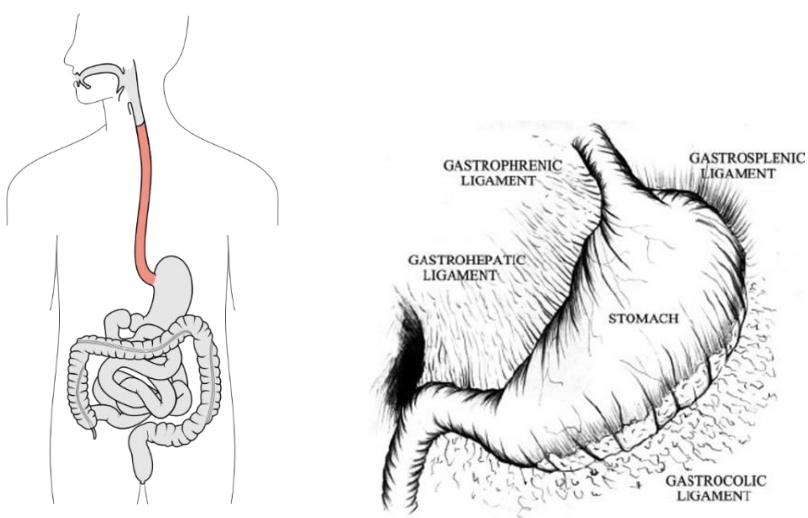


(a) (b)

Figure 2.1: Anatomy of the human GI tract.

(a) Esophagus in human GI tract [25]

(b) Surrounding ligaments of the stomach [26]

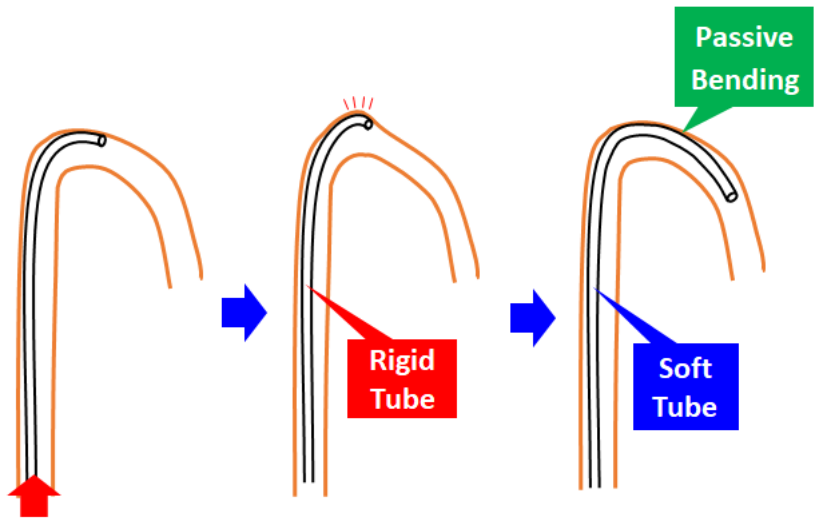


Figure 2.2: Passive bending in GI tract.

(a) Medical tube at the curved pathway

(b) Tissue distension increases when rigid tube is passing

(c) Tissue distension decreases when soft tube is passing

### 2.1.2 Tension Spring Model for Stomach Distension

Prediction of the tissue distension in interventional procedure is effective in terms of perforation risk factor. In general, the puncture force of GI tract is estimated as 3 – 5 N (concentrated force) [27, 28], therefore, the exerted pushing force to the stomach wall through a tube must not exceed this force range during GI intervention. The first contact occurs at the stomach wall after the medical tube passing through the esophagogastric (EG) junction (see Figure 2.3(a)). After EG junction passing, the stomach is distended by a pushing force that is applied to the tube. To determine the relationship between the pushing force and stomach distension, a lumped model that consists of tension springs (see Figure 2.3(b)) was constructed.

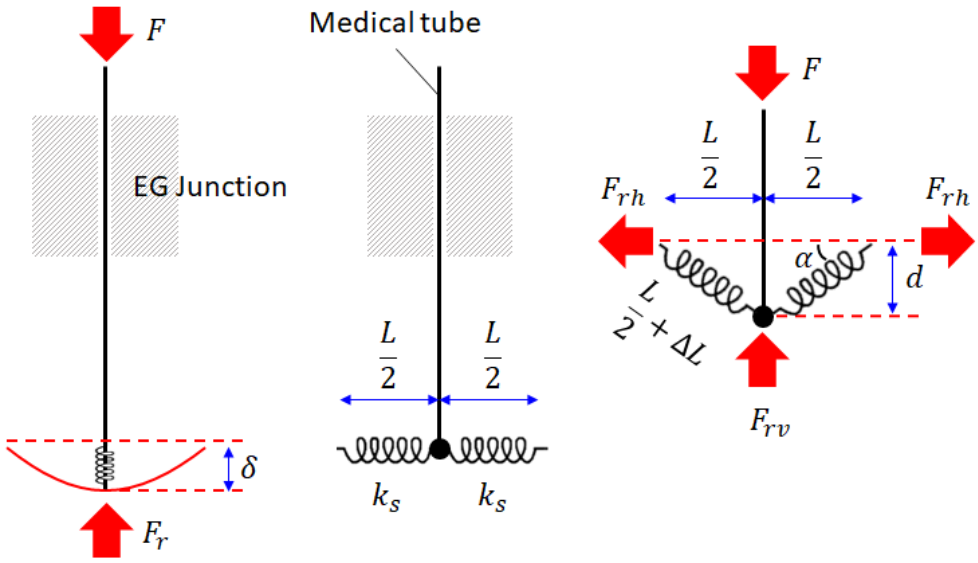


(a) (b) (c)

Figure 2.3: Tension spring model for tissue distension.

(a) Geometry change of the stomach wall by tube pushing

(b) Soft tissue model with two tension springs

(c) Free body diagram of soft tissue distension

$k_s$ is the spring constant of the soft tissue, $F$ is the exerted force, $F_r$ is the reaction force of the stomach wall, $\alpha$ is the angle between a horizontal line and a deformed line, $d$ is the tissue deflection, and $L$ is the horizontal length in the deflection range. $L$ is assumed as **50 mm** by the average bottom length of the stomach geometry [29]. The vertical deflection $F_{rv}$ and horizontal deflection $F_{rh}$ are given as

$$F_{rv} = k_s \Delta L \sin\alpha \tag{2.1}$$

$$F_{rh} = k_s \Delta L \cos\alpha \tag{2.2}$$

$$\left(\alpha = tan^{-1}\frac{2d}{L}, \Delta L = \frac{L}{2}\left(\frac{1}{cos\,\alpha} - 1\right)\right)$$

To obtain a spring constant of the stomach wall (bottom area in the stomach) in the lumped model, the following equation (2.3) gives a conversion from the modulus of elasticity of stomach wall to spring constant.

$$F_r = F = k_s\delta \Leftrightarrow k_s = \frac{F}{\delta} = \frac{48E_sI_s}{L^3} \tag{2.3}$$

To obtain an area moment of inertia of the stomach, the simple stomach wall model (see **Figure 2.4**) was proposed. To define the dimensions of the stomach wall area, the computational model data from the average value in actual patients was adopted [29].

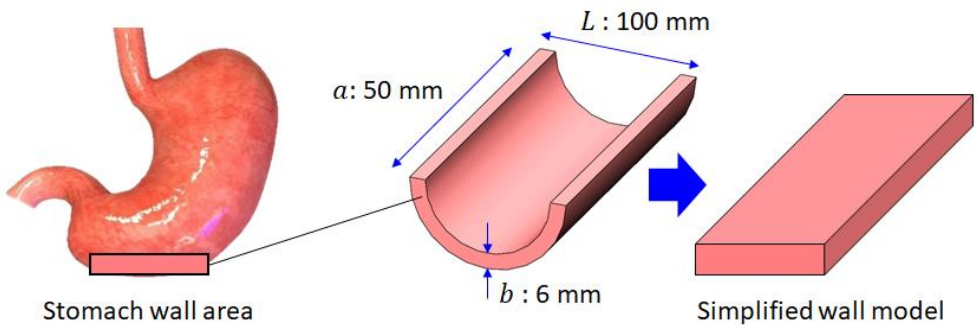


Figure 2.4: Simple stomach wall model

The Young's modulus of the stomach wall $E_s$ was given as **1.7 MPa** [30–32]. The area moment of inertia of the stomach wall $I_s$ was calculated as **900 mm$^4$**. Finally, $k_s$ was obtained as **0.7949 N/mm**.

Table 2.1: Simulation parameters in tension spring model

| $L$ (mm) | $E_s$ (MPa) | $I_s$ (mm$^4$) | $k_s$ (N/mm) |
|---|---|---|---|
| 50 | 1.7 | 900 | 0.7949 |

The simulated result for tissue distension – distension relationship was illustrated in Figure 2.5. The tension spring model, which is on the basis of the assumption that the soft tissue distension is similar to the trampoline deflection was suggested. The contact surface was assumed as the stomach wall.

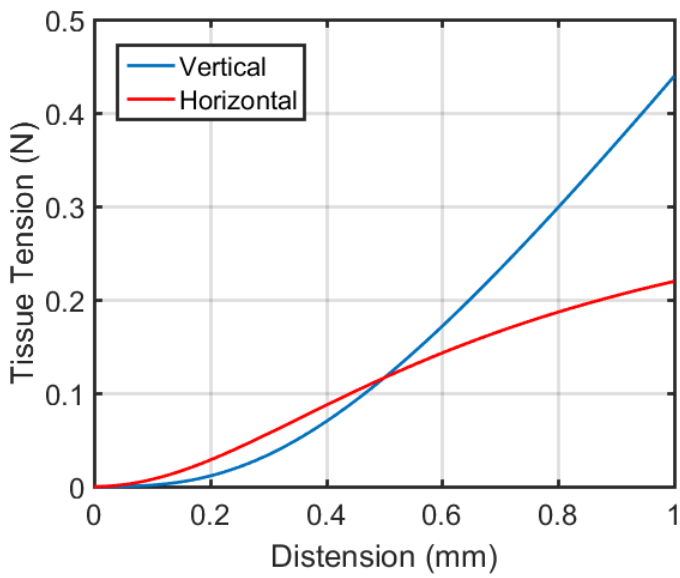


Figure 2.5: Tissue tension prediction by distended stomach in simple stomach model

As illustrated in Figure 2.5, the tensions in two axes show the different profile by distension increase in the simple stomach model. The model can describe the very first interaction between the medical tube and the stomach wall. As a result, the horizontal reaction force can be extended into the three-dimensional force under the assumption that a lot of tension springs aligned omnidirectional. However, the stomach distension does not occur only by the concentrated force at the tip during the interventional procedure. Due to the curved pathway in GI tract, the distal tip of the medical tube follows the stomach wall to slip into the distal side in the GI tract.

Wall-following in the stomach requires appropriate flexibility that makes the inserted medical tube conforms in the curved pathway. Passive bending characteristics of the medical tube in the various region in the GI tract requires a model to predict an allowable range in terms of the curve configurations and perforation safety. Therefore, the multi-body contacts should be considered to simulate a complete behavior of the interaction between the tube and the stomach wall. Furthermore, a vertical reaction force and a deflection are not only dependent on the tissue stiffness but the various ligaments and anatomical constraints such as a hepatoduodenal ligament, a peritoneum, and an abdominal wall (see Figure 2.1(b)).

### 2.1.3 Curves in Stomach

To insert a medical tube into the distal upper GI tract, the anatomy in the GI tract should be considered. The duodenum is a $20-30$ cm C-shaped hollow viscus predominantly on the right hand side of the vertebral column. It lies at the level of L1-3 and the convexity of the duodenum usually encompasses the head of the pancreas [33]. In general, due to the limited degrees of freedom by a long esophagus, the distal tip of a guidewire or an endoscope does not follow the minimum path from the esophagogastric junction to the pylorus. In endoscopic-guided approach, a clinician can see the frontal scene by CCD in its tip and manipulate a distal tip angle by a control handle. By contrast, in a fluoroscopic-guided procedure, an approach to the duodenum is relying on the passive bending and wall-following condition. For this reason, the distal tip should follow the greater curvature region in the stomach wall (see Figure 2.6(a)). The angle between the stomach and a pylorus is different by a patient. Moreover, an angle of the greater curvature is extremely acute in

patients with gastroptosis [34, 35]. Thus, the passive bending (or wall-following) characteristic of a guidewire is important in fluoroscopic-guided approach.

To investigate a passive bending behavior of the guidewire at the stomach, Finite Element Analysis (FEA) using a commercial software ABAQUS 6.12 (Dassault Systèmes, France) was conducted under the assumption that the greater curvature of the stomach is similar to a curved bowl (see Figure 2.7). Based on the condition that the circumferential surface of the bowl is completely constrained, the concentrated force was exerted on the bottom center of the specimen.

The deformation of the soft tissue should be considered in terms of hyperelastic and viscoelastic behaviors in time scale. In general, viscoelastic effect should be observed if the time scale is long. To simulate an actual situation that the tubular structure bending in steering can occurs in short or long time, both properties should be considered. The Neo-Hookean model was selected for use here, which is widely used in soft structure simulations. The Neo-Hookean material model does not predict that increase in modulus at large strains and is typically accurate only for strains less than 20%. Nevertheless, the simple buckling and kinking can be predicted with two parameters which can be obtained from a shear modulus and a Poisson's ratio. The strain energy function of the three dimensional incompressible material Neo-Hookean model is given by $C_{10}$ and $D_1$. where $C_{10}$ and $D_1$ is a mechanical parameter having a unit of stress. A Neo-Hookean model is a hyperelastic material model, similar to Hooke's law that can be used for predicting the nonlinear stress-strain behavior of materials undergoing large deformations. In contrast to linear elastic materials, the stress-strain curve of a Neo-Hookean material is not linear. Instead, the relationship between

applied stress and strain is initially linear, but at a certain point the stress–strain curve will plateau. The Neo–Hookean model does not account for the dissipative release of energy as heat while straining the material and perfect elasticity is assumed at all stages of deformation [36]. The Neo–Hookean model is based on the statistical thermodynamics of cross–linked polymer chains and is usable for plastics and rubber–like substances. Cross–linked polymers will act in a Neo–Hookean manner because initially the polymer chains can move relative to each other when a stress is applied. However, at a certain point the polymer chains will be stretched to the maximum point that the covalent cross links will allow, and this will cause a dramatic increase in the elastic modulus of the material.

For positive values of the coefficient $C_{10}$ the neo–Hookean form is always stable. The form of the neo–Hookean strain energy potential is

$$U = C_{10}\left(\bar{I}_1 - 3\right) + \frac{1}{D_1}(J^{el} - 1)^2 \tag{2.4}$$

where $U$ is the strain energy per unit of reference volume; $C_{10}$ and $D_1$ are the Neo–Hookean material parameters. $J$ is determinant of the elastic deformation gradient. $\bar{I}_1$ is the first deviatoric strain invariant defined as

$$\bar{I}_1 = \bar{\lambda}_1^2 + \bar{\lambda}_2^2 + \bar{\lambda}_3^2 \tag{2.5}$$

Furthermore, viscoelasticity was considered in the simulation. Viscoelasticity is the property of materials that exhibit both viscous

and elastic characteristics when undergoing deformation. Prony series is the most popular model for a prediction of the viscoelastic behavior of polymer-based material [37]. The mathematical form of viscoelastic behavior is given by Prony series as

$$g_R(t) = 1 - \sum_{i=1}^{N} g_i\left(1 - e^{-t/\tau_i}\right) \quad (2.6)$$

where $g_i$ is the material constant and $\tau_i$ is the relaxation time. $g_R$ is the dimensionless shear relaxation modulus defined as

$$g_R(t) = \frac{G(t)}{G_0} \quad (2.7)$$

where $G(t)$ and $G_0$ are the time dependent and the initial shear modulus, respectively. Prony series parameters are merged into one set of parameters $g_i$ (Normalized shear modulus), $k_i$ (Normalized bulk modulus), and $\tau_i$ (Relaxation time). Neo-Hookean parameters $C10$ and $D1$ are determined from the shear modulus $\mu_s$ and the bulk modulus $\kappa_s$. Normally, the bulk modulus is $0$ in incompressible material, and $C_{10}$ is set to be a half value of the shear modulus. The shear modulus of stomach wall is estimated as $25\,\text{kPa} - 60\,\text{kPa}$ [30, 31, 38]. Table 2.2 and 2.3 show the specific parameters in the FEA.

Dynamic explicit analysis was conducted with aforementioned parameters. For the simple prediction of the viscoelastic model parameters of the typical rubber analysis was used in the analysis. However, the simulation time was set to $0.1$ seconds, the viscoelastic effect was almost ignored in the analysis. The friction coefficient between the tube and the stomach wall was assumed as $0.025$ [41]. Figure 2.7(c, d) show a stress - strain relationship at the center point on the wall surface and a stress - vertical deflection

relationship point on the wall surface. The stress – strain did not show a linear relationship at the center point because the curvature of the guidewire is continuously change during the passing. As a result, during the tube passing, stress distribution and deflection of the stomach constantly change. For this reason, the interaction between the medical tube and the stomach wall should be considered in terms of the contact behavior in a broad area.

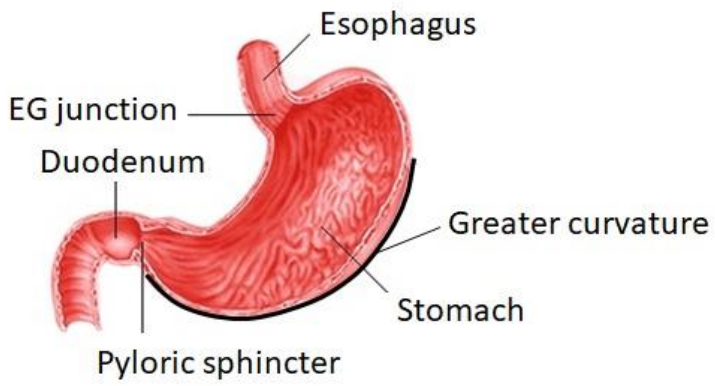


(a)

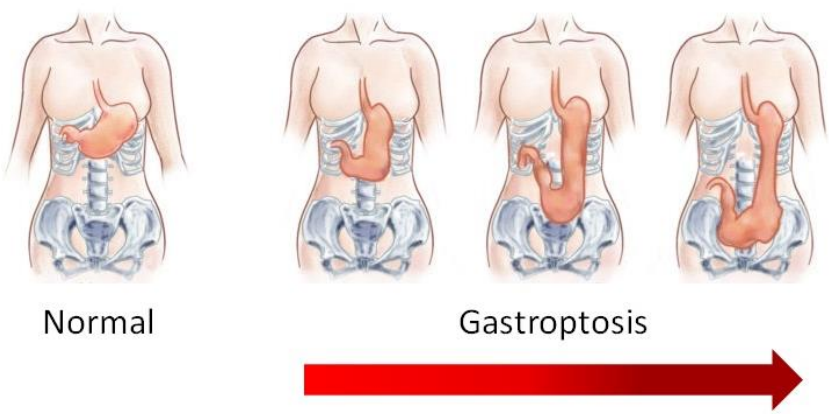


(b)

Figure 2.6: Anatomy of stomach. (a) Stomach – duodenum region [33] (b) Insertion angle difference by gastroptosis [34]

Table 2.2: Parameters for stomach wall deformation analysis

| Hyperelastic Parameters (Neo Hooke) | | Viscoelastic Parameters (Prony series) | | |
|---|---|---|---|---|
| $C_{10}$ | $D_1$ | $g_i$ | $k_i$ | $\tau_i$ |
| 0.388 | 0 | 0.3 | 0 | 0.1 |

Table 2.3: Dimensions for stomach wall deformation anlaysis

| $L$ (mm) | $E_s$ (MPa) | Thickness (mm) | Radius of curvature R (mm) |
|---|---|---|---|
| 50 | 1.7 | 6 | 25 |

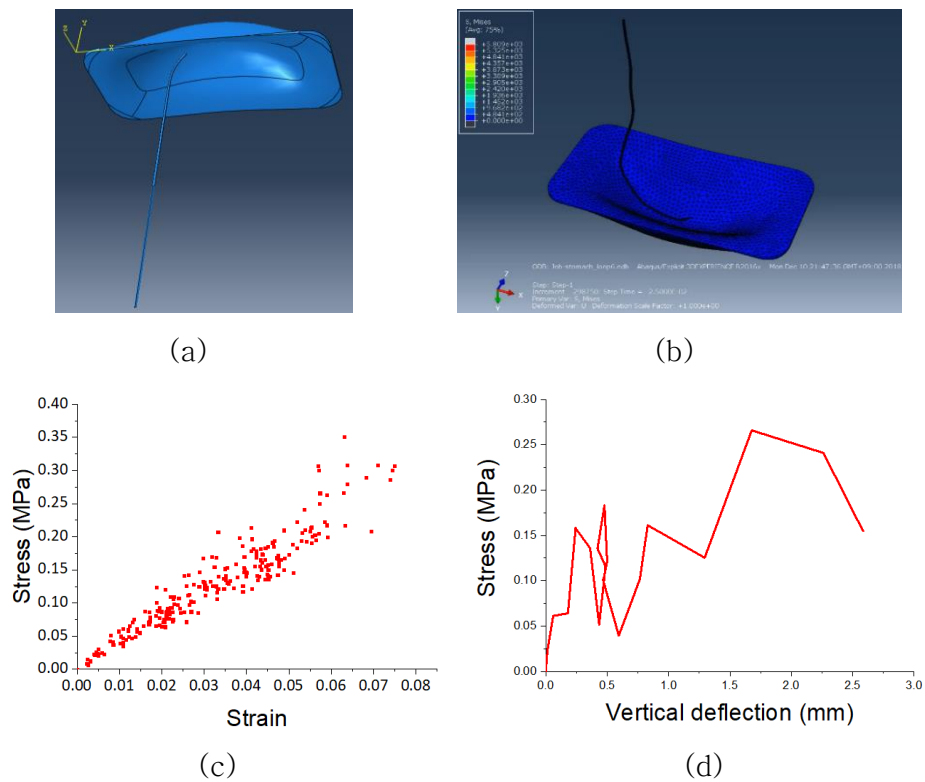


Figure 2.7: Simulation of mechanical behavior during the contact at stomach wall. (a) Stomach wall model (b) Analysis result (c) Stress – strain relationship at center point on wall surface (d) Stress – vertical deflection relationship point on wall surface

The bending motion after the guidewire collide into the greater curvature is initiated by column buckling. In science, buckling is a mathematical instability that leads to a failure mode. When a structure is subjected to compressive stress, buckling may occur. Buckling is characterized by a sudden sideways deflection of a structural member. This may occur even though the stresses that develop in the structure are well below those needed to cause failure of the material of which the structure is composed. As an applied load is increased on a member, such as a column, it will ultimately become large enough to cause the member to become unstable and it is said to have buckled. Further loading will cause significant and somewhat unpredictable deformations, possibly leading to complete loss of the member's load-carrying capacity. If the deformations that occur after buckling do not cause the complete collapse of that member, the member will continue to support the load that caused it to buckle [32].

The wall-following on the stomach wall is based on the buckling of the guidewire (Figure 2.8). The guidewire bends when the reaction force from the soft tissue exceeds a critical buckling load. A typical guidewire which is commonly used by interventional radiologists is nitinol wire. The Young's modulus of the nitinol guidewire (Radifocus, TERUMO corp.) was estimated as 63.54 GPa. The length of the guidewire is 260 cm and 0.89 mm in diameter. The critical buckling load is given as follows:

$$P_{cr} = \frac{m\pi^2 E_{GW} I_{GW}}{{L_{GW}}^2} \qquad (2.8)$$

$$\left( I_{GW} = \frac{\pi d^4}{64} \right)$$

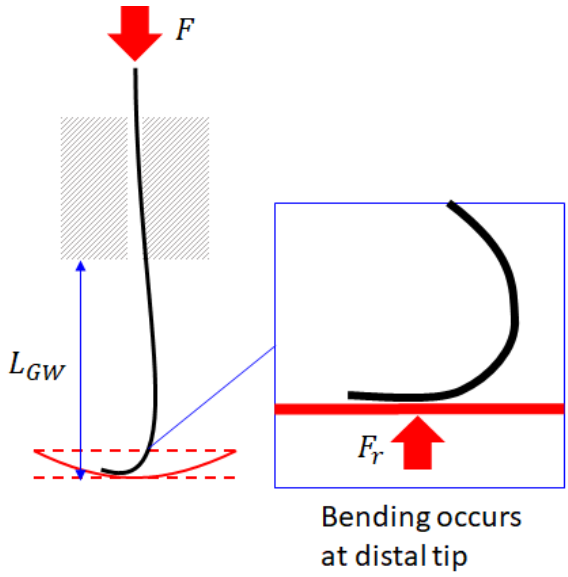


(a)

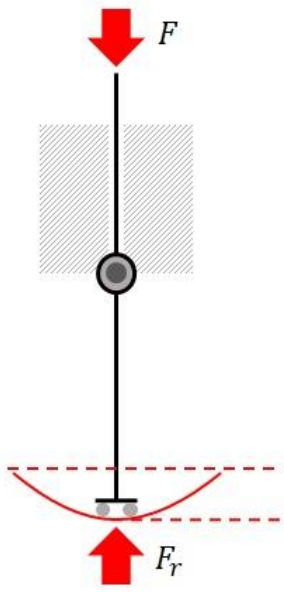


(b)

Figure 2.8: Buckling on stomach wall.

(a) Tip bending by buckling (b) Buckling coefficient at stomach wall

where $m$ is the factor accounting for end conditions, $E_{GW}$ is the Young's modulus of the guidewire, $I_{GW}$ is the moment of inertia of the guidewire, $L_{GW}$ is the maximum distance from the EG junction to the greater curvature, $F_r$ is the reaction force by the distended stomach, and $d$ is the diameter. If the condition $F_r > P_{cr}$ is satisfied, the distal tip of a guidewire bends.

Table 2.4: Parameters for critical buckling load prediction of guidewire in stomach

| $m$ | $E_{GW}$ (GPa) | $I_{GW}$ ($mm^4$) | $L_{GW}$ (mm) |
|---|---|---|---|
| 1 | 63.54 | 0.0308 | 100 |

The buckling load converges to approximately 0.19 N when the inserted guidewire length is assumed as 100 mm and contacts to the distended stomach. Incidentally, the contact point is wider than the diameter of a guidewire due to the J-shaped tip. It means that the reaction force and the inserted length determine whether the bending motion occurs or not.

Passive bending phenomenon after buckling continues by an increase of the pushing force onto the guidewire. When a guidewire is pushed into the stomach, the curve configuration is determined by the force equilibrium at the stomach wall. Right after the buckling, the radius of curvature will decrease by 10 mm (Figure 2.9(b)). This can be assumed as a bending curve at the stomach.

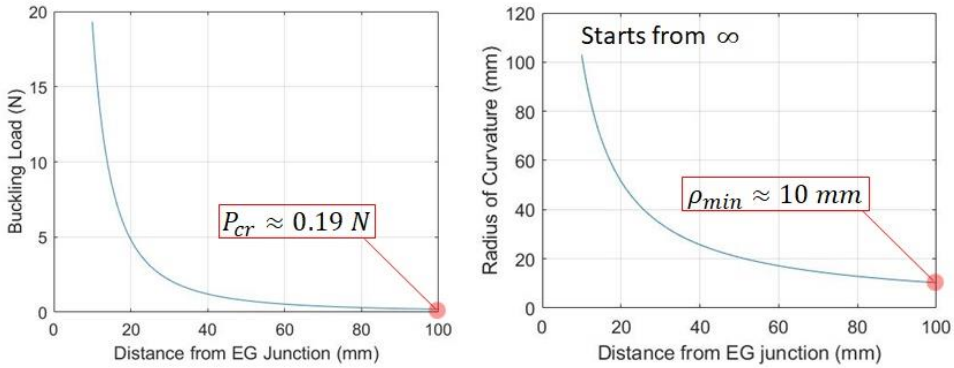


(a) (b)

Figure 2.9: Buckling load and radius of curvature prediction of guidewire. (a) Buckling load prediction (b) Radius of curvature at stomach wall

### 2.1.4 Friction in Stomach

Organ friction is a factor that can affect the slip conditions in the interventional radiology. The inner surface of the stomach is lined by a mucous membrane known as the gastric mucosa. The mucosa is always covered by a layer of thick mucus that is secreted by tall columnar epithelial cells. Gastric mucus is a glycoprotein that serves two purposes: the lubrication of food masses in order to facilitate movement within the stomach and the formation of a protective layer over the lining epithelium of the stomach cavity. This protective layer is a defense mechanism the stomach has against being digested by its own protein-lyzing enzymes, and it is facilitated by the secretion of bicarbonate into the surface layer from the underlying mucosa. The acidity, or hydrogen ion concentration, of the mucous layer, measures pH7 (neutral) at the area immediately adjacent to the epithelium and becomes more acidic (pH2) at the luminal level. When the gastric mucus is removed from the surface epithelium, small pits, called foveolae gastrique, may be observed with a magnifying glass.

There are approximately 90 – 100 gastric per $1\,mm^3$ of surface epithelium. Three to seven individual gastric glands empty their secretions into each gastric pit. Beneath the gastric mucosa is a thin layer of smooth muscle called the muscularis mucosae, and below this, in turn, is loose connective tissue, the submucosa, which attaches the gastric mucosa to the muscles in the walls of the stomach [39].

Friction behavior on gastric tissue is known that "Stick–slip" phenomenon occurs and there are multiple stages which are based on the repetitive elastic deformation accumulation and the release of the stored energy [40]. In GI intervention, the guidewire is lubricated by saline, therefore, the hydrophilic coated surface is highly slippery. In endoscopy, the friction coefficient of esophagus depended on the variations of normal load and sliding speed. However, the guidewire insertion into the duodenum can be assumed that the insertion speed is not dominant due to the number of the contact point is relatively fewer than an endoscope. The friction between the distal tip of the guidewire and the stomach wall is an important issue in intervention. Sometimes, the deformed stomach wall plays a role as a crater–like constrained space. When the top surface of the distal tip contacts at the stomach wall surface, the distal tip will bite into the epithelial layer as illustrated in Figure 2.10. The contact angle cannot be determined by a clinician in the fluoroscopic–guided procedure because the fluoroscopic image can only provide a perception of the contrast difference between a radiopaque section and organs. Therefore, the clinicians push and pull back the guidewire repetitively to make the guidewire in a curved configuration at the stomach.

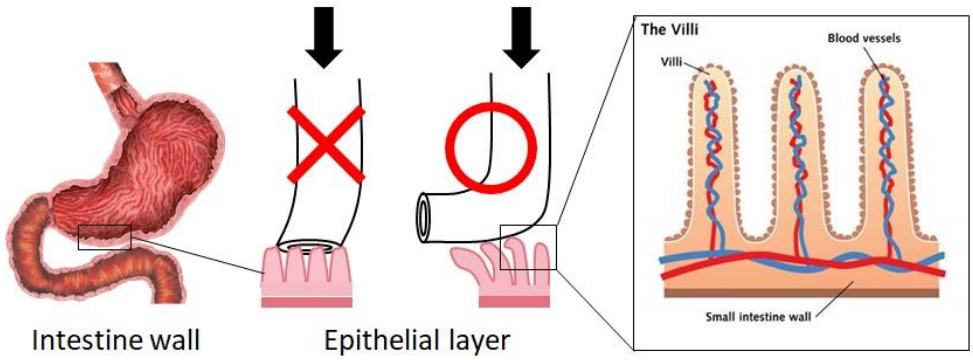


Figure 2.10: Interaction on stomach wall

The friction of the stomach wall had been measured by many researchers and the coefficient of static friction is known as **0.025 – 0.040** in endoscopy [41]. The lubricant and the covering materials determine the friction coefficient in endoscopy can be assumed as same in the interventional devices. To verify a friction effect during a tube insertion, a free body diagram of the stomach wall interaction was verified through a simple model (see **Figure 2.11**). Due to the flexibility of the stomach wall, the stomach wall changes during the interaction. Therefore, an interaction between a tube and the stomach is divided into two forces: 1) Internal and 2) External. The internal force occurs by the stomach wall reaction. The external force is exerted on an inserted structure (guidewire, catheter). Here, a guidewire insertion process was simulated.

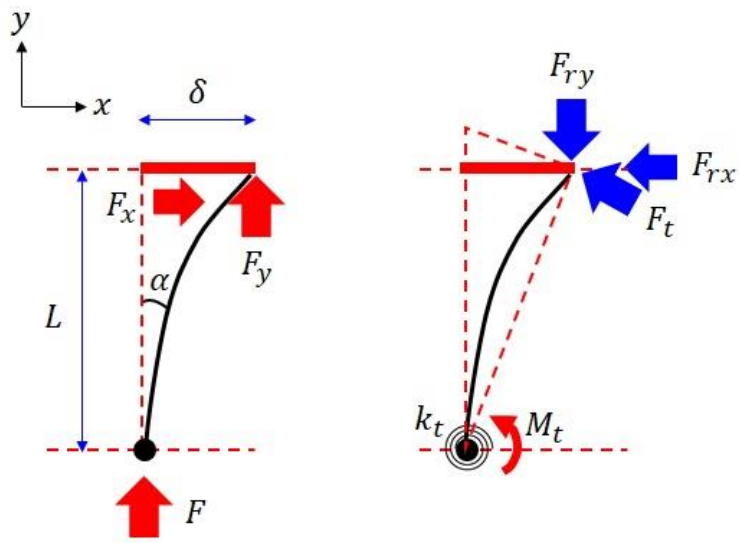


(a) (b)

Figure 2.11: Force decomposition at stomach wall.

(a) Free body diagram of external force at the stomach

(b) Free body diagram of internal force at the stomach

The external force is given as following equation.

$$F_x = F\sin\alpha = \mu N \tag{2.9}$$

$$F_y = F\cos\alpha \tag{2.10}$$

$$\left(\alpha = \tan^{-1}\frac{\delta}{L}\right)$$

The internal force is given as following equation.

$$F_{rx} = \frac{3EI\delta}{L^3} \tag{2.11}$$

$$F_{ry} = F_t \sin\alpha \tag{2.12}$$

$$\left(k_t\alpha = F_t L, \qquad k_t = \frac{2E_{GW}I_{GW}}{L_{GW}}\right)$$

$\alpha$ is the deflection angle, $\delta$ is the maximum horizontal deflection at the stomach wall, $\mu$ is the coefficient of static friction, $N$ is the normal force to the stomach wall which is same as the vertical force $F_y$, $F_x$ is the horizontal force, $L_{GW}$ is the maximum distance from the EG junction to the greater curvature, $M_t$ is the straightening moment by the beam deflection, and $k_t$ is the torsional spring constant of the curved guidewire as above under the assumption that the beam bending occurs between the EG junction and the stomach wall. $F_t$ is the horizontal load at the tip by the reaction force of the distended stomach. The external force and the internal force can be decomposed by horizontal and vertical direction as illustrated in **Figure 2.12 (a, b)**. As a result, $F_{rx}$ increases that follow a quadratic curve by the $F_x$ increase. **Figure 2.12(c)** shows the force ratio into the horizontal direction. The friction effect is not significant because the friction force is dependent on the vertical force on the stomach wall.

To slip into the duodenum, the pushing force should be maintained which is to satisfy the following conditions.

$$F_x > \mu' F_y + F_{rx} \tag{2.13}$$

The kinetic friction coefficient can be approximated as $\mu' \cong \mu/2$. From the simulation result, the friction is not dominant during the pushing force increase because of the friction at stomach is extremely low. Furthermore, the guidewire is generally lubricated by the saline. Therefore, the friction effect is almost negligible in intervention.

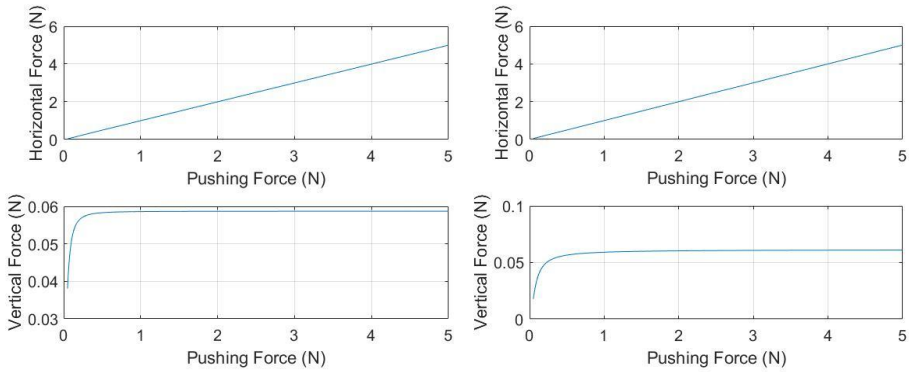


(a) (b)

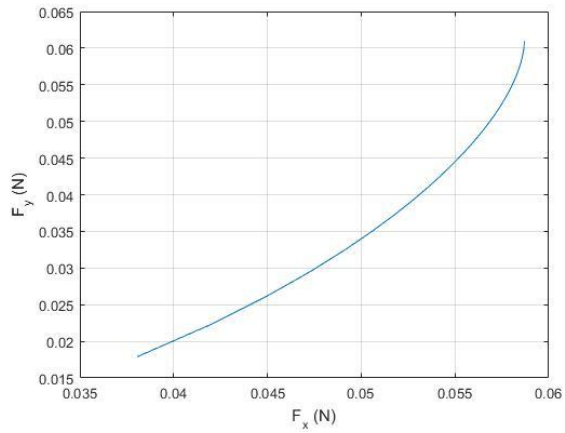


(c)

Figure 2.12: Force decomposition analysis (Upper: horizontal force, Lower: vertical force). (a) Decomposition of external force analysis (b) Decomposition of internal force analysis (c) $F_{ry} / F_{rx}$ ratio

## 2.2 Conformability Model

### 2.2.1 Conformability Factor

In an interventional procedure, the physical interaction occurs between the flexible environment (soft tissue) and the inserted structures (guidewire, catheter, stent introducer/endoscope). To determine the appropriate mechanical characteristics of the medical tube that is designed to be inserted into the GI tract, the conformable

force and tactile could be the main interests in terms of safety. In other words, a conformability of the medical tube against the soft tissue is a key factor in an interventional procedure.

Conformability in the tube insertion into the soft tissue is considered as the degree of shape adaptiveness in static equilibrium. If conformability between a certain environment and an interacting structure is high, curved configuration of the inserted tube is close to the geometry of an anatomical tortuosity (see **Figure 2.13(a)**). Contrary to this, if conformability is low, the soft tissue deforms by an inserted tube (see **Figure 2.13(b)**). To avoid the patients' discomfort and perforation during the interventional procedure, conformability should not be too low. However, to predict a conformability with a multi-body contact model requires a huge computational effort. For this reason, the design parameters of a medical tube for an interventional procedure cannot be determined by a simple one.

Conformability of a continuum structure against a curved environment can be determined by the bending stiffness. If the bending stiffness of a tube is too high during an insertion process, the bending points of the structure decreases due to the high resistance. A bending point of the structure can be considered as a joint, however, a continuum structure has an infinite number of joints.

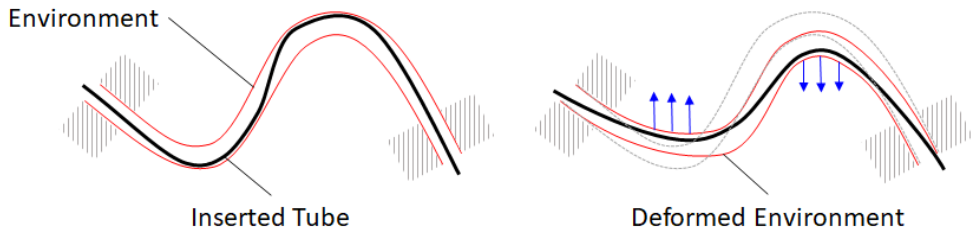


(a) (b)

Figure 2.13: Conformability between continuum structure and flexible environment. (a) Highly conformable state (b) Less conformable state

Thus, the bending point in a continuum structure is determined by its bending stiffness. Bending stiffness, namely flexural rigidity $K$ is the resistance of a member against bending deformation. It is a function of elastic modulus $E$, the area moment of inertia $I$ of the beam cross-section about the axis of interest, length of the beam and beam boundary condition as follows:

$$K = EI \tag{2.14}$$

The flexural rigidity difference between the environment and the structure affects a shape adaptiveness during an insertion. Thus, conformability of the environment-inserted tube interaction can be considered as a normalized flexural rigidity of the environment as follows:

$$C = \frac{EI_{ENVIRONMENT}}{EI_{INSERTING\ TUBE}} \tag{2.15}$$

where $C$ is the conformability factor.

To calculate a conformability factor in the simple stomach wall

model (see **Figure 2.5**), the Young's modulus of the stomach wall $E_s$ was determined as **1.7 – 2.3 MPa** [30, 31, 38] and the area moment of inertia $I_s$ was calculated as **1,800 mm$^4$**. The equation (2.16) defines the area moment of inertia of the contact region in the stomach wall.

$$I_s = \frac{ab^3}{12} \tag{2.16}$$

To obtain the bending stiffness of each devices and stents for GI intervention, bending stiffness test machine was developed (see **Figure 2.14(a)**). **Table 2.5** shows the dimensions and the evaluated Young's modulus of the common GI stents at the compressed state inside a silicone tube (see **Figure 2.14(b, c)**). The medical tubes for GI intervention was also evaluated using the bending stiffness test machine (see **Table 2.6**).

Table 2.5: Young's modulus of GI stents

| Stent | Dimension L x D x t (**mm**) | $E_{MAX}$ (**MPa**) |
|---|---|---|
| #1 | 70 x 23.5 x 0.6 | 31.9 |
| #2 | 64 x 19 x 0.3 | 30.1 |
| #3 | 85 x 20 x 0.3 | 43.3 |
| #4 | 64 x 25 x 0.3 | 30.5 |

Table 2.6: Bending stiffness comparison in GI intervention

| Object | Bending Stiffness (**$Nmm^2$**) |
|---|---|
| Stomach wall (bottom) | 3,060 |
| Soft guidewire (Φ0.89, Terumo, Ni-Ti) | 1,957 |
| Stiff guidewire (Φ0.89, Boston Scientific, steel) | 6,256 |
| Esophageal-Duodenal Stent | 2,769 |
| GI Stent introducer (PTFE) | 7,157 |
| Coil Catheter (S&G Biotech) | 4,721 |
| GI Sheath (Φ6, PTFE) | 12,944 |

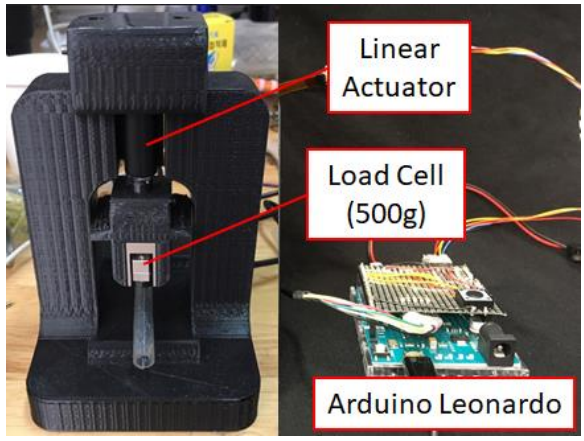


(a)

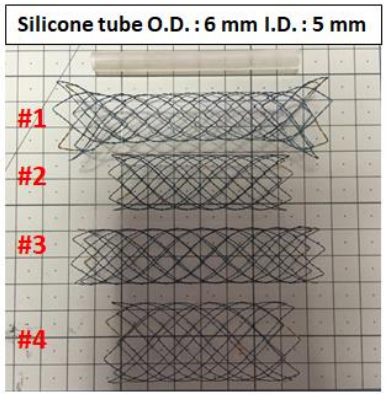


(b)

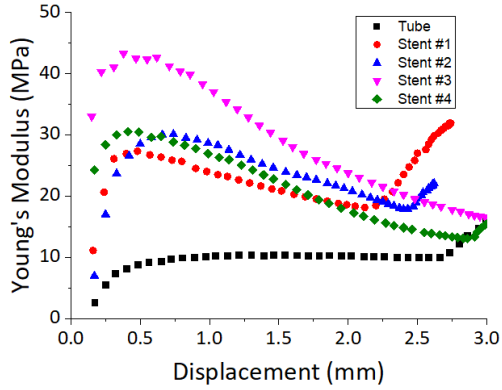


(c)

Figure 2.14: Bending stiffness evaluation.

(a) Three-point bending test machine for interventional devices

(b) Silicone tube test piece and GI stents

(c) Young’ s modulus change in three-point bending test

For example, during the guidewire insertion into the duodenum, the guidewire should pass through a bottom wall region of the stomach. The maximum contact region is determined as a pathway of the guidewire. At the first step, the soft guidewire is inserted (see **Figure 2.15(a)**). The conformability factor of the guidewire passing in the stomach wall (see **Figure 2.5**) is calculated as $C_{GW-s} = E_s I_s / E_{GW} I_{GW} = 1.56$. The subscripts **s** and **GW** represent the stomach and the guidewire respectively.

To deliver a stent into the target site, a stent introducer with a compressed stent is inserted (see **Figure 2.15(b)**). In this process, the conformability factor $C_{SI-GW,s}$ is decreased by **0.56** (Subscript **SI** represents the stent introducer) because the environment in the conformability model is replaced by the stomach and the inserted guidewire (see **Figure 2.16**). In fact, in the clinical situation, the perforation risk factor increases in this combination. Therefore, the soft guidewire is replaced by a stiff guidewire after catheter insertion. The conformability factor $C_{SI-SGW,s}$ is increased by **0.94** (see **Figure 2.15(c)**). Subscript **SGW** represents the stiff guidewire. Consequently, the stent placement procedure is prolonged because of the catheter insertion and guidewire replacement. Furthermore, the pre-curved guiding sheath is used in the difficult situation during the procedure. The curve configuration of the inserted guidewire is changed by the guiding sheath insertion. Due to the high stiffness of the guiding sheath, the conformability factor is increased by **1.50** even though the stiff tube such as stent introducer is passing. In this case, the stiffness of the stomach wall is ignorable because the guiding sheath is supported from the proximal side.

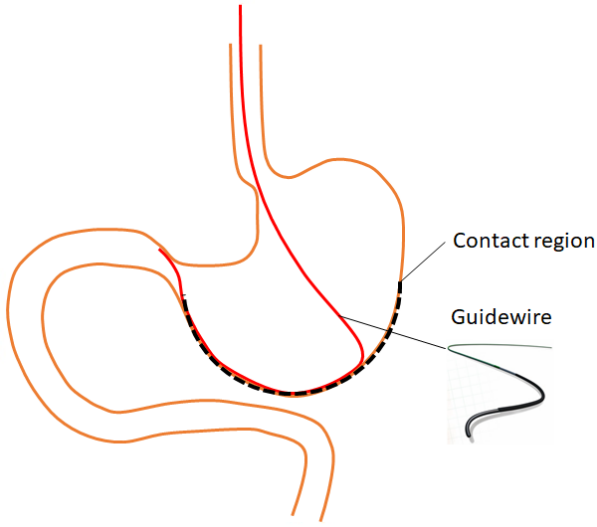


(a)

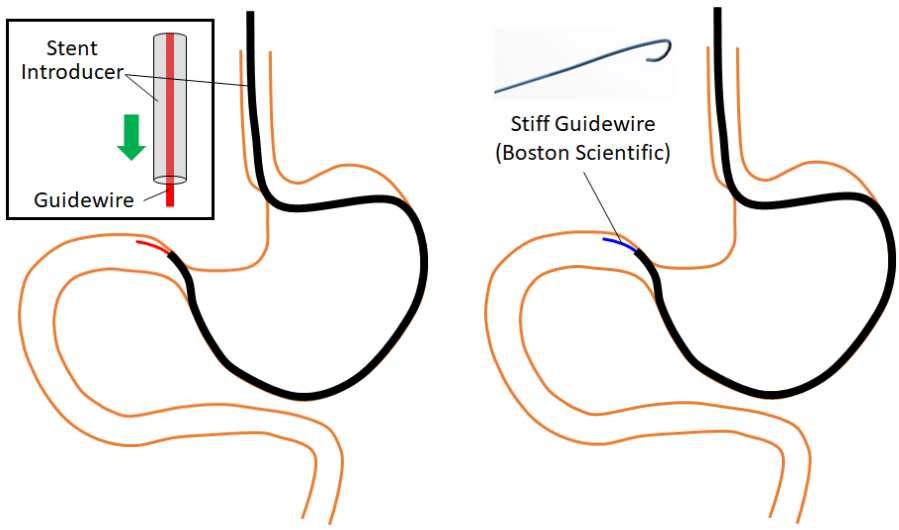


(b) (c)

Figure 2.15: Insertion process of guidewire and stent introducer. (a) Soft guidewire is inserted (b) Stent introducer is overlapped on the soft guidewire (c) Stent introducer is overlapped on the stiff guidewire

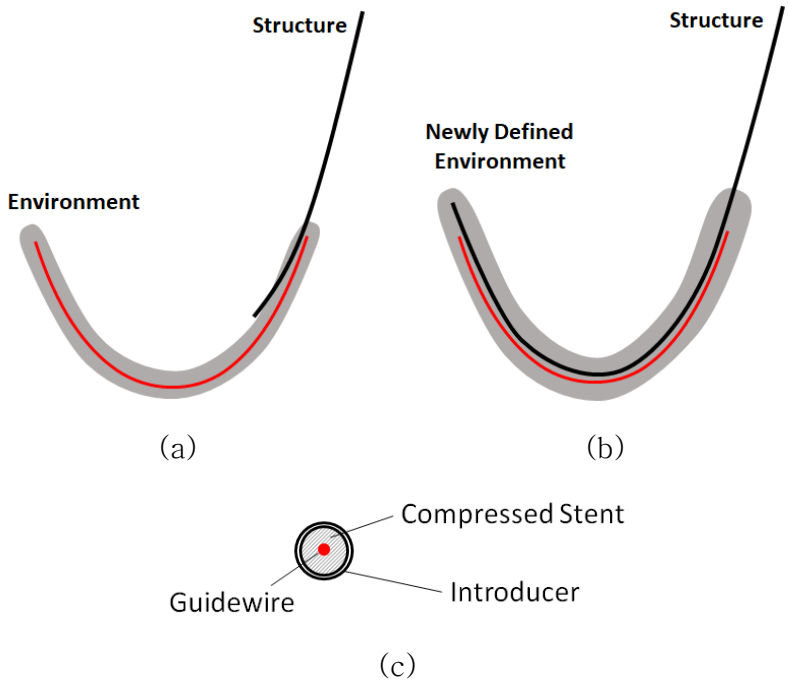


Figure 2.16: Environment - structure relationship in conformability model. (a) Environment - structure in initial state (b) Newly defined environment - structure after tube insertion (c) Cross-sectional view of overlapped stent introducer

The conformability factors in various combinations of GI interventional device were calculated as represented in Figure 2.17. The conformability factor of the stent introducer against the soft guidewire is low, therefore, the combination of these devices is not desirable in the actual procedure [42, 43]. Commonly, the soft guidewire is replaced with the stiff guidewire through the catheter. The bending stiffness of the steel guidewire is almost three times of the nitinol guidewire. The steel guidewire generates a higher bending stiffness compared to the nitinol guidewire. For this reason, a direct insertion increases the perforation risk factor during the procedure.

As a result, the additional procedure is required for stent placement.

| Environment | Inserting Tube | Conformability |
|---|---|---|
| Soft Tissue | Soft Guidewire | 1.56 |
| Soft Tissue | Stiff Guidewire | 0.49 |
| Soft Tissue + Soft Guidewire | GI Stent + Stent Introducer | 0.56 |
| Soft Tissue + Stiff Guidewire | GI Stent + Stent Introducer | 0.94 |
| Soft Tissue + Soft Guidewire | Coil Catheter | 1.06 |
| Soft Tissue + Coil Catheter | Stiff Guidewire | 1.24 |
| Soft Guidewire + Guiding Sheath | GI Stent + Stent Introducer | 1.50 |
| Guiding Sheath | Soft Guidewire | 6.61 |

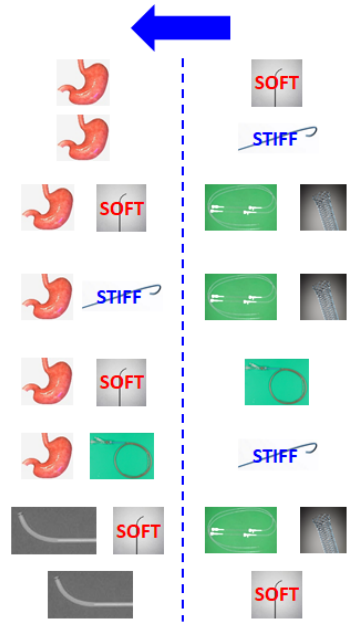


Figure 2.17: Conformability factors in various combinations of GI interventional device

### 2.2.2 Geometry in Conformability Factor

In GI intervention, to avoid a large deformation of the soft tissue in the GI tract, the concentrated load at the tortuosities should be distributed. The bending stiffness is a dominant factor for tissue deformation, however, the stiffness issue is irrelevant during the tube is passing through in the straight portion (see Figure 2.18). Consequently, the curvature that the medical device is supposed to be overcome should be considered in the conformability model.

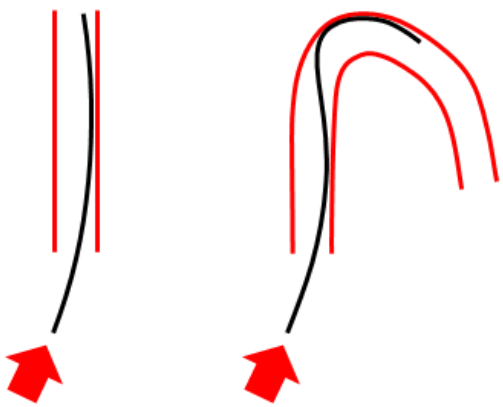

(a) (b)

Figure 2.18: Geometry difference in GI intervention.
(a) Tube insertion into straight portion
(b) Tube insertion into curved portion

The geometry in curved space is illustrated in Figure 2.21. The modified conformability factor is defined as follows:

$$C' = \frac{2R}{L_t} \frac{EI_{ENVIRONMENT}}{EI_{INSERTING\ TUBE}} \tag{20}$$

where $R$ is the radius of the circle that is approximated at the curve and the effective length $L_t$ is the minimum distance between

the input point $P_{IN}$ and the output point $P_{OUT}$. Both points are determined by the natural curve configuration in anatomy.

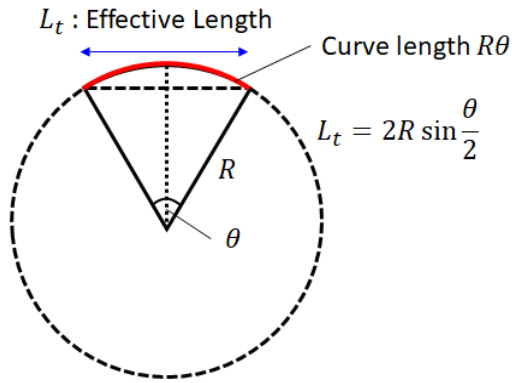


(a)

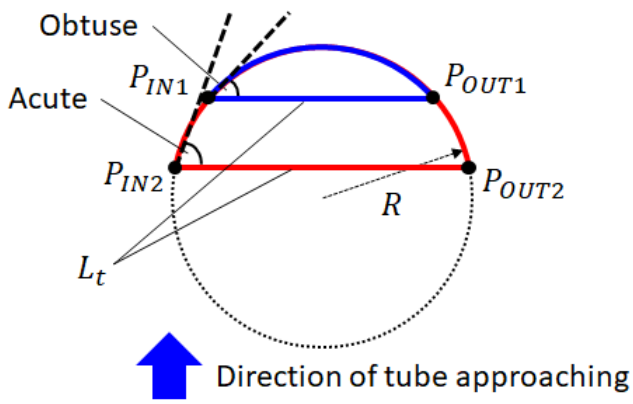


(b)

Figure 2.19: Geometry of curved space in conformability model.

(a) Approximation of curved space by circle

(b) Geometry difference between obtuse and acute angle in circle with same radius

### 2.2.3 Conformability Space in Stent Placement

In general, a compressed stent inside a tube is pushed out by a clinician (see Figure 2.20). To deliver the tip of the stent introducer into the target site, the guidewire should be located at the distal side in advance. During the insertion process, the stent introducer follows the pathway of the guidewire as though overlaps the guidewire body. The stent introducer can be inserted by a pushing force with resistance from kinetic friction between the stent introducer and the guidewire. As described in the previous chapter, the stent introducer is made of PTFE for several reasons such as the lowest friction coefficient of any polymer, high-use temperature and highly resistant to UV radiation [44]. However, the bending stiffness of the PTFE tube is high compared to the other device in GI intervention.

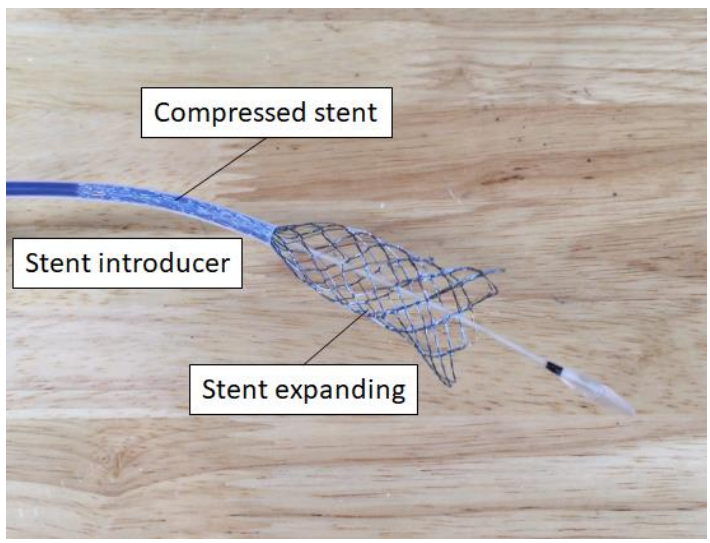


Figure 2.20: Stent placement using introducer

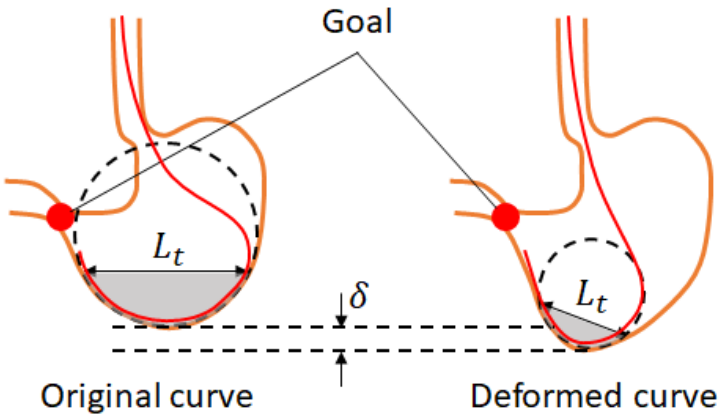


Figure 2.21: Curve configuration change by tissue deformation

Deformation of the soft tissue in GI tract should be considered in the design of the interventional devices. If the guidewire tip is located in the distal jejunum, the deformation of the soft tissue will increase when the stent introducer with a large bending stiffness is overlapped. For this reason, the conformability during GI intervention should be considered in terms of curve configuration change (see Figure 2.21). With the modified conformability model, a conformability space can be evaluated in various effective length and radius of curvature (see Figure 2.22). Figure 2.22(b) shows that the safe and the dangerous ranges in terms of the perforation safety. As illustrated in the plot, the soft guidewire insertion into the stomach can be done safely in a curve configuration with a large effective length and a large radius of curvature. In contrast, the stent introducer passing with a soft guidewire cannot be achieved safely in any curve configuration.

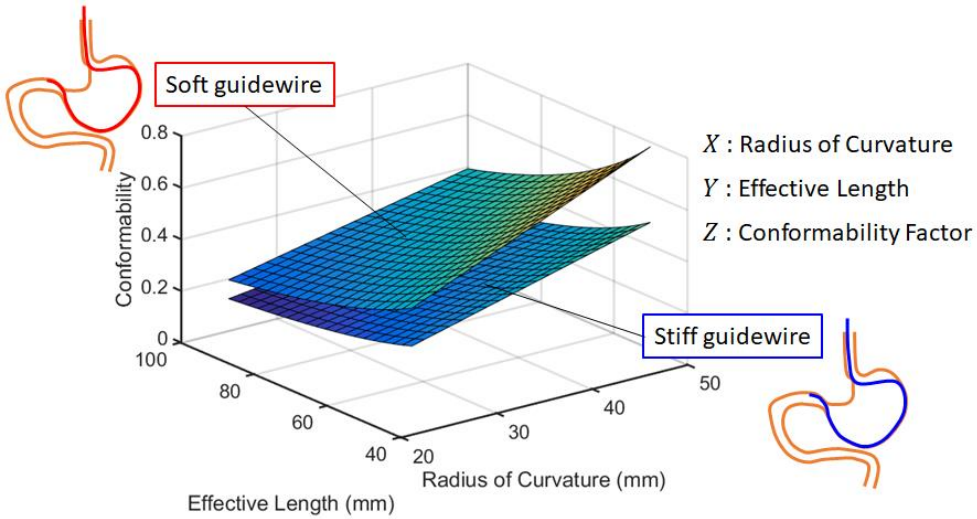


(a)

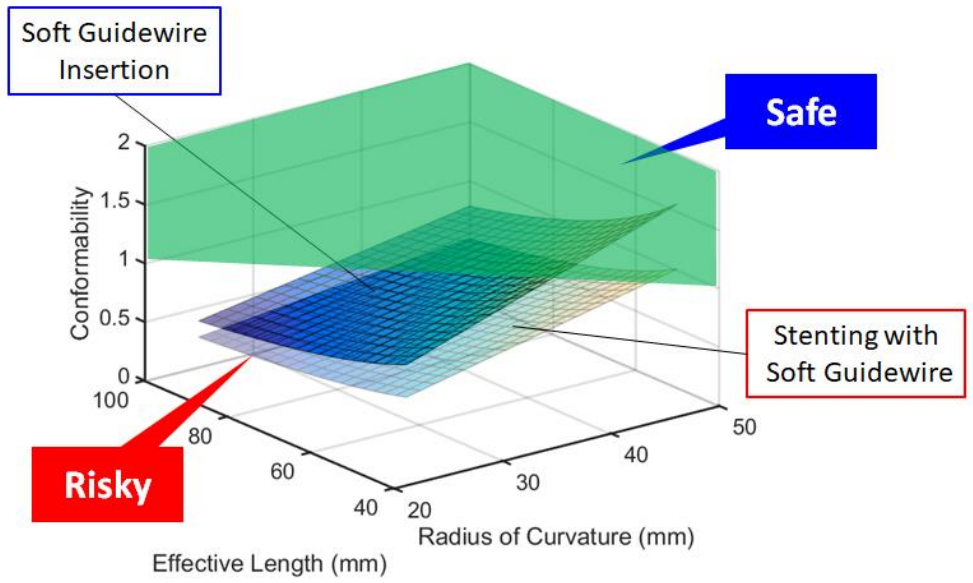


(b)

Figure 2.22: Conformability space in GI intervention.

(a) Conformability space in guidewire insertion

(b) Difference in conformability space of the procedures

# Chapter 3. Steerable Catheter Design

## 3.1 Conventional Designs and Mechanisms of Steerable Catheter

### 3.1.1 Steerable catheters

A catheter is a tubular device for medical use that has the capability to pass another device or drug through the inner lumen. Therefore, a catheter is made from medical grade materials serving a broad range of functions. The flexible catheter can be inserted into the body to treat diseases or perform a surgical procedure including radiofrequency ablation, tissue resection, and biopsy (see Figure 3.1). By modifying the material or adjusting the way catheters are manufactured, it is possible to tailor catheters for cardiovascular, urological, gastrointestinal, neurovascular, and ophthalmic applications [45].

Recently, a steerable catheter has been one of the most promising devices in the interventional radiology. Steerability refers to the ability to turn or rotate the distal end of the catheter with a like-for-like movement of the proximal section or catheter handle. It is achieved through strong torque transfer along the length of the shaft. Cardiac catheterization performed by steerable catheters, is one of the significant domains in Minimally Invasive Surgeries (MISs) for electrophysiology studies, heart rhythm abnormality treatment, and cardiac valve replacement. In past, cardiac catheters are steered with limited degrees of freedoms (DOFs) in the vascular path to the heart chambers and on the targeted cardiac tissues. However, with a steerable catheter, the interventionalists can navigate the catheter by means of translating and twisting the proximal end with the bending of the distal shaft using the steering knob on the handle. The long and

flexible structure of catheters along with fast cardiac motions restrain accurate positioning and consequently maintaining stable contact with the endocardium [46].

In GI intervention, the catheter for the biliary tract balloon dilation is a common product for dilation treatment (see **Figure 3.2(a)**). Endoscopic balloon dilatation of the biliary sphincter is an important adjunct to the therapeutic arsenal of the biliary endoscopist for removal of bile duct stones during endoscopic retrograde cholangiopancreatography (ERCP). On the other hands, other types of catheters for diagnosis of gastrointestinal motility disorders are commercially available (see **Figure 3.3(b)**). Motility catheters are air-charged single-use catheters for esophageal motility studies and anorectal manometry. The steerable catheters in ERCP are known as a better device for the initial cholangiogram than the standard catheter [47]. In addition, steerable catheters for neurovascular intervention have been widely studied recently. Shape Memory Alloy (SMA) (see **Figure 3.3(a)**) [48, 49], magnetic (see **Figure 3.3(b)**) [50], hydraulic (see **Figure 3.3(c)**) [51], Ion-Polymer-Metal Composite (see **Figure 3.3(d)**) (IPMC) [52-54] and wire (see **Figure 3.3(e)**) [55-58] mechanisms were adapted for the steerable catheter. Most of these actuation mechanisms are based on the electric actuation. The electric mechanisms are classified as 1) direct electric actuation and 2) indirect electric actuation. Direct electric actuation in steerable catheters can rely on different actuation mechanisms, yet in all cases, an electric current is provided to create a bending force and motion at the distal tip like SMA and IPMC catheters. For direct methods, the most common is by the use of a PZT (Pb-Zr-Ti transducer or, as it is sometimes called, piezoelectric z-axis actuating transducer), which is capable of

vibrating at different frequencies very accurately depending on the driving voltage. Indirect actuation includes using acoustic vibration to shake a microsensor much like a piece of paper in front of a speaker vibrates from the compression waves in the air. Despite the recent developments in both categories, all known electrically actuated steerable systems are currently experimental prototypes [59]. Likewise, most of the other catheters are yet in the state of basic research and not for the clinical use. Commonly, pull-wire type mechanism is considered as the simplest and verifiable mechanism to bend a tip of the catheters in the clinical field.

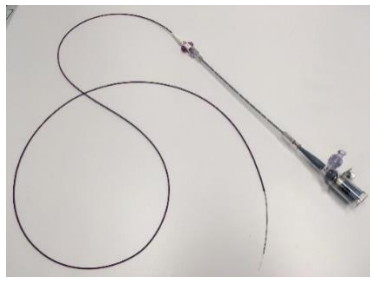

(a)

(b)

(c)

(d)

Figure 3.1: Catheters. (a) Cardiac catheter (UC Davis) (b) Urinary catheter (Birth Supplies) (c) Neurovascular catheter (MERCI) (d) Ablation catheter (St. Jude Medical)

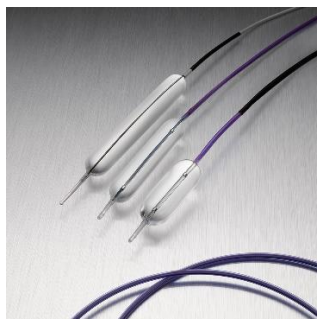

(a)

(b)

Figure 3.2: GI catheters. (a) Balloon Dilatation Catheters (Boston Scientific, Inc.) (b) Catheters for GI motility (MMS, Inc.)

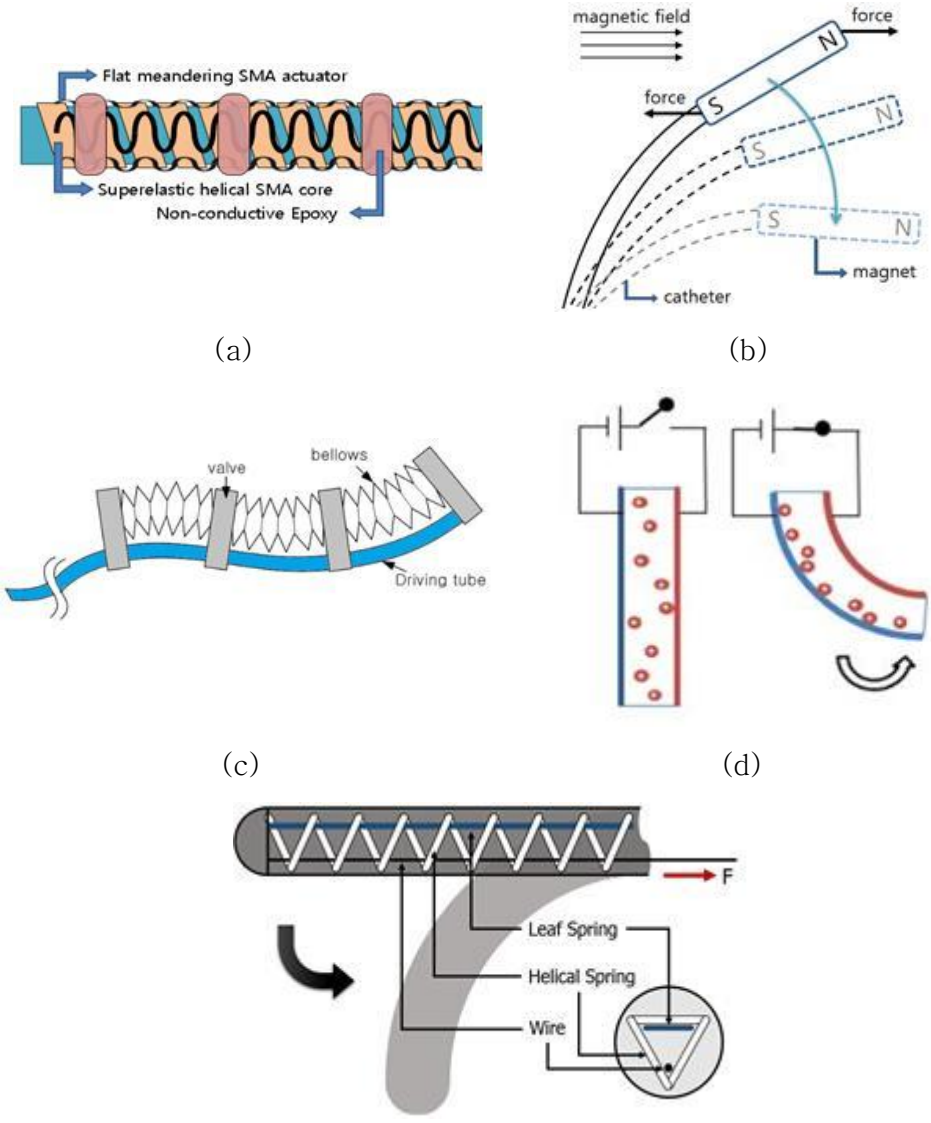


Figure 3.3: Actuation and mechanisms in steerable catheters.

(a) Shape memory alloy-actuated catheter [48]

(b) Magnetic catheter [50] (c) Hydraulic catheter [51]

(d) Ion-polymer-metal composite catheter [52]

(e) Pull-wire catheter [55]

### 3.1.2 Continuum Robots as Catheter

Continuum robot manipulator has been considered as a delivery system including an endoscope, biopsy forceps, surgical tool, and ablation tip. This concept was featured as the platform of Natural Orifice Transluminal Endoscopic Surgery (NOTES) over the decade. Furthermore, research on multi-degree of freedom manipulators with flexible structure has been widely conducted, and various flexible joint mechanisms have been proposed with a simple structure and high versatility [60-63]. The most typical one is the bending mechanism of the active endoscope. Breedveld et al. proposed a Cable-ring mechanism in which drive cables are annularly arranged between a Ring-spring having annular plate springs bonded together and a double coil spring and proposed an active endoscope "Endo-Periscope" (see **Figure 3.4(a, b)**) [64, 65]. Arata et al. proposed a compact two degree of freedom bending mechanism combining a leaf spring and a link mechanism and developed a general purpose tool manipulator including an endoscope (see **Figure 3.5(c)**) [66]. Ikuta et al. [67] And Dario et al. [68] proposed a bending mechanism for an active endoscope using a shape memory alloy wire which has the property of being deformed by heat. In addition, pseudo-flexible manipulators with cable-driven multi-section link structure [69, 70] and active probes with flexible bending modules using hydraulically driven actuators have been proposed [71].

Next, the surgical manipulators have been widely studied in a continuum robotic platform. Dupont et al. proposed a compact flexible manipulator in which elastic tubes with different curvatures are arranged in multiple layers (see **Figure 3.4(d)**) [72]. The system has 6 DOFs with a simple mechanism in order to achieve positioning the distal forceps by controlling straight advancement and rotation of

each tube. Nevertheless, due to the low rigidity of the manipulator, applicable techniques are limited. The flexible bending mechanism by Simaan et al. [73] adapts hyperelastic alloys for joint structure and transmission, so that backlash is reduced and the bending portion becomes long while being a simple structure (see **Figure 3.4(e)**). The structure is considered that the joint part becomes longer and provides an insufficient torsional rigidity that can be a drawback because only the hyperelastic alloy at the center can play a role as a supporting structure. Peirs et al. proposed a flexible bending structure in which a hyperelastic alloy pipe was slit processed (see **Figure 3.4(f)**) [74]. Compared to the structure using a rigid link structure, it is a simple structure and has an advantage in miniaturization. In general, the design of a flexible joint mechanism capable of realizing a compact bending motion while ensuring the sufficient rigidity for surgery leads to solving the issues in surgical manipulators.

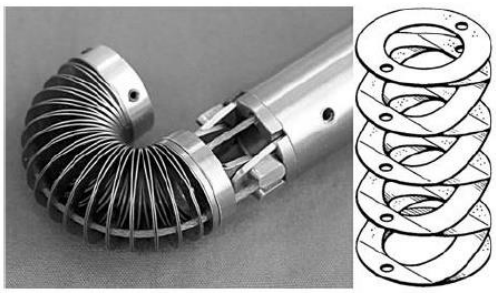

(a)

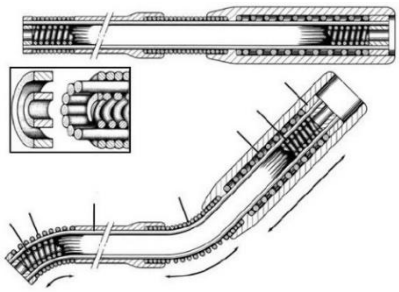

(b)

(c)

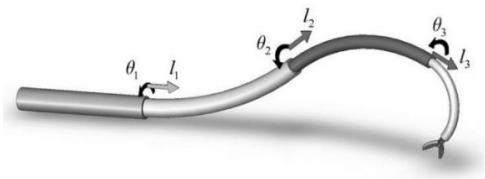


(d)

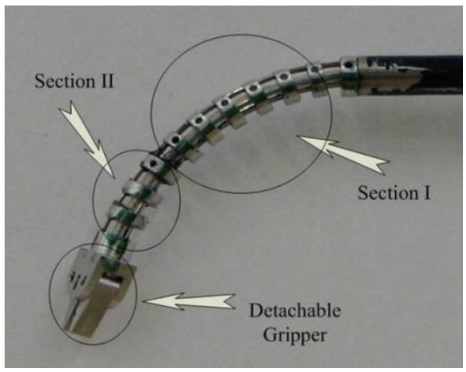


(e)

(f)

Figure 3.4: Continuum manipulators.

(a) Ring-spring mechanism [64] (b) Cable-ring mechanism [65]

(c) Spring-link mechanism [66] (d) Concentric robot [72]

(e) The multi-backbone continuum robot [73]

(f) Flexible distal mechanism [74]

Robotic catheter systems have been developed and used in the clinical field (see **Figure 3.5(a, b)**) [75–81]. It provides various advantages such as high precision, dexterity, and radiation–free environment. However, the drawback that loss of tactile feedback is one of the most critical problems in the robotic interventional procedure. To address the issue related to the loss of haptic feedback, force feedback systems have been proposed recently (see **Figure 3.5(c)**) [82, 83]. Robotic catheters can be used for a variety of applications and provide the physician with greater control and less exposure to radiation. Nevertheless, a robotic system requires a large footprint in the operating room, and it is still expensive due to the complex design.

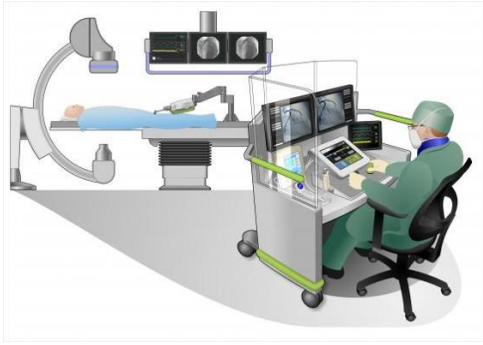

(a)


(b)

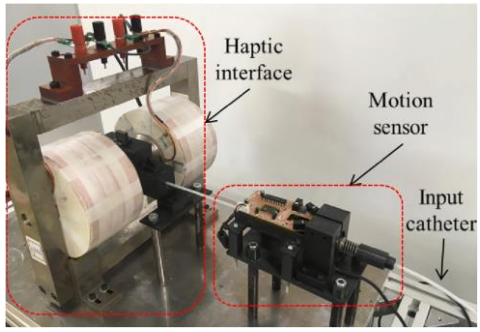


(c)

Figure 3.5: Robotic catheter system.
(a) CorePATH (Corindus, Inc.) (b) Sensei robotic catheter system (Hansen Medical, Inc.) (c) Catheter robot with haptic interface [82]

## 3.2 Steerable Catheter Design for GI Intervention

### 3.2.1 Structure Design based on Anatomy

In GI intervention, a catheter has two types of roles: 1)Stiffen the anchoring point at the acute angle for easy negotiation of a guidewire, 2)Injection of contrast medium. Commonly, the vascular catheters are essential in diagnostic angiography as well as in vascular and nonvascular interventional procedures. As in guiding a guide wire to the area of interest, vascular catheters have some limitations in upper gastrointestinal interventional procedures because of the acute angulations of the esophagus, gastric antrum, duodenum, and small bowel. In addition, in procedures in the stomach with long durations, it is often difficult to control a hydrophilic guide wire within a vascular catheter because of friction between the inner lumen of the vascular catheter and the outer surface of the hydrophilic guide wire. To overcome the limitations of vascular catheters in the upper gastrointestinal tract, Song et al. had designed a multifunctional coil catheter through which they could inject contrast medium to opacify the area of interest with a guide wire in place [84].

The functional requirement of steerable catheter had been considered on the basis of gastrointestinal system anatomy (human digestive system) and the form factor analysis of the conventional medical devices such as a guidewire, a coil catheter, guiding sheath, a flexible endoscope, and an overtube. Every device is designed to have a specific and a limited property to satisfy the situation that requires a specific function in the interventional procedure. Most of the interventional devices have a length of more than 1,200 mm. In upper gastric system anatomy, the distance from mouth to distal jejunum is approximately up to 90 cm along the organ path. The

diameter of the upper gastrointestinal tract is up to 2.54 cm.

Table 3.1: Dimensions in upper GI tract [42]

| Organ | Length (cm) | Thickness (mm) |
|---|---|---|
| Esophagus | 25 – 30 | 4 |
| Stomach | 20 – 50 | 4 – 6 |
| Duodenum | Overall : 25 – 30<br>($1^{st}$ portion : 5<br>$2^{nd}$ portion : 5<br>$3^{rd}$ portion : 7.5<br>$4^{th}$ portion : 10) | 3 |
| Jejunum | 90 | 0.9 |

### 3.2.2 Structure Design based on Interventional Devices

In general, the upper GI tract lumen diameter is known as 2.5 – 3 cm. The size of each interventional device varies with a device function (see Figure 3.7). The diameter of the guidewire is 0.68 – 0.89 mm and they are normally made of nitinol or stainless steel wires [85, 86]. Stent introducer is a tubular structure that consists of various material and diameter section in it. A peek tube section with 1.5 – 2.5 mm in diameter is aligned at distal side. The peek tube is used as a supporting structure to coil a loaded stent and make a guidewire pass through an inner lumen. The outer diameter of the stent introducer is 2.5 – 4.5 mm. A smaller diameter provides a chance to perform a more safe treatment.

In addition, there are size limitations related to the GI SEMS design. Normally, the GI SEMS is a meshed structure made of a hyperelastic material. In the manufacturing process, the knitted wires surrounding a cylinder jig (see Figure 3.7) form a meshed tubular

structure, therefore, the strut thickness (overlapped diameter of wires) is a dominant factor in the design of a GI SEMS. Major design parameters of GI SEMS are divided into the axial force and the radial force (see Figure 3.8(a)). GI SEMS is designed on the basis upon the desirable expansion force. To expand a SEMS in a narrow space, SEMS should be compressed in the delivery process. For this reason, SEMS is designed as a highly compressible tubular structure. Especially, an esophageal-duodenal stent is compressed in a radial direction up to $2 - 3.5\,mm$ in the introducing tube. In endoscopic-guided approach, the stent introducer should pass through a working channel (smaller than $3.5\,mm$ in diameter). That is, the outer diameter of a stent introducer is limited to smaller than $2 - 2.5\,mm$ due to the minimum wall thickness of the tube.

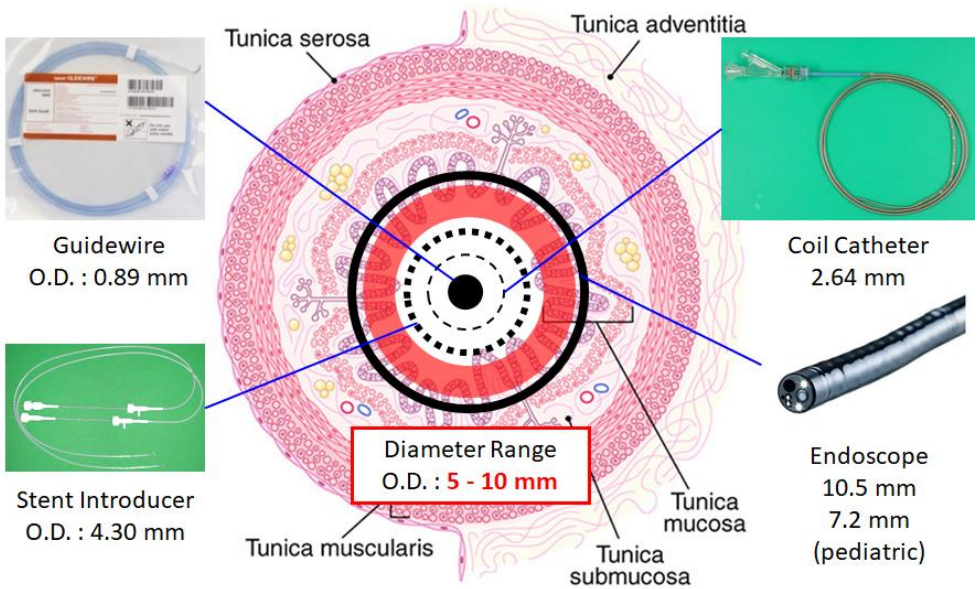


Figure 3.6: Form factor limitation in interventional devices related to the average diameter of upper GI tract

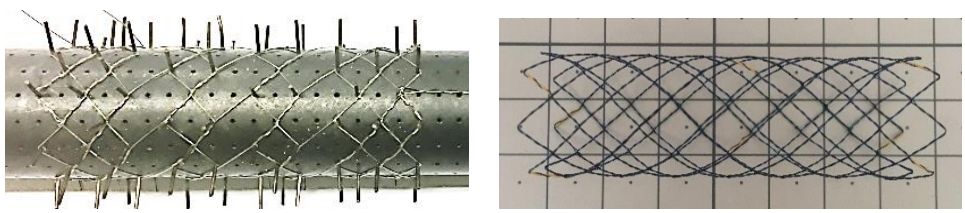

(a) (b)

Figure 3.7: GI SEMS pattern design.
(a) Jig for pattern design of GI SEMS (b) Knitted GI SEMS

The shape of the SEMS after the compression is almost the same as a solid cylinder. Due to the minimum desirable expansion force of SEMS [87], the strut thickness of SEMS should not exceed a certain level. Generally, the esophageal–duodenal stents have a knitted strut which is 0.35 mm in diameter (see Figure 3.8(c)). In most cases, the axial force of the stents is relatively small compared to the expansion force inside a lumen. This is because of the necessity of increased

conformability after placed in the stenosed lumen. Stents should be compressed in a uniform distribution into a radial direction because the shape collapse of stents comes to the deployment failure [88]. For this reason, the outer sheath of stent introducer for esophageal–duodenal stents is commonly designed to endure the large expansion force by the compressed stent in the tube. Maintaining a radial stiffness means that the bending stiffness will increase consequently. Commonly, an outer sheath of the stent introducer is made of Polytetrafluoroethylene (PTFE). PTFE is the most popular material for medical tubing that requires maximum surface lubricity, high chemical, and thermal resistance, biocompatibility, and/or exact extrusion tolerances. However, the increased bending stiffness of the stent introducer with a loaded stent generate a straightening moment and it hinders to overcome the acute angle at the tortuosity in GI tract. Thus, the steerable catheter should be designed in the basis of consideration on the stiffness and size limitations in the conventional devices.

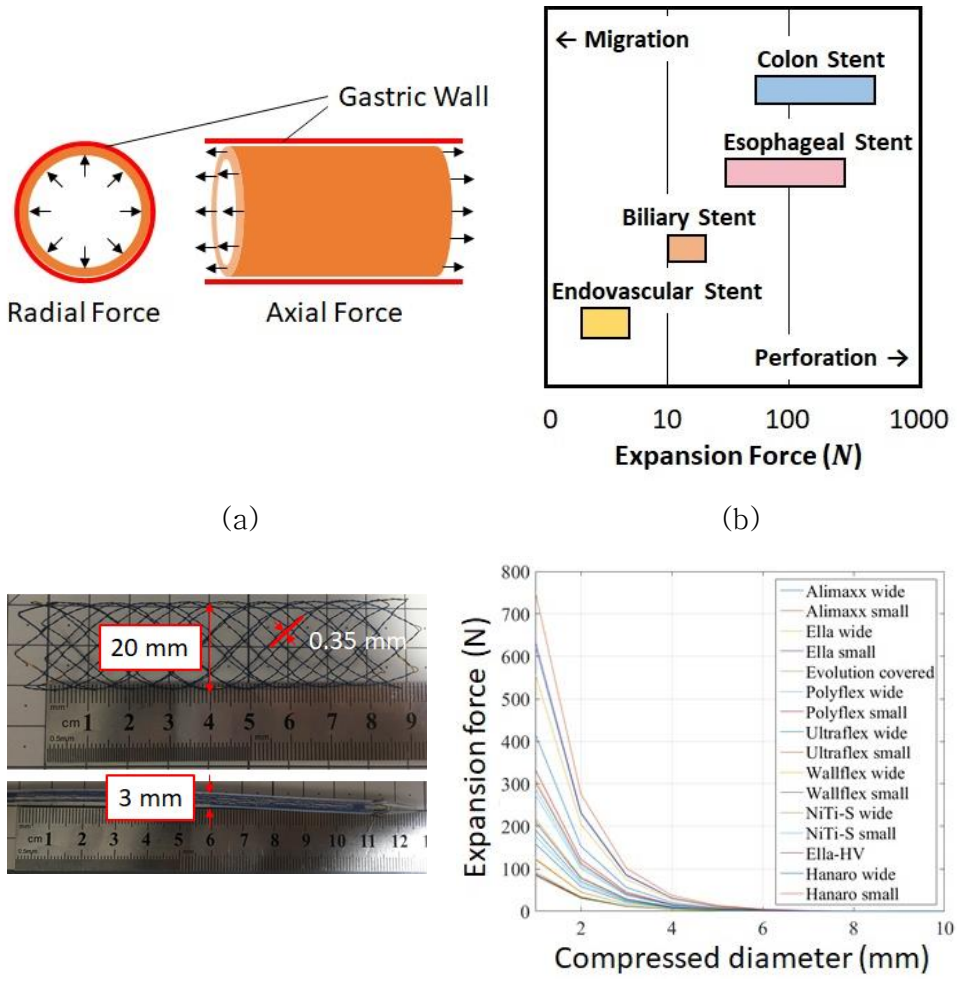


Figure 3.8: Form factor limitation related to SEMS.

(a) Design parameter of SEMS

(b) Expansion force of various stents

(c) GI stent sample (upper:original shape, lower:compressed in stent introducer) (d) Expansion force of esophageal-duodenal stents by the compressed diameter change [88]

### 3.2.3 Structure Design based on Required Configurations

In this study, the steerable catheter was designed in terms of a soft manipulator to be a guiding overtube which can deliver the conventional stent introducers or other devices through the inner lumen. Delivering the various treating devices through the continuum structure means that the treating options in a non-invasive manner can be expanded. The desirable bending curvatures of a steerable joint had been considered on the basis of knowledge for the organ curvatures including the sections from an esophageal-gastric junction to a duodenal bulb and from a duodenal bulb to a proximal jejunum. As illustrated in the Figure 3.9, there are three types of curvature and length to be overcome during the GI interventional procedure. The first anatomical tortuosity exists as a virtual path along the stomach wall. Stomach wall is slightly inflated by the gas. Tension on the wall surface can be replaced as compressed spring, therefore, the stomach wall will be in the state of relatively stiff. The tip of catheters or guidewires should be passively bent at the stomach wall. The first curve forms with approximately $25 - 50\,\mathrm{mm}$ ($R_1$) in a radius of curvature. The second anatomical tortuosity starts from the duodenal bulb to proximal jejunum with approximately $80 - 90\,\mathrm{mm}$ ($R_2$) in a radius of curvature. The third anatomical tortuosity exists in the proximal jejunum in highly curved shape with approximately $5 - 10\,\mathrm{mm}$ ($R_3$) in a radius of curvature. Strictly, the radii of curvature of these portion in GI tract vary in the patient to patient, therefore, the steerable catheter should have a steering curvature which can cover the broad range during the insertion.

The steering mechanism for the steerable catheter had been selected under the consideration of the limited space in the tubular structure and the motion range. The pull-wire mechanism gives an

advantage in terms of the simplicity and a force transmission for the far side actuation.

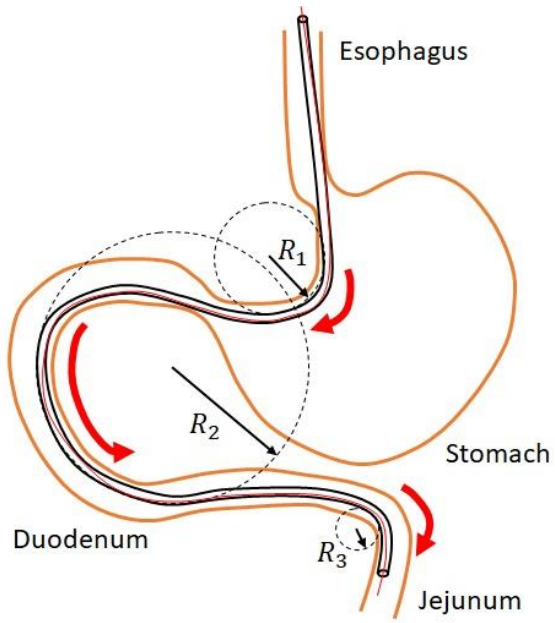


(a)

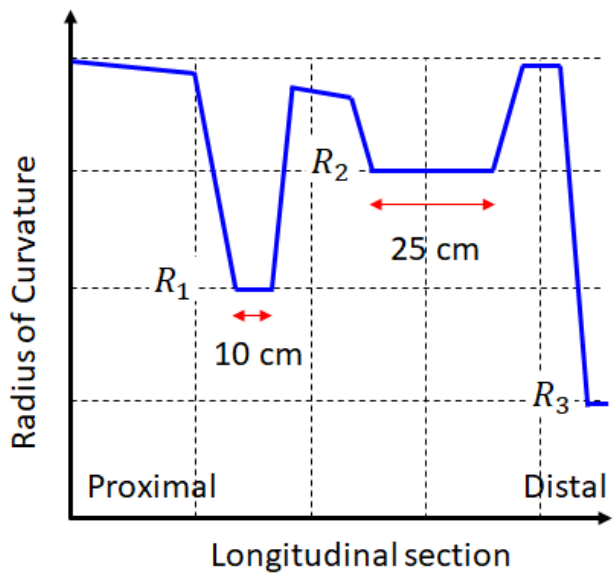


(b)

Figure 3.9: Desired catheter curve configurations.

(a) Curvature in GI tract (b) Steering configurations in GI tract

### 3.2.4 Fabrication of Tubular Joint

At first, the available materials in 3D printing was investigated before the prototyping of a flexible tubular joint. FilaFlex with Shore hardness 56A (Recreus) was chosen for the tubular joint material for the initial prototyping due to the highest flexibility and high adaptability in 3D printing (see Figure 3.10(a)). Filaflex was fabricated by a commercial Fused Deposition Modeling (FDM) type 3D printer (see Figure 3.10(b)).

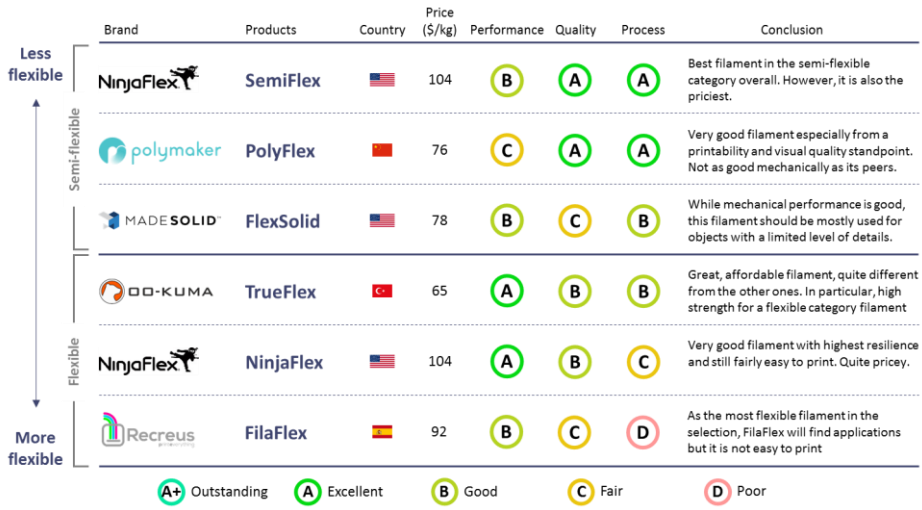


(a)

(b)


(c)

Figure 3.10: 3D printing with flexible material.

(a) Flexible materials in 3D printing (3DPrinterOS)

(b) FDM 3D Printer for flexible tube prototyping (Cubicon 310F)

(c) Flexible TPU-TPE filament (FilaFlex 56A, Recreus)

Figure 3.11 shows a model and the prototyped joint structure. To achieve a bi-directional bending, a tip that can be pulled in two opposing directions is required. This is achieved by using two pull wires connected to a distal tip as shown in Figure 3.12. A steering wire was passed through in the PTFE tube and fixed at the tip structure. By pulling a wire from the proximal side, bending motion of the steering joint occurs (see Figure 3.13(a)). When the bending curvature of the steering joint exceeds the specific value, the flexible tubular structure collapses. This phenomenon is called tube kinking in general (see Figure 3.13(b)).

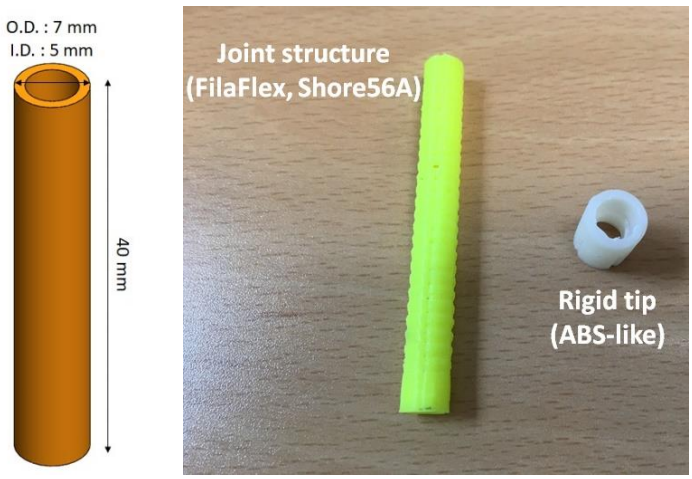


(a) (b)

Figure 3.11: Steerable joint with a steering wire.
(a) Drawing of joint structure (b) Prototyped tubular joint

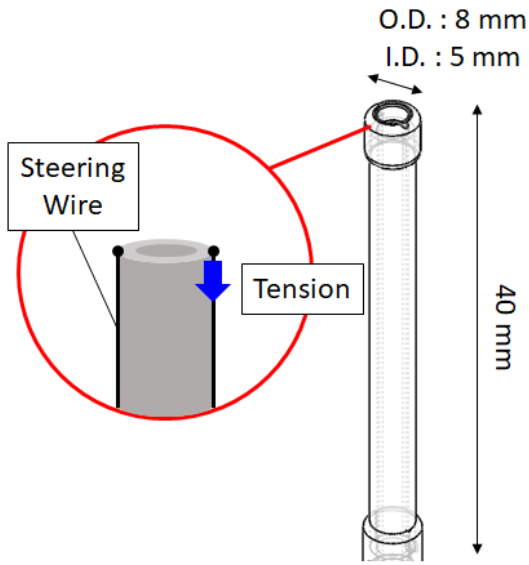


Figure 3.12: Steering mechanism for continuum structure

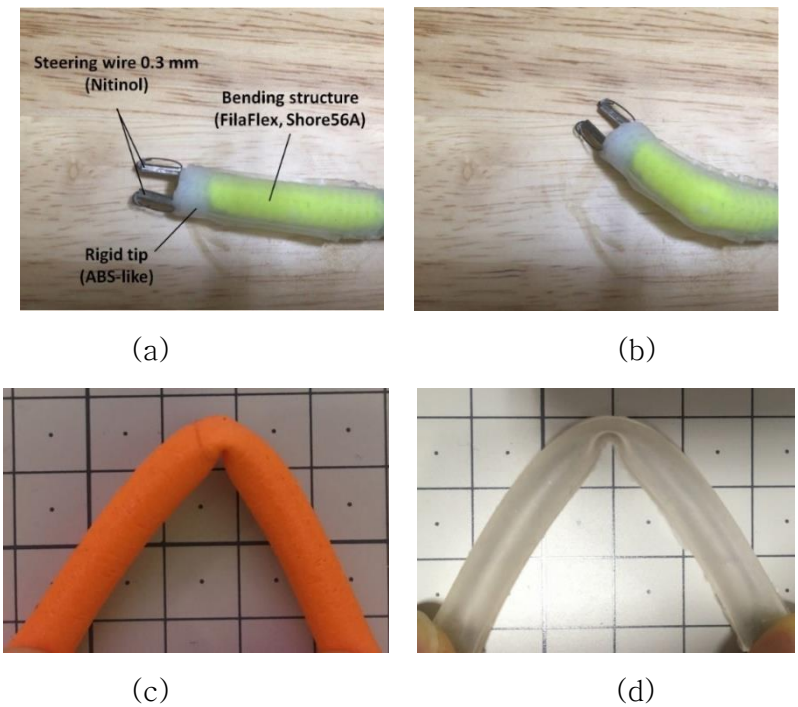


Figure 3.13: Kinking in tubular structure.

(a) Steering setup for prototyped joint

(b) Kinking in the curved joint (c) Filaflex tube kinking

(d) Silicone tube kinking (Shinetsu, KE-1606, Shore 30A)

Under the assumption that the steering joint is flexible and easy to bend, the kinking in a shell structure should be considered in the joint design. The shell structure can be easily kinked by the increased curvature during the bending motion. Because the rubber or the silicone is not a compressible material, kinking is an intrinsic issue. For this reason, most of the medical tubing adapts a braiding wire or a coiling wire reinforcement around or inside the tube. However, the reinforcement of a medical tube with a braided wire or a coiled wire makes hard to fabricate, therefore, the complex design is required.

To verify a shape deformation which is followed by kinking during the flexible tube bending, a computational prediction was performed using a commercial Finite Element Analysis (FEA) software ABAQUS 6.12 (Dassault Systèmes, France). The shell tube model (Diameter: 7 mm, length: 40 mm, thickness: 1 mm) for FEA was designed. To obtain a typical tendency of the flexible tube kinking, the material property of a typical rubber was assigned on the model under the assumption that the hardness and shell thickness of the incompressible material can show a significant tendency of the tube kinking.

Bottom hoop of the tubular structure was pinned in every direction for a mechanical constraint. A uniform force 1 N was exerted on the upper hoop of the shell tube in the simulation. Shear Modulus of the silicone model was calculated as 0.16 MPa from the typical Young's modulus (1 MPa) of the silicone rubber.

Table 3.2: Parameters for a flexible tube buckling analysis

| Hyperelastic Parameters (Neo−Hooke) | | Viscoelastic Parameters (Prony series) | | |
|---|---|---|---|---|
| $C_{10}$ | $D_1$ | $g_i$ | $k_i$ | $\tau_i$ |
| 0.16 | 0 | 0.3 | 0 | 0.1 |

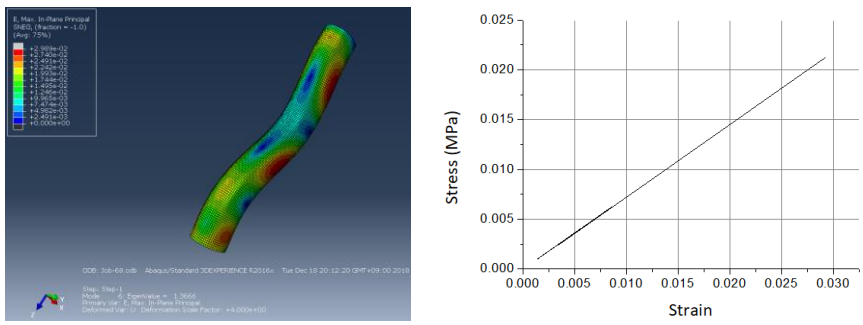


(a) (b)

Figure 3.14: Analytical kink prediction combined with buckling phenomenon. (a) Kink analysis (b) Stress−strain relationship into the horizontal direction by the progress of kink

In the analytical prediction on bending of a flexible tubular structure, relatively large stress into the horizontal direction was observed (see Figure 3.14(a)). The tendency of the Stress−strain curve during the bending shows that the most stressed point in the simulation (red nodes in Figure 3.14(a)) was in a linear relationship with strain (see Figure 3.14(b)). In fact, the volumetric increase into horizontal direction can be observed at the initial stage of bending in both actual situation (see Figure 3.13(c, d)) and the simulation result.

### 3.2.5 Kink Prevention Ring Design for Tubular Joint

To increase a critical buckling load, the flexural rigidity of the structure should be increased. Or, the length of the joint should be decreased from the critical buckling load definition:

$$T_{cr} = \frac{m\pi^2 EI}{L^2} \tag{3.1}$$

where $m$ is the factor accounting for the end conditions, $E$ is the Young's modulus (MPa), $I$ is the moment of inertia ($m^4$), and $L$ is the joint length (mm). That is, tube kinking during the bending in flexible material cannot be completely avoided by the design parameter change of the tubular structure. One of the solutions is reinforced tubing so far, which allows the significant reduction of the bend radius of small silicone tubes [89]. Especially, the lumen size limitation is a critical issue in the medical application that the lumen size should not be decreased as in the interventional devices.

As illustrated in Figure 3.15, tube kinking in a flexible material occurs by the geometrical inconsistency between the elongated tube surface and compressed surface during the bending. The tube kinking

phenomenon is considered as caused by a local column buckling due to the incompressibility of the material during the bending. If the bending motion is induced by the moment equilibrium at both ends, the center of rotation can be always determined as the center point of the compressed surface. The center of rotation is expanded into a horizontal direction by the increased compressive stress. The expanded center of rotation forms a folding line. If the volume change into horizontal direction is partially suppressed, the tube will not be kinked even in the highly curved shape.

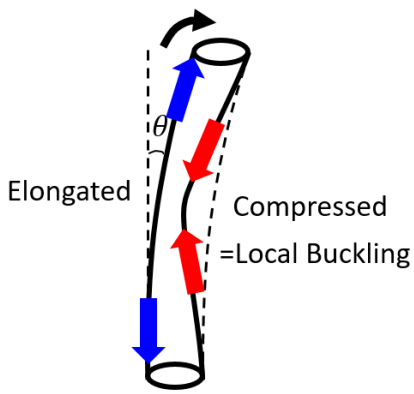


Figure 3.15: Local buckling in flexible tube

To suppress the horizontal deflection, a backbone ring was designed as shown in **Figure 3.16(a)**. The prototype of the designed backbone rings were fabricated by 3D-printing (CONNEX 260, Stratasys) using an ABS-like material Vero-white. The ring-shaped structure has two or four grooves inside and these are the paths for the steering wires. The backbone rings are fixed on the joint structure. As shown in **Figure 3.15(c)**, the maximum deflection can be suppressed by the backbone ring. However, the material is still incompressible, thus, the stretch occurs into axial direction. Putting the backbone rings is similar to the hoops on a barrel. The alignment span and amount of the backbone rings were determined in

trial and errors so far, however, the qualitative prediction of the suppression effect by the backbone ring was achieved by the ring alignment test (see **Figure 3.17**). The span of backbone ring optimization can be achieved through the further study on local column buckling condition during the bending.

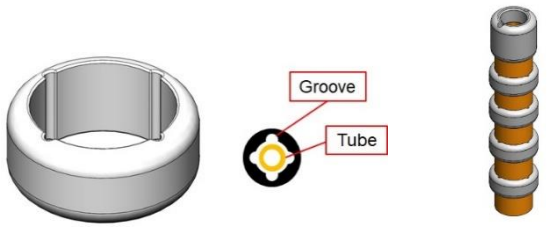


(a) (b)

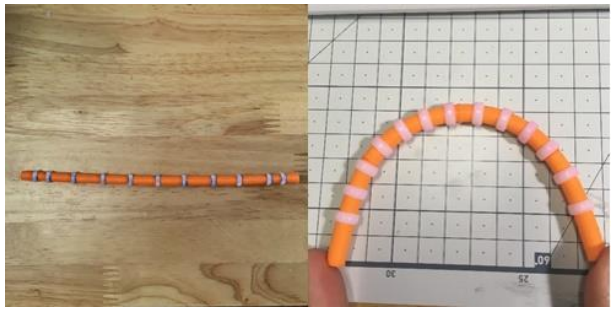

(c)

Figure 3.16: Kink-free design for a flexible tubular structure.
(a) Backbone ring for kink prevention (b) Drawing of reinforced tubular joint with backbone rings (c) Bending test scene

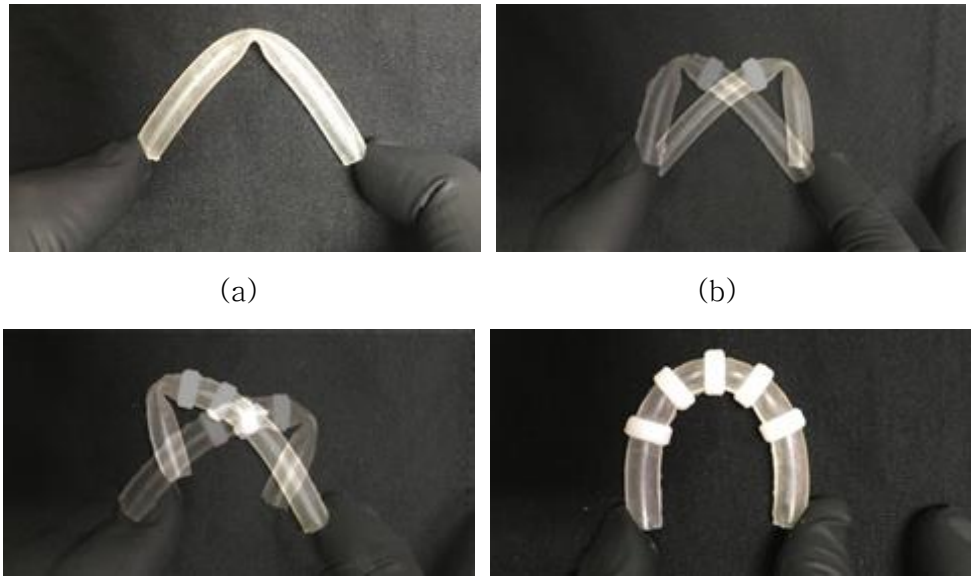

(a) (b)

(c) (d)

Figure 3.17: Ring alignment test.
(a) No ring (b) 1 ring at the center (c) 3 rings (d) 5 rings

A joint tip and a middle connector for the 1st and the 2nd joint were designed. The steering wires are passed through the backbone rings and fixed at the catheter tip with a tied knot (see **Figure 3.18(a)**). To guarantee enough axial stiffness and a durability in the limited channel size, SMA wire with **0.2 mm** in diameter was used (Flexinol, Dynalloy, Inc.). Bending motion of the steerable joint can occur by pulling a wire as illustrated in **Figure 3.18(b)**.

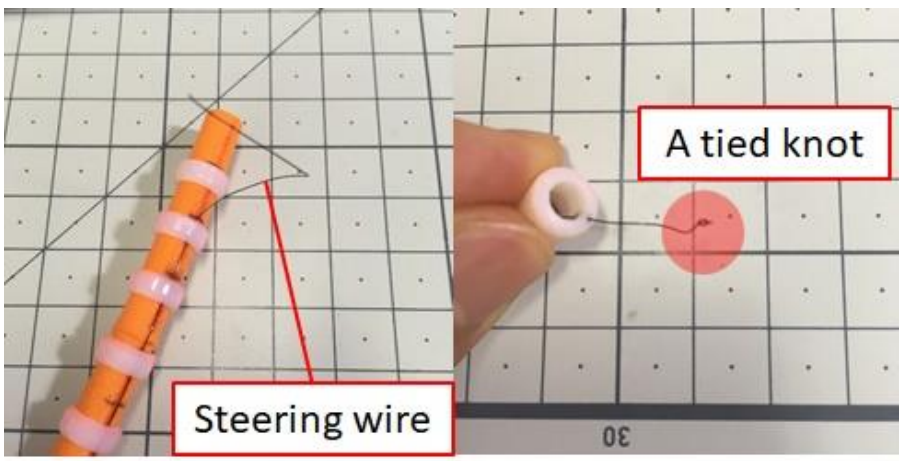


(a)

(b)

Figure 3.18: Steering in tubular joint. (a) Assembly with steering wire (b) Bending motion by pull-wire actuation

### 3.2.6 Steerable Joint for Multiple Curvature

For bi-planar and bi-directional bending, four steering wires should be embedded in the joint structure (see Figure 3.19(a)). The first joint and the second joint are connected by a middle connector. Another two wires are fixed at the middle connector and the alignment is shifted in 90° from the first set of the steering wires (see Figure 3.19(b)). Therefore, the plane which connects two parallel wire paths is perpendicular to another bending motion plane. These two sets of wires form an antagonistic pair. The bending motion of steerable joint assembly follows the bi-planar trajectory. Because the anatomical curves form in a different length and a curvature (and three dimensional), two different motion planes are required. Total assembly of the steerable joint are illustrated in Figure 3.19(c). The components of the steerable joint are shown in Figure 3.20. Figure 3.21 shows the bi-direction bending test scene using the developed steerable joint. The bending angle for each joint was almost 180°.

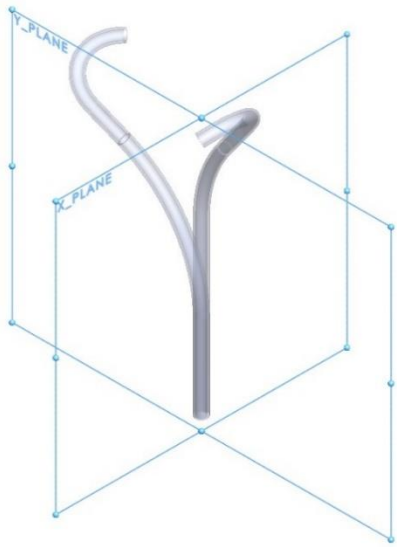


(a)

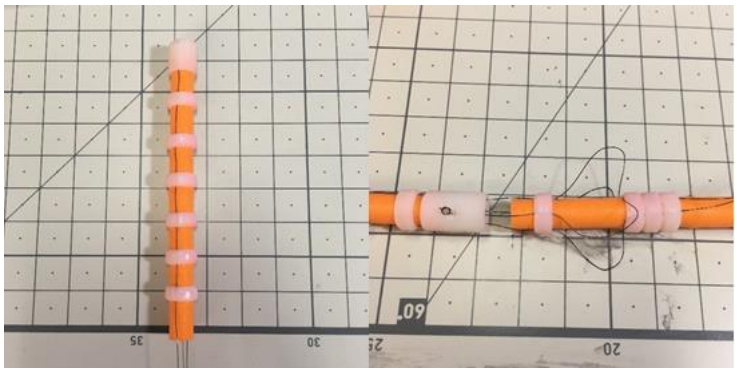

(b)

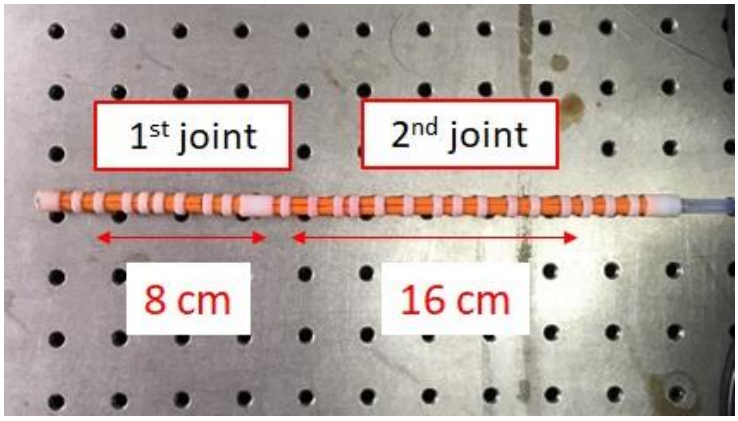


(c)

Figure 3.19: Steering joint assembly. (a) Bending motion plane assignment (b) Assembly process (c) Joint assembly

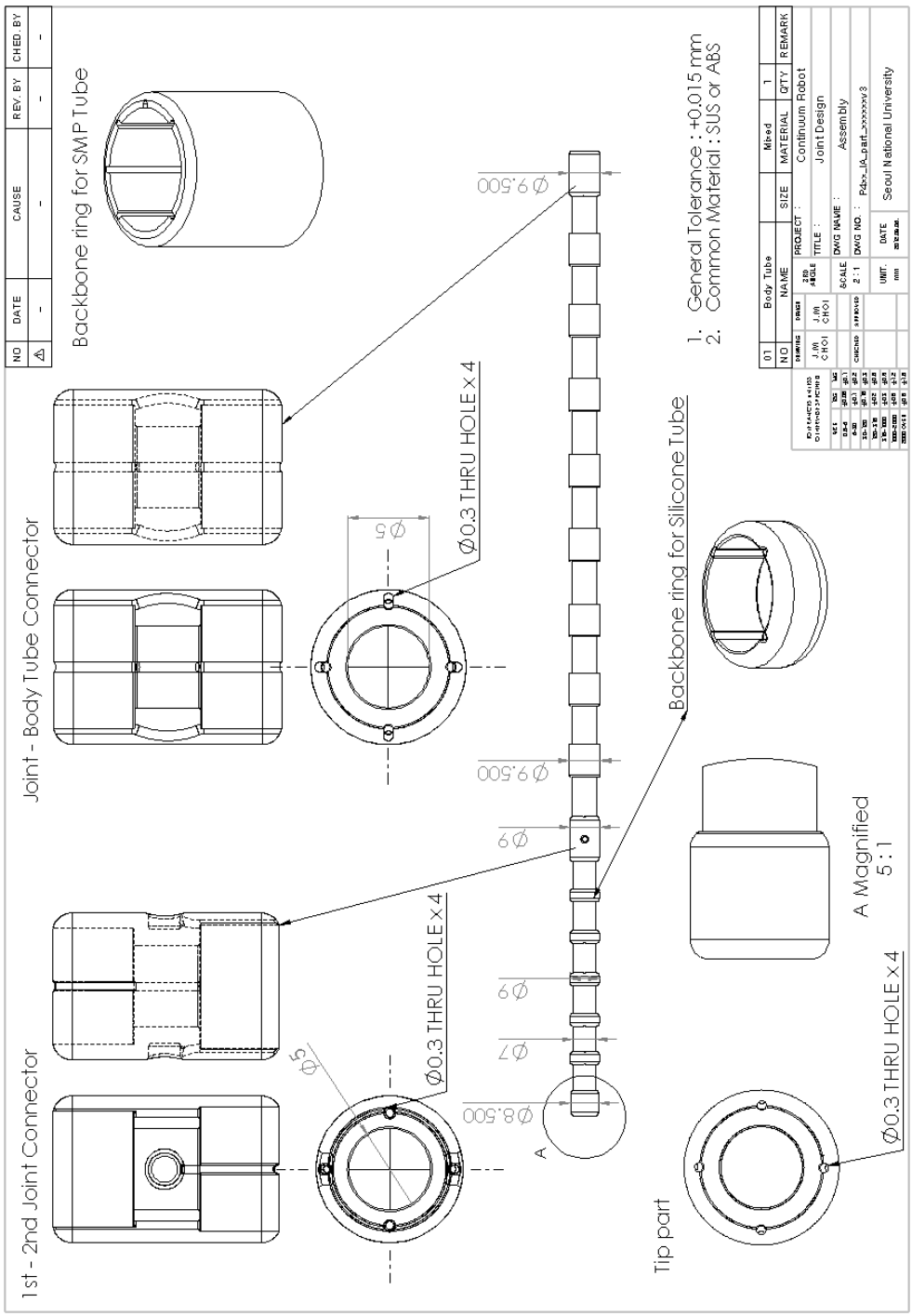


Figure 3.20: Components of the steerable joint

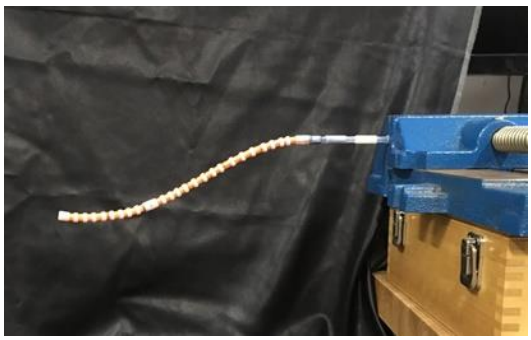

(a)

(b)

(c)

Figure 3.21: Bending test scene of steerable joint.
(a) Bending test setup (b) 2nd joint bending
(c) Bi-direction bending trajectory

In the antagonistic actuation, a tension coupling is a major issue due to the bi-planar bending. Those two sets of the antagonistic pair cannot be decoupled mechanically because they are embedded in the same structure. Pulling a wire which is fixed at the endpoint will apply a bending moment to the first joint, however, the flexible second joint will be deformed even though the material of a middle connector is rigid. Thus, the end position is determined by a combination of the

joint deformation and the joint bending. For this reason, the available trajectory of the steerable joint should be considered in terms of a stiffness difference in the joint materials. Figure 3.23 shows the result from an analytical prediction of the bi-planar joint configurations. The analytical model is constructed based on Euler-Bernoulli beam bending theory. Constitutive equations of the trajectory simulation are described as follows:

$$P = -\frac{2}{x^2 - 2Lx}\theta EI \tag{3.2}$$

$$y = \frac{Pdx^2}{6EI}(3L - x) \tag{3.3}$$

$$x_2(i+1) = x_1 \cos\theta(i) \tag{3.4}$$

where $P$ is the arbitrarily determined lateral component of the tension, $x$ is the longitudinal displacement, $L$ is the joint length, $\theta$ is the deflection angle, $E$ is the Young's modulus, $I$ is the moment of inertia, $y$ is the lateral deflection, and $dx$ is the infinitesimal longitudinal displacement.

Figure 3.22(a, b) show the overall scheme and the result example of the trajectory simulator. The Young's modulus, dimensions (length and diameter), and a desired joint deflection angle of the tube are given as input parameters. The output parameters are entire trajectory, approximated radius of curvature of the deflected joint, and the tip position. Approximated radius of curvature was calculated from the circle that passes through the both ends of the joint after the deformation. In the condition that is given as Table 3.3, the radius of curvature was calculated as 48.93 mm. The body structure was set

to be a rigid shaft.

Table 3.3: Input parameters of trajectory simulator example

| $L_{BODY}$ (mm) | $L_{JOINT}$ (mm) | $E_{JOINT}$ (MPa) | $I_{BODY,JOINT}$ ($mm^4$) | Tension (N) |
|---|---|---|---|---|
| 60 | 40 | 63,547 | 0.0308 | 1 |

Table 3.4 shows the input parameters for the trajectory simulator. The simulation results which are illustrated in Figure 3.23 are based on the extension of the calculation into the three dimensional space with two joint deflection. After the calculation of the second joint trajectory is completed, the first joint trajectory is calculated and the entire points on the first joint trajectory are rotated around the second joint tip position.

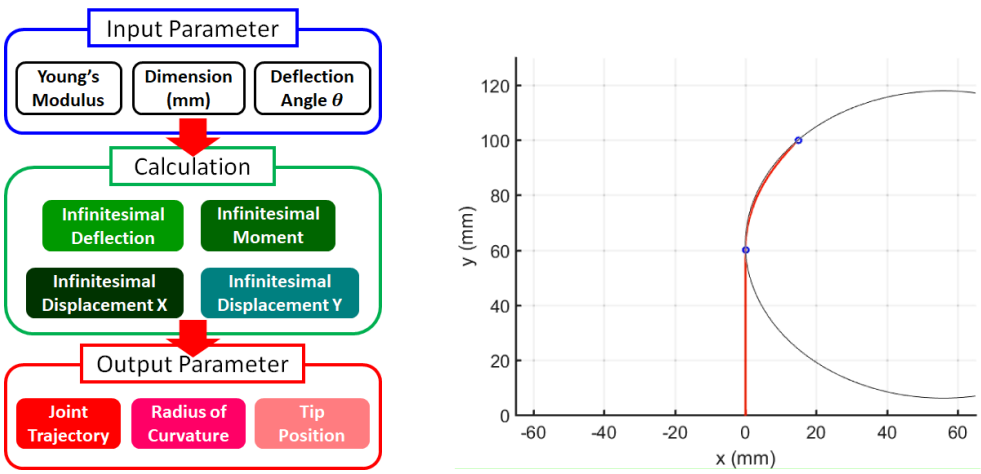


(a) (b)

Figure 3.22: Trajectory simulator of the steerable joint. (a) Structure of trajectory simulator (b) Trajectory and approximated radius of curvature of the joint bending example

Table 3.4: Parameters for trajectory simulation

| $L_{BODY}$ (mm) | $L_{JOINT}$ (mm) | $E_{BODY,JOINT}$ (MPa) | $I_{BODY,JOINT}$ ($mm^4$) | Tension (N) |
|---|---|---|---|---|
| 200 | 80 | 3 | 87.18 | 0.5 – 1 |

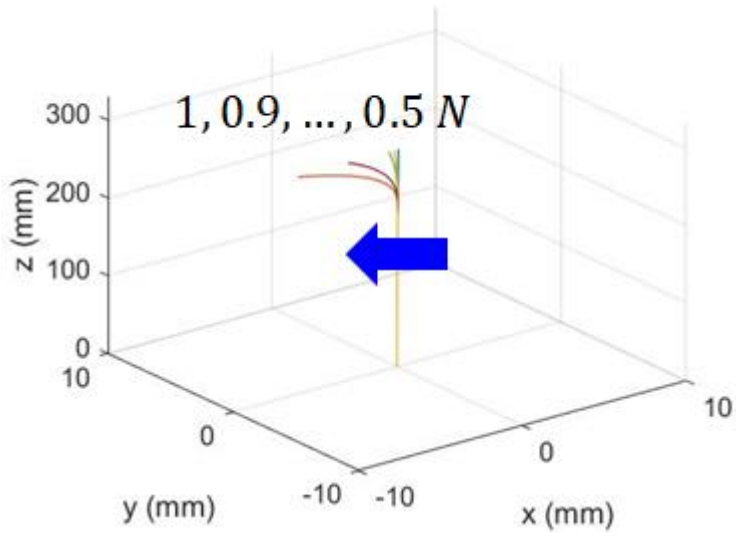


(a)

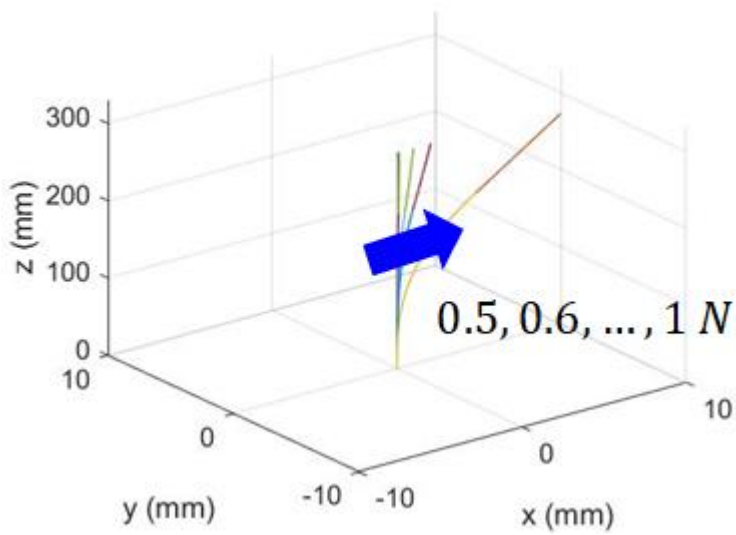


(b)

Figure 3.23: Trajectory analysis in two joint. (a) Bending configurations of 1st joint (b) Bending configurations of 2nd joint

### 3.2.7 Body Structure of Steerable Catheter

To realize the steerable joint as an interventional device, a tubular body structure should be designed under the consideration of medical use and the anatomical constraints. From the aforementioned design constraint, a total length of the continuum structure should be 120 cm – 140 cm to reach a distal jejunum. Besides the tube length, the diameter was set to 7.5 mm. This is because of the backbone rings on the joint sections. The overall scheme of the steerable catheter is illustrated in Figure 3.24. To make a simple and a stiff structure, a 1,200 mm long PTFE tube for GI sheath was (S&G Biotech, Inc.) connected to the steerable joints assembly. The GI sheath had been developed and established its usefulness in the interventional radiology over the decade [22, 24].

On the other hands, the kink in the PTFE tube is also an issue when the tube bends along the GI tract. Once the kink occurs in PTFE tube, the shape is not recoverable due to the plastic deformation. To avoid a kink in a PTFE tube, the backbone rings were designed and fabricated by a 3D printer using an ABS-like material. A backbone ring (see Figure 3.25(a)) consists of two half-cylinder structure for the easy assembly process. The half-cylinders are aligned in every 10 mm into the longitudinal axis and bonded using a medical adhesive (4C30, Permabond®), and a Polyolefin Primer (POP, Permabond®, see Figure 3.25(b)). POP has been developed for surface treatment of polyolefins, PTFE and silicones prior to bonding with the cyanoacrylate adhesives (see Table 3.5).

Table 3.5: Physical properties of POP [90]

| | |
|---|---|
| Appearance | Colorless Liquid |
| Viscosity at 25℃ | 0.6 mPa. s (cP) |
| Specific Gravity | 0.7 |
| Boiling Point | 98℃ |
| Flash Point | −4℃ |
| Evaporation Rate | 2.8 (butyl acetate = 1) |
| Drying time at 23℃ | 30 sec. |
| UV−fluorescence | Yes |

Due to their low surface energy, plastics such as PTFE, Polypropylene (PP), Polyethylene (PE) and Silicones are difficult to bond without special surface treatment. After the treatment with POP, durable bonds stronger than the substrate material can be achieved [90]. As shown in **Figure 3.25(c)**, the back bone ring could resist kink at the acute curve configuration.

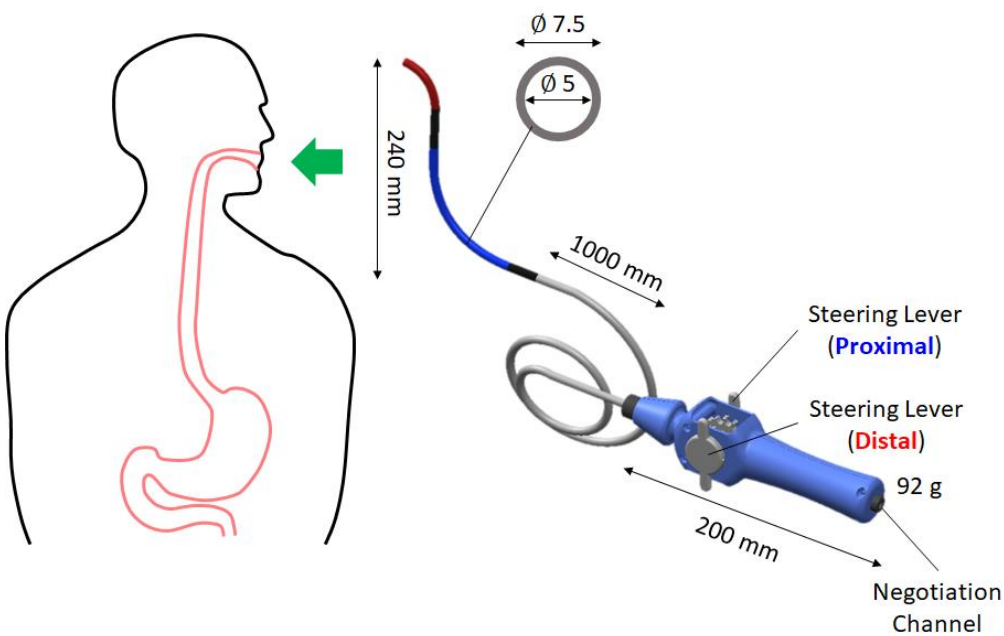


Figure 3.24: Overall scheme of the steerable catheter


(a) (b)

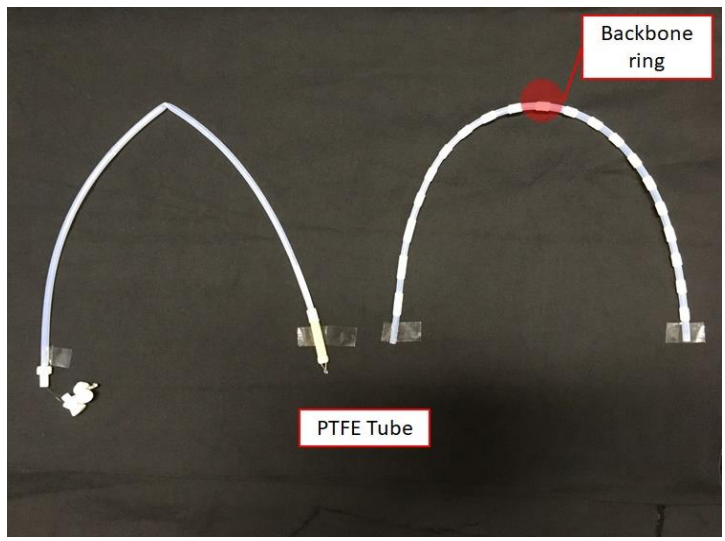


(c)

Figure 3.25: Kink-free design for the body tube. (a) Backbone rings (Left: 10 mm, Right: 20 mm in length) (b) Medical adhesive and POP primer (c) Comparison between a body tube with (Right) and without (Left) the backbone rings

### 3.2.8 Steering Wire Path Design

In overall, the wire path should be formed inside the joint connectors because the bending moment at the distal tip on each joint section should be generated by an applied tension from the proximal side. At the initial state, a wire tension is not involved in generating bending moment of each joint. To make a conversion from an axial load to the bending moment, the joint structure should be pre-curved.

Otherwise, in the straight shape, the buckling should occur by the pull-wire tension. Once the bending motion is initiated by the buckling, the bending moment by the pull-wire actuation after the buckling will dramatically increase. Therefore, the required steering force will decrease to bend the same amount of angles during the motion. Furthermore, due to the condition for column buckling of the joint structure, the joint connector should be rigid and completely fixed. The alignment of the steering wire path does not require a high level of accuracy, because when the wires are pulled, the wires tend to bite into the grooves in the backbone rings. Compared to the backbone rings, the joint connectors have a sophisticated structure inside as illustrated in **Figure 3.26**. The wire path follows the continuous trajectory from the distal to the proximal side.

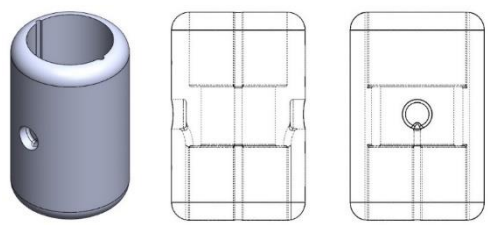

(a)

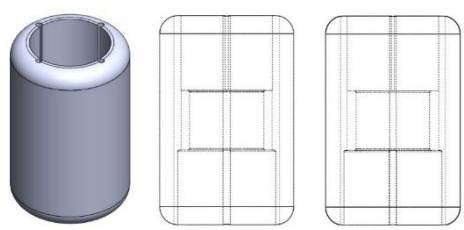

(b)

Figure 3.26: Tendon path design in joint connectors (Left: Isometric view, Center: front view, Right: Side view). (a) $1^{st}$ – $2^{nd}$ joint connector (hidden lines visible) (b) $2^{nd}$ joint – body tube connector (hidden lines visible)

## 3.3 Integration of Steerable Joint

### 3.3.1 Steering Handle Design

To improve the usability of the steerable joint, a steering handle was designed. The handle was designed under the considerations that the simultaneous use with other interventional devices in an actual procedure. To consider the steerable catheter as a GI interventional device, the existence of the through hole from the proximal to the distal is required because the guidewires, catheters, and stent introducers should be passed through the catheter lumen. Sometimes, the holes in the catheters delivery the contrast medium or the drugs.

First, the steering wires in the antagonistic pair were connected to the originally designed tendon connector (see Figure 3.27(b)). A wire with ball forms in Pearl-necklace structure. The balls are connected by a slightly flexible wire, therefore, the distance between each ball is variable with a small elongation (longitudinal elongation was $0.1 - 0.5\,mm$ in tension $1 - 2\,N$). This feature facilitates the connecting process in the connector assembly for tendon actuation. The gear tooth profile was designed to fix the balls in the wires as shown in Figure 3.27(c). To make an antagonistic pair in two wires, slack in the neutral position of the steerable joint should be prevented. Thus, the pre-tension (approximately $1\,N$) was applied in the process of assembly.

Second, the steering handle was fabricated by a 3D printer (CONNEX 260, Stratasys) with an ABS-like material Vero-white. The outer shell was designed as $2\,mm$ in thickness (see Figure 3.28 (b)). Several components including a middle tube, adaptors, and a body tube connector were designed and prototyped. In the assembly process, the four steering wires are easily aligned by passing through the body tube connector holes (see Figure 3.29(a, b)). Several

components are fixed by M3 and M4 bolts.

Finally, the penetration test was done as illustrated in **Figure 3.30(d)**. The **120 cm** long stent introducer was completely passed through the handle and the steerable catheter.

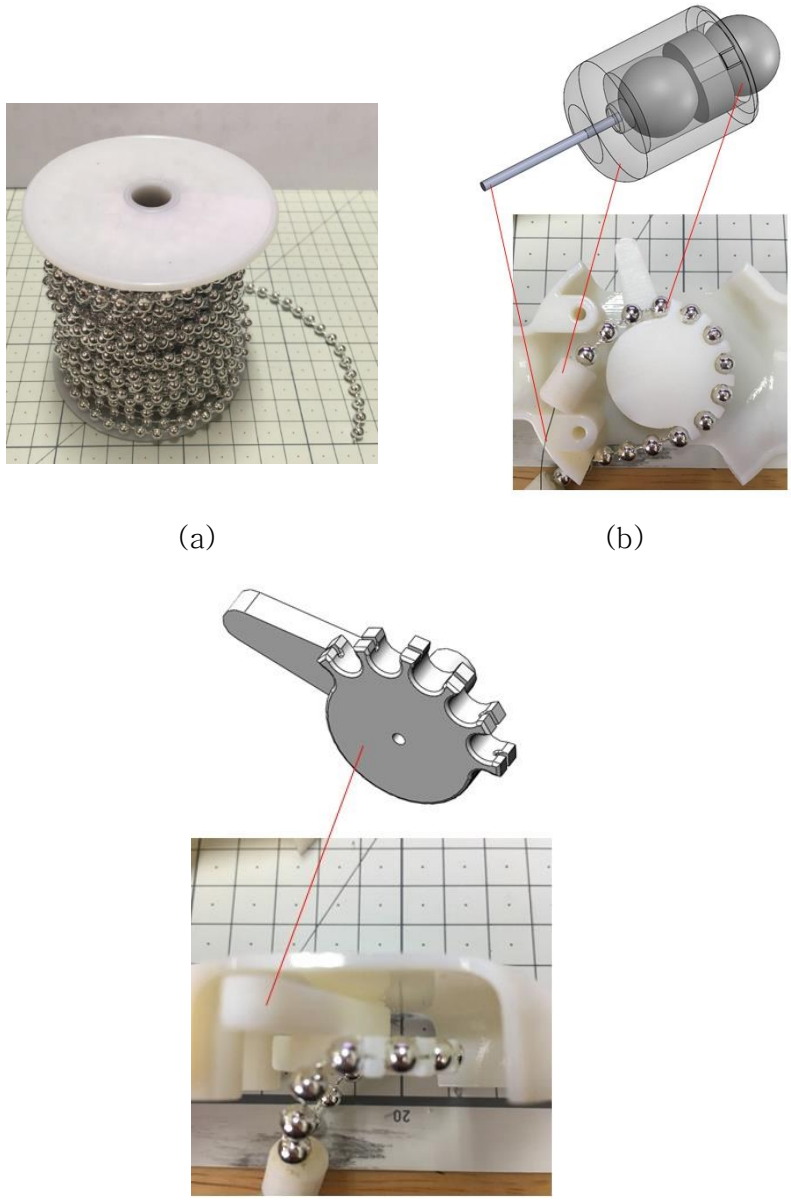

(a) (b)

(c)

Figure 3.27: Transmission components. (a) Wire with ball (b) Tendon connector (c) Rotating gear with lever (d) Adaptor for antagonistic alignment for steering wires

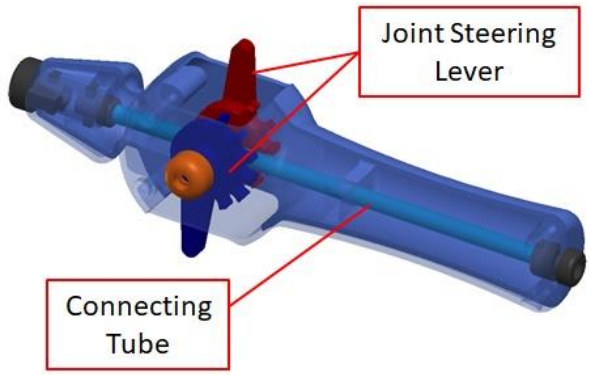


(a)

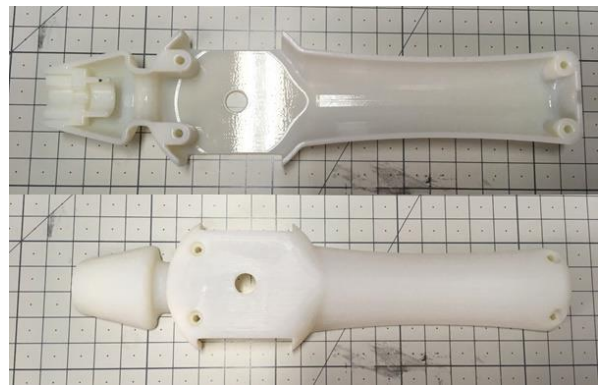

(b)

(c)

Figure 3.28: Steering handle for steerable catheter.
(a) Handle design for steerable catheter (b) Outer shell for steering handle (c) Handle prototype for steerable catheter

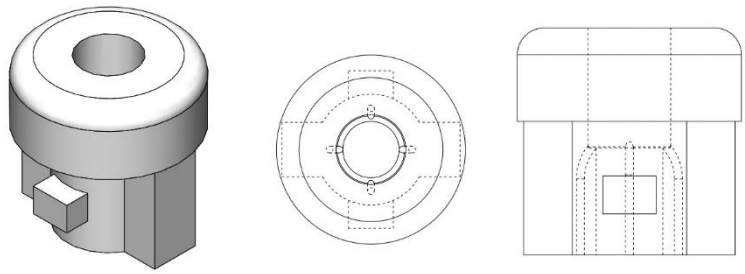

(a)

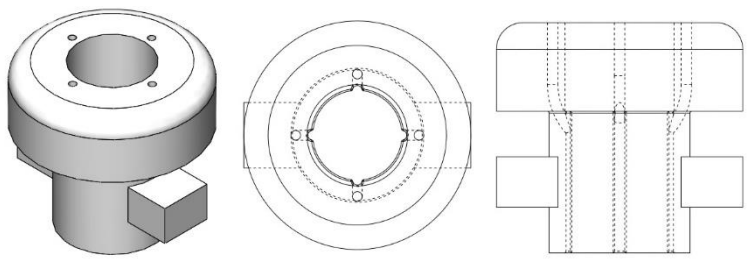

(b)

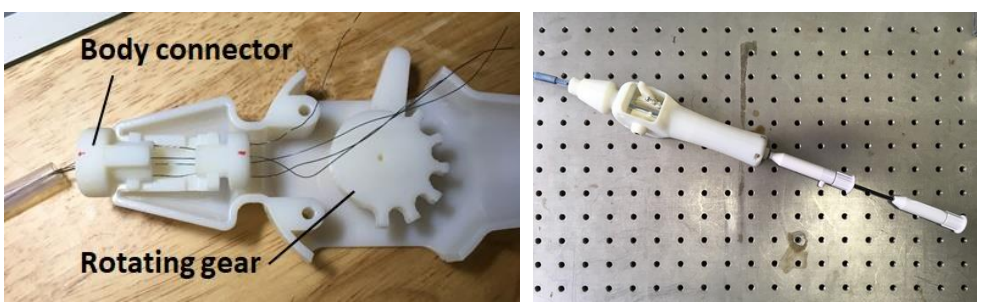


(c) (d)

Figure 3.29: Handle components and assembly process. (a) Body tube connector design (Left: Isometric view, Center: Top view, Right: Front view) (b) Middle connector design (Left: Isometric view, Center: Top view, Right: Front view) (c) Assembly process of the body tube connector and handle structure (d) Penetration test using stent introducer

The complete assembly of the steerable catheter was fabricated as shown in Figure 3.30. A control gear contains fixed tendon wires and it shows an antagonistic motion in the steerable catheter. Figure 3.31 shows schematic of steerable catheter assembly.

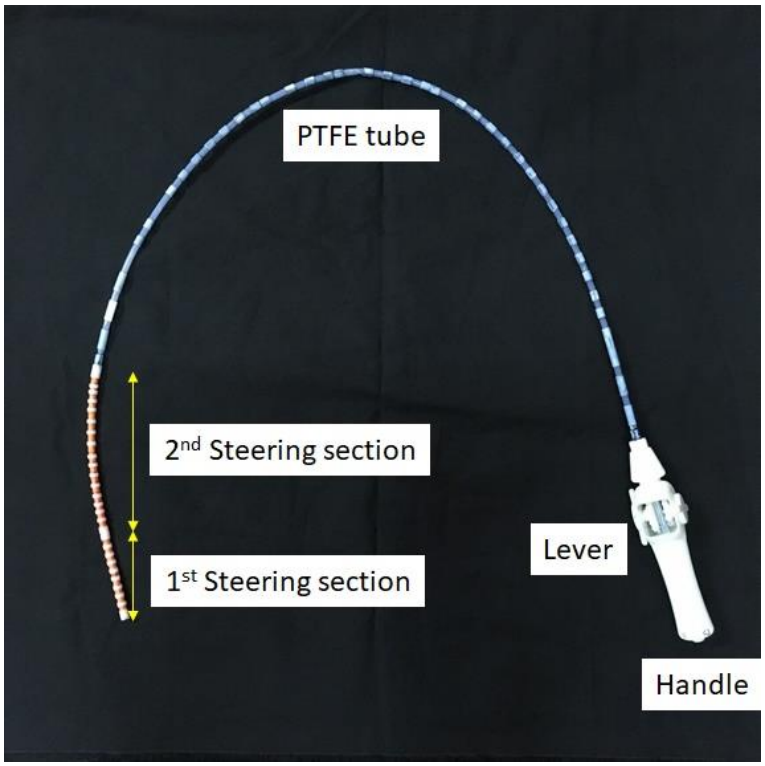


Figure 3.30: Prototype of steerable catheter with handle

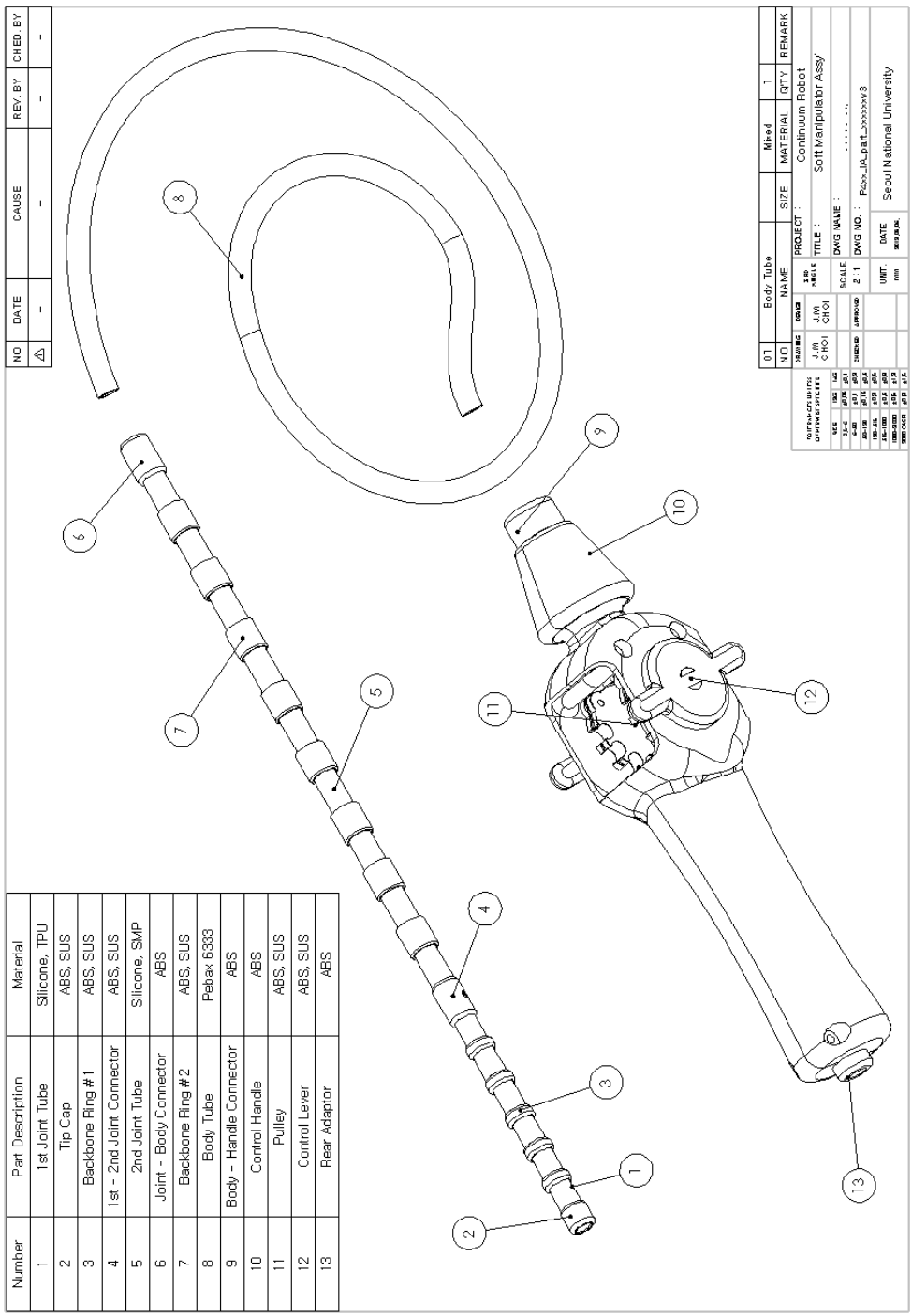


Figure 3.31: Schematic of steerable catheter assembly

To obtain an approximation of the bending stiffness when using the developed steerable catheter, the payload test was conducted. A push–pull gauge (DTG–20, DigiTech, Japan) was used to measure the pulling force of the steering wires (see Figure 3.32). The distal tip of the manipulator was weighted with the weights $10, 20, 30, 40,$ and $50\,g$ to produce a vertical deflection. As a result, the bending stiffness of the steerable catheter with/without steering were $2{,}993\,Nmm^2$ and $623\,Nmm^2$ respectively. With steering, the wire tension did not exceed $5\,N$ for a safety issue during the test.


(a) (b)

Figure 3.32: Evaluation of bending stiffness in steerable catheter.
(a) Push–pull gauge DTG–20 (b) Payload test scene

The conformability space in stenting with the developed soft manipulator as an overtube is illustrated in Figure 3.33. Stenting with a soft guidewire and the overtube shows significantly low conformability as 0.36. In fact, the overtube cannot maintain the curved shape when the stent introducer is passing. Consequently, a shape–locking function without additional tension is required for the stent placement in the GI tract. In other words, the variable stiffness characteristic is required for the safe GI stent placement.

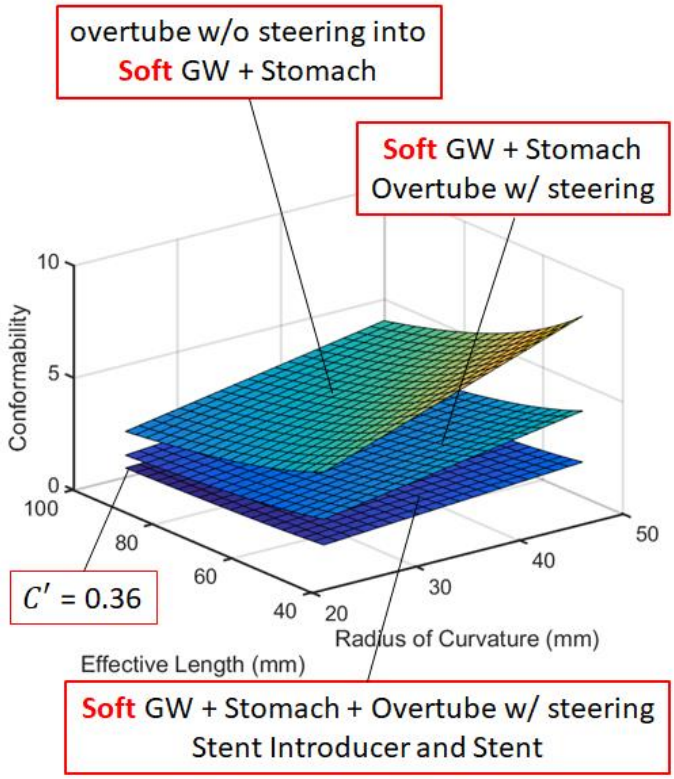


Figure 3.33: Conformability space in stenting with developed steerable catheter as overtube

# Chapter 4. Variable Stiffness for Steerable Catheter

## 4.1 Stiffness Control Method

Various stiffness methods have been reported in the literature and a number of classifications of such methods have been reported. In a soft structure, there have been several methods for stiffness control. However, the stiffness control in medical devices is limited in terms of safety, a material, and a form factor constraint by the organ size. For this reason, there are two possible types of variable stiffness methods are considered for medical use: 1)Structure-based methods, 2)Phase transition-based methods.

### 4.1.1 Structure-based Variable Stiffness Methods

Variable stiffness can be achieved in soft structure mechanically by structural designs. Shiva et al. [91] designed a continuum silicon-based manipulator with controllable stiffness realized by antagonistic actuation of pneumatic actuation and tendon (Figure 4.1(a)). The antagonistic actuation configuration increased the manipulator's load bearing capabilities. Except for stiffness modulation, the pneumatic and tendon-based actuation method endows the soft structure with the ability to control its pose. Another example of variable stiffness soft structures using antagonistic actuation is by combination of contracting and extending fluidic actuators as in Figure 4.1(b) [92]. By driving the contracting and extending actuators concurrently, the combined mechanism can achieve stiffening effect. A variable stiffness continuum manipulator with active-braid inspired by muscular hydrostats is proposed [93]. In this research, the stiffness of the manipulator could be changed when the radial actuators and the longitudinal tendons were actuated in antagonistic manner.

Segment locking is also a common approach for variable stiffness structures especially for flexible manipulators in medical applications such as MIS. By using central or multiple tensioning cables to lock the segments, stiffness change can be achieved [94, 95]. The tension in the cables leads to friction between segments and causes stiffness variation of the manipulator to adapt to different application scenarios. Except for controlling the tension of cables, segment locking of the manipulator could also be obtained via locking joints in the mechanism as shown in **Figure 4.1 (c)** [94]. The unique geometry in the segment design facilitates that the segments of the manipulator can be mechanically locked and stiffened by the applied air pressure. These working principles showed feasibility, however, the design principles of the manipulators that are based on the structure–based principles have either limited stiffness–changing properties or too complex and bulky bodies to be miniaturized.

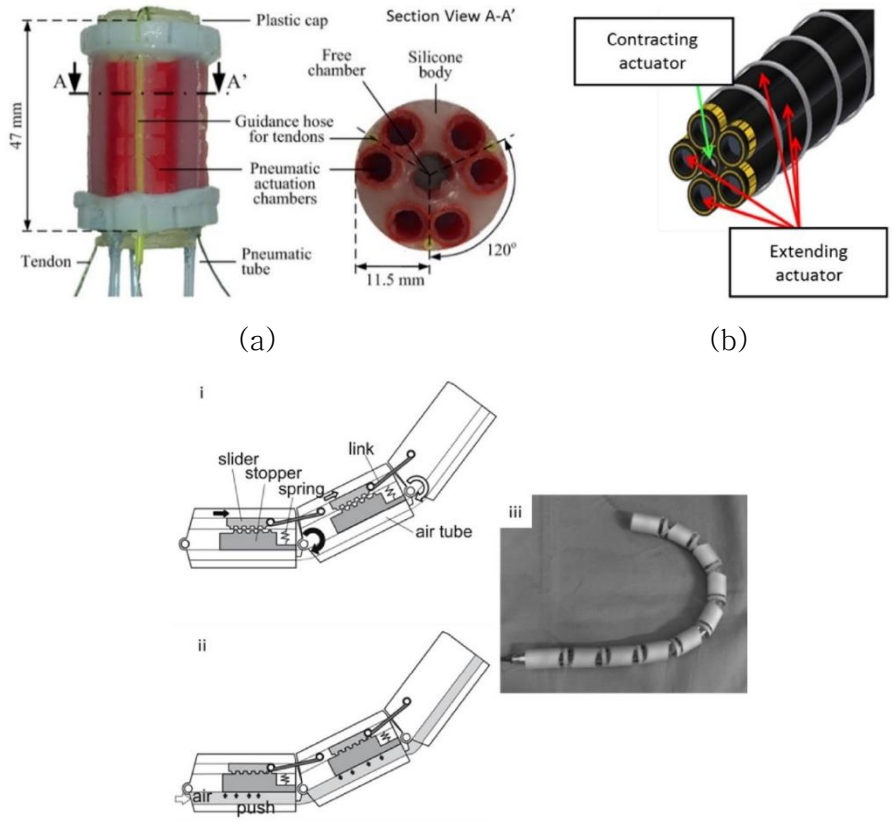


Figure 4.1: Structure-based variable stiffness methods. (a) Pneumatically actuated soft manipulator using tendons for stiffening [91] (b) Configuration of combined contracting and expanding fluidic actuators to achieve variable stiffness [92] (c) Flexible endoscopic [94]

### 4.1.2 Phase Transition-based Variable Stiffness Methods

Among the stiffness control strategies for soft manipualtors, phase transition-based methods are widely used. Mechanical properties of thermoplastics show variation during thermal transitions including glass transition temperature $T_g$ and melting temperature $T_m$. The elastic modulus of thermoplastics changes dramatically when heated to around its glass transition temperature. Similar phenomenon is also found in shape memory polymer (SMP). The change of SMP's Young's modulus with temperature change is drastic (see Figure 4.2(a)) [97]. SMP is at glassy phase with high elastic modulus below $T_g$. Above $T_g$, SMP transforms to rubbery phase that can be easily deformed. The Young's modulus ratio between glassy and rubbery states of SMP can be as high as hundreds.

Yang et al. reported variable stiffness ball joints that its stiffness was tuned by thermal stimulus and cascaded a number of these joints to form a hyper-redundant robotic arm [98]. The ball joint is made of two materials: ABS and SMP. When heated above $T_g$, the joint exhibits low resistive torque and can move freely because SMP is at rubbery state. When the SMP cools down to below $T_g$, the SMP structure is at glassy state and the joint's resistive torque increases dramatically. In their further study, variable stiffness soft fingers were developed using SMP for stiffness control and bending shape control [99, 100]. They attempted the SMP materials with an integrated pin heaters and with conductive elastomers. The main novelty of using conductive elastomers was that they could not only provide Joule heating for the SMP part but also enable the finger joint with position feedback capability (see Figure 4.2(b)) [100]. The three bending joints are realized by heating SMP material above $T_g$

at the joint regions. As a result, the finger would bend at low stiffness joints when pressurized air flows in the air chamber. Except for soft pneumatic fingers, SMP has also been applied in tendon-driven under-actuated robotic origami structure for stiffness control [101].

Thermoplastics have been used for developing multifunctional robotic fibers to mimic the capabilities of human muscle fibers in a research conducted by Yuen et al. [102]. In their study, the glass transition in PLA ($T_g$ = 55 – 65 ℃) or ABS ($T_g$ = 105 ℃) was tapped for stiffness control and thus the long-time lifting of a soft robotic arm was accomplished without continuous energy input. Except for thermoplastics and SMPs, SMAs also exhibit modulus variation when transforming from Austenite to Martensite through variation of thermal energy. The phase transition of SMA is presented in **Figure 4.2(c)** [103]. However, the range of the elastic modulus change of SMAs is relative small (< 4x) and its absolute modulus is still high (**83 GPa** as Austenite [104]), which limits SMAs' application for stiffness control in soft structures.

On the other hands, low melting point alloys (LMPAs) has been emerging for variable stiffness applications recently since a large stiffness range can be achieved when LMPAs changing between solid and liquid states. Schubert et al. developed a variable stiffness composite with LMPA. The melting temperature of LMPA is approximately **47** ℃. The small-sized channels in LMPA were covered with Polydimethylsiloxane [105]. The composite demonstrated stiffness change of **25** folds from **40 – 1.5 MPa** when LMPA was heated from solid state to liquid state. Moreover, the composite possessed inherent strain sensing capability by monitoring its resistance change since LMPAs were also electrical conductors. Using this composite, variable stiffness actuators have been

developed by using dielectric elastomers actuators (DEA) and a LMPA substrate as stiffness tuning module as shown in **Figure 4.2(d)** [106].

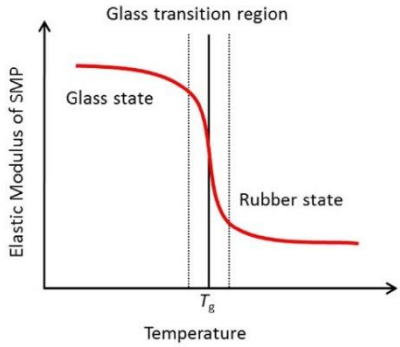


(a)

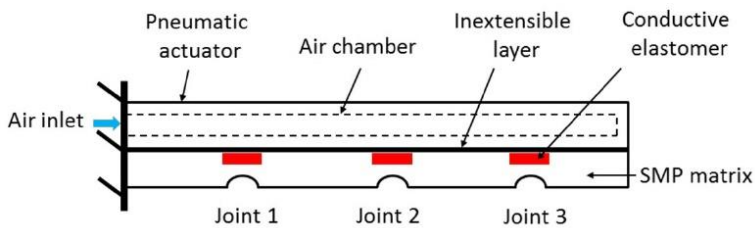


(b)

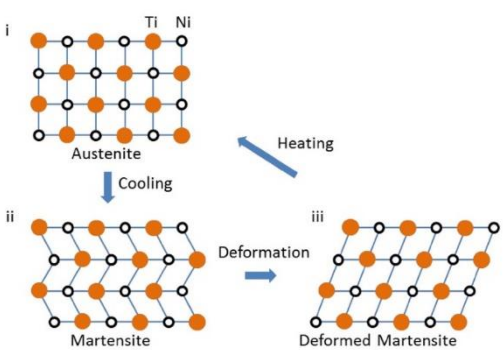


(c)

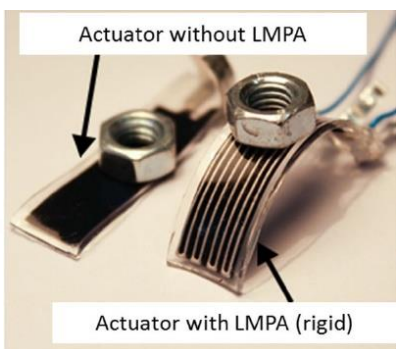


(d)

Figure 4.2: Phase transition-based variable stiffness methods. (a) SMP's elastic modulus change with temperature [97] (b) Variable stiffness soft finger based on SMP and conductive elastomer [100] (c) Phase transition in Ni-Ti SMA [103] (d) LMPA applied in DEA-based soft actuator for stiffness modulation [106]

## 4.2 Shape Memory Polymer

### 4.2.1 Backgrounds

SMPs can retain two or sometimes three shapes, and the transition between those is induced by temperature. In addition to temperature change, the shape change of SMPs can also be triggered by an electric or magnetic field, light or solution. As well as polymers in general, SMPs also cover a wide property-range from stable to biodegradable, from soft to hard, and from elastic to rigid, depending on the structural units that constitute the SMP. SMPs include thermoplastic and thermoset (covalently cross-linked) polymeric materials. SMPs are known to be able to store up to three different shapes in memory. SMPs have demonstrated recoverable strains of above 800 % [107]. SMPs are considered that are suitable for medical use due to the broad elastic range, bio-compatibility, and a shape-locking capability with no energy input.

### 4.2.2 Fabrication of SMP Structure

As described previously, the SMP has a frozen strain characteristic which makes the structure be deformed by the external load and shape-locked in the room temperature (Figure 4.3(a)). A temporary shape can be maintained unless the structure is heated. Recently, the fabrication of the SMP is available due to the advance in 3D-printing technology. There are several material sources such as a pellet for extrusion process and molding, or filament (SMP Technologies and Kyoraku, Japan) for 3D printing (Figure 4.3(b)). $T_m$ of the SMP filament is around 210 ℃. Therefore, the printing temperature was set to be 220 ℃, and the travel speed was 80 mm/s.

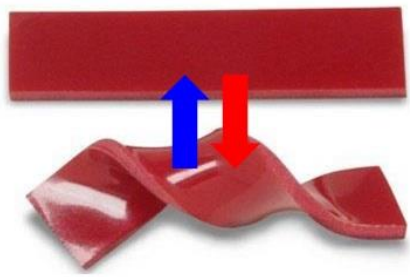

(a)

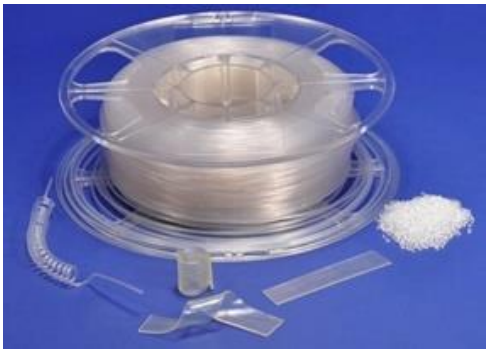

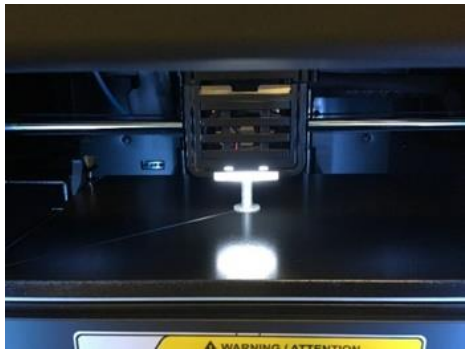

(b) (c)

Figure 4.3: Shape Memory Polymer. (a) Frozen strain in SMP (Advanced Polymer Research lab.) (b) SMP filaments and pellets (SMP Technologies, Inc.) (c) 3D-printing process of SMP

The designed sample structure (**Figure 4.4(a)**) was printed by a typical FDM 3D printer. The prototyped structure showed a fine shape accuracy as illustrated in **Figure 4.4(b)**. In addition, the tubular structure was fabricated using the SMP filament as shown in **Figure 4.4(c)**. The tube layer was overlapped by **30 %**, leakage was not observed under the water flow condition. The feasibility test of the SMP tube was conducted. Before the test, the SMP tube was heated and cooled down in a curved shape. The bending radius of curvature was **57 mm**. The stent introducer could path through the inner lumen of the curved SMP tube, and the curvature was maintained (**Figure 4.5**).

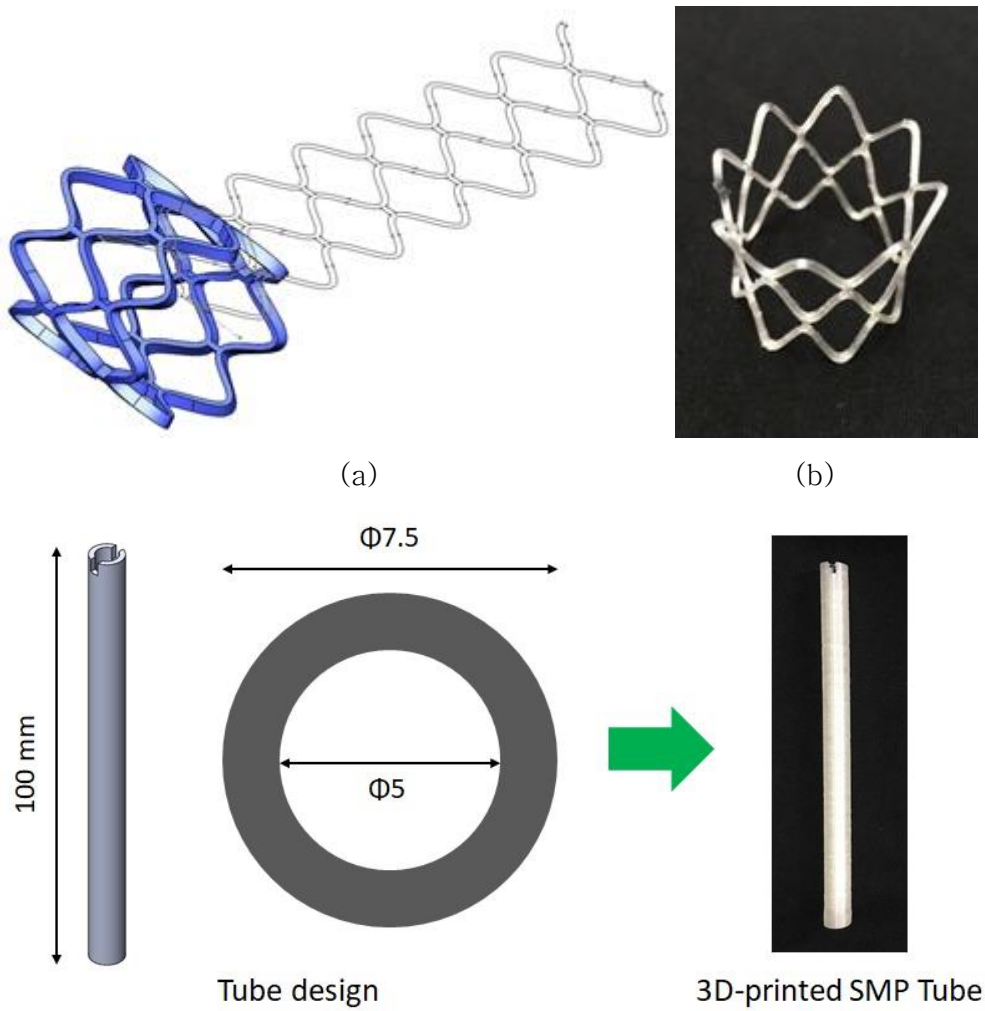


Figure 4.4: Stent structure. (a) SMP structure design
(b) 3D-printed SMP structure (c) Tube design and SMP tube

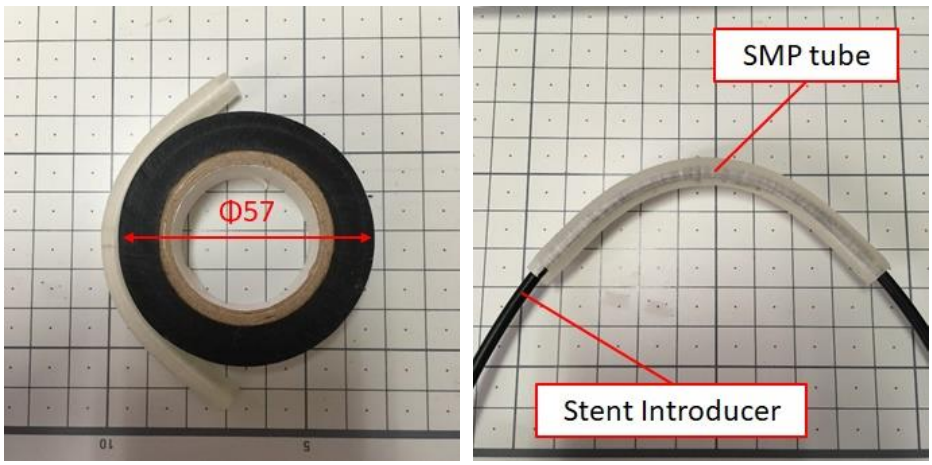


(a) (b)

Figure 4.5: Feasibility test of SMP tube. (a) Radius of curvature of SMP tube (b) Shape-locking capability test with stent introducer

### 4.2.3 Material Property of SMP

Generally, two states exist in SMP structure by the temperature change that induces the phase transition. Thus, in SMP structure design, two possible behaviors in a rigid state and a flexible state should be considered. To predict two states in design process, the property of the SMP was measured by tensile testing machine. The tensile testing was conducted using a standard specimen as shown in Figure 4.6(a, b). The thickness of the fabricated specimen was 3.2 mm. To measure the elongation in the rubbery state of the specimen, the center of the specimen was coiled by the PTFE tube which contains nichrome wires ($\Phi$ 0.3 mm) inside. The local heating was done by the electric current to the coiled wires. The electric current was applied by a DC power supply (0.1 A) for more than 30 seconds. After the SMP specimen was heated enough (around $T_g$), the specimen were pulled by a tensile testing machine, and a load cell

(maximum load = 20 kgf) was used to measure the applied load in every test. The results show that the stress-strain curve in the flexible state is similar to the typical rubber or silicone (see Figure 4.6(d)).

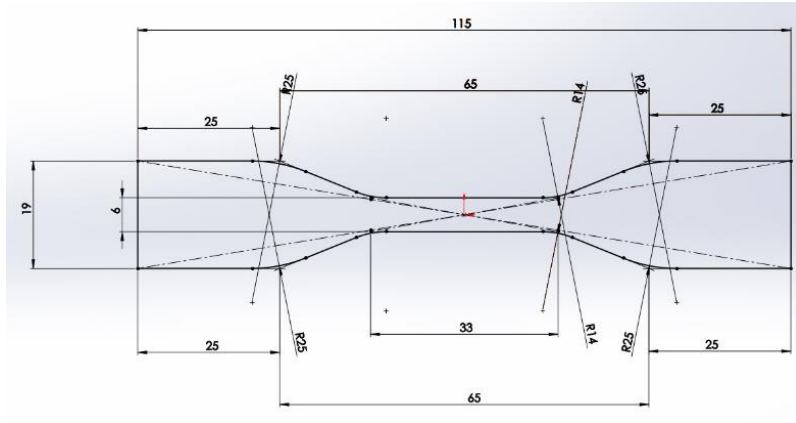


(a)

(b)

(c)

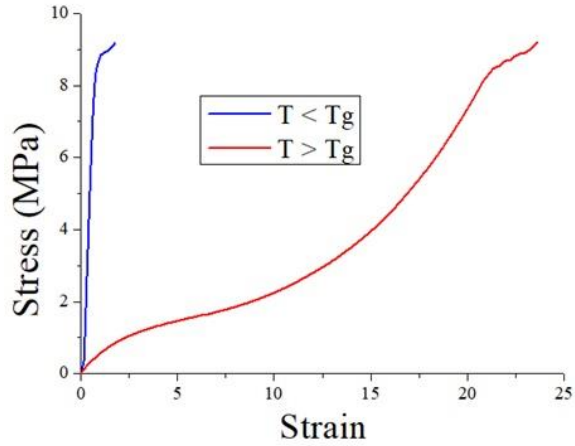


(d)

Figure 4.6: SMP property test. (a) Specimen for tensile test (b) Fabricated SMP test piece (c) Tensile test setting for SMP (d) Tensile test result for SMP

### 4.2.4 Heating and Cooling Method for SMP Structure

The heat-induced phase transition requires the instant heating for the shape deformation. Embedding a nichrome or a nitinol wire is considered as the simplest method to an entire SMP structure. As illustrated in Figure 4.7(a), Joule heating can be achieved by the direct current from the DC power supply. A test piece for joule heating test was designed (Figure 4.7(b)). The thru-hole makes the heating wire pass through and both ends are connected to the metal electrodes for closed circuit formation. The electric current 0.1 A was applied to the inner lumen of the SMP structure through the heating wire during 10 seconds. After the heating, the structure was deformed by the applied load (Figure 4.7(c)).

Joule heating using a heating wire showed a feasibility in the SMP structure, however, the heat transfer is not efficient due to the heating area is limited with a thin wire. To address the issue related to heating area limitation, coiling a heating wire was considered for the broad range heating of the tube surface. The experiment using a coiled heating wire was designed to verify the effectiveness of the electric heating method (see Figure 4.8(a)). The load cell (maximum load = 500 gf) was used to measure a small amount of the pulling force with a high accuracy. Figure 4.8(b) shows an experimental result. When the lateral deflection of the SMP tube did not bend more than 1 - 2 mm even though lateral load 150 g was applied. When the SMP tube is heated above glass transition temperature, the SMP tube can be bent with a small amount of the lateral force (see Figure 4.8(c)). As a result, the embedded heating method that contains Joule heating method can be a candidate for the steerable catheter with a variable stiffness.

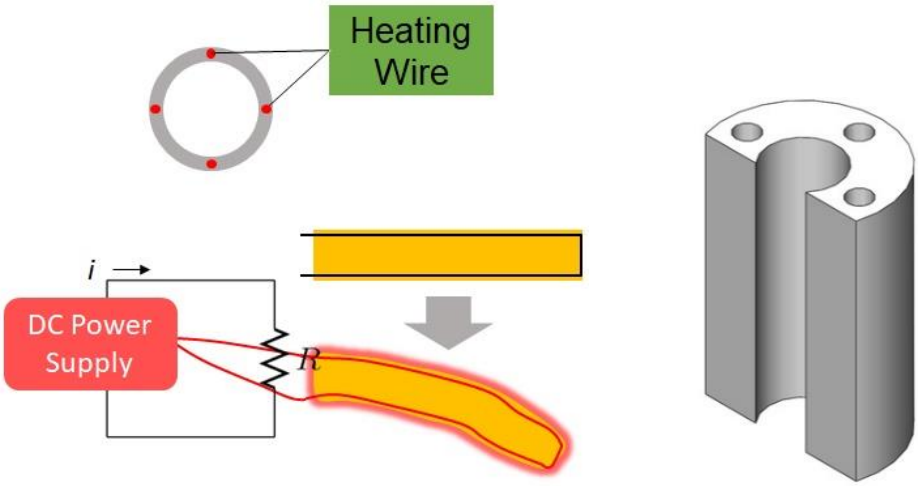


(a) (b)


(c)

Figure 4.7: Heating and cooling methods.

(a) Electric heating method (b) Test piece for heating test

(c) Heating setup and test scene

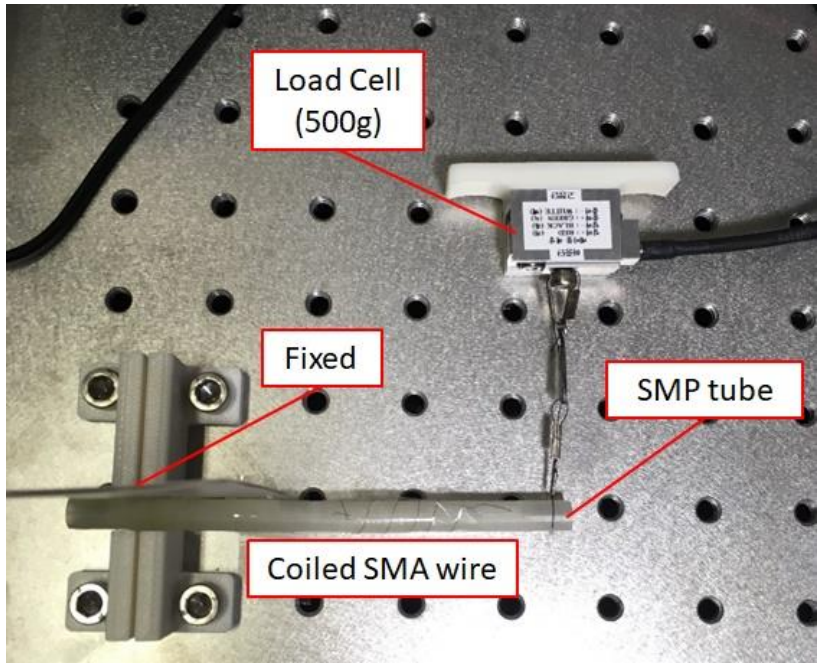


(a)

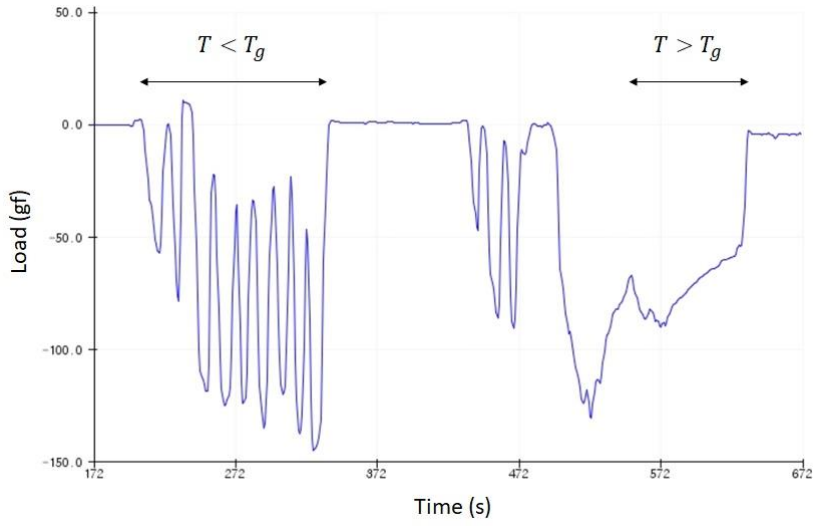


(b)

Figure 4.8: SMP heating test. (a) Heating test setup
(b) Experimental result of joule heating

On the other hands, the cooling method is required to achieve a shape-locking of the steerable catheter. In thermoelectric heating, the heat transfer efficiency is low because of the temperature influence by the surrounding tissue. A low heat transfer efficiency may not be a critical issue in heating process, however, the cooling should be instant because the desired shape can be maintained only with an appropriate wire tension until the cooling is complete.

To evaluate a cooling performance with a thermoelectric cooling, Peltier module (see **Figure 4.9(a)**) was used in the thermoelectric cooling test (see **Figure 4.9(b)**). A copper wire ($\Phi$ 0.25 mm) was coiled on the SMP tube surface and connected to the Peltier module for heat transfer. The cooling fan was attached on the Peltier module. A thermocouple-type temperature sensor with a display (M002, makepcb, Korea) was set up to monitor the temperature during the test. In test, Electric current 6 A by a DC power supply was constantly applied to the Peltier module, The temperature of the Peltier module was cooled down instantly by 10 – 15 ℃, however, the cooling performance of the SMP tube was extremely low due to the low heat transfer efficiency. To increase heat transfer efficiency, the area of the coiled surface should be widened with a shorter connecting length. Consequently, another method should be considered for phase transition to the glassy state of the SMP tube.

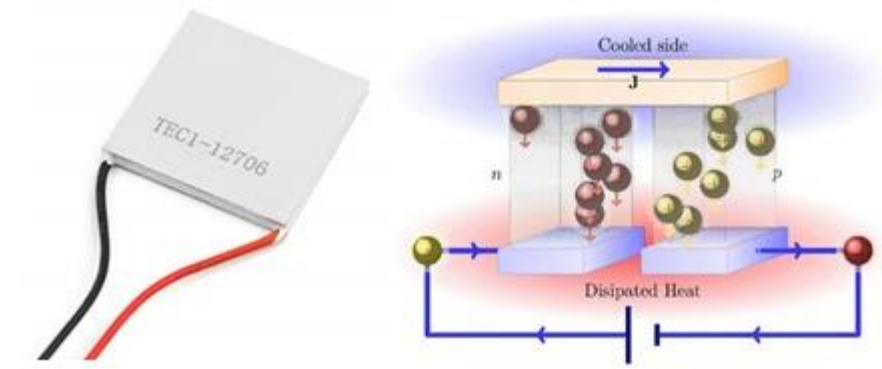


(a)

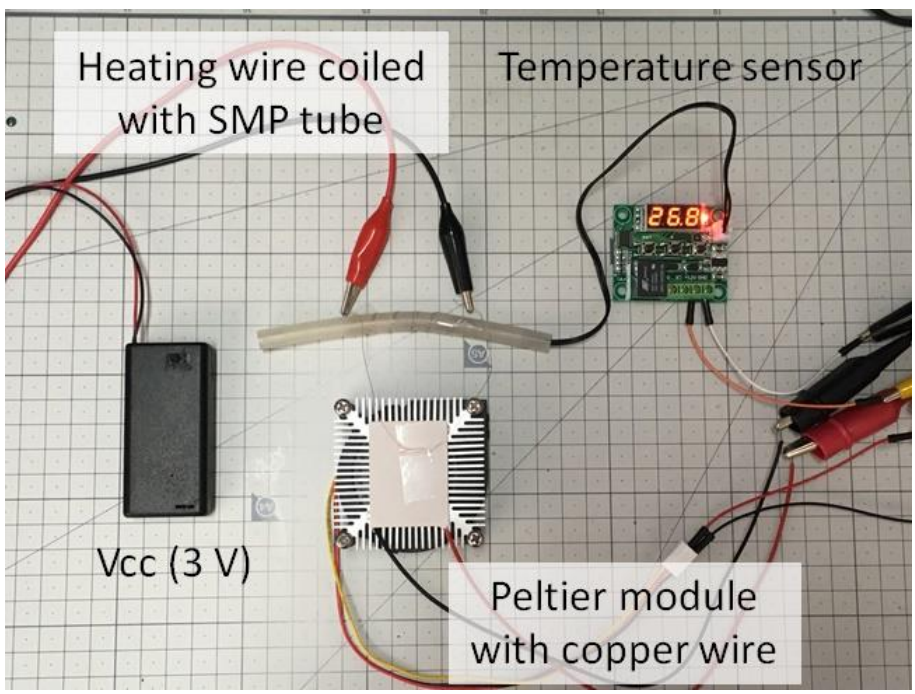


(b)

Figure 4.9: Thermoelectric cooling test for SMP tube.

(a) Peltier module (FALC1-09506T150, Huimao, Inc.)

(b) Cooling test setup using Peltier module

To use the simplest way to cool down a heated SMP structure for medical use, the water chilling method was proposed (see **Figure 4.10(a)**). In general, the water chilling method requires a circulation system, however, the flowing the saline into the GI tract through the medical tube is commonly used to wash and sterilize a soft tissue in the surgical and the interventional procedures. Thus, direct injection of water is considered as an effective method in terms of safety. Moreover, a PTFE tube (O.D.: **4 mm**, I.D.: **2 mm**) and a syringe (**5 mL**) was used for cool water injection into the SMP tube (see **Figure 4.10(b)**). The heated SMP tube was cooled down using cool water (**3 – 6.5** ℃) injection for 10 seconds. As a result, the cool water method showed a feasibility that can easily cool down the heated SMP structure compared to the thermoelectric cooling. Furthermore, the electric heating method has limitations in a temperature control and requires an additional component for temperature sensing. To achieve the instant phase transition of the SMP tube, the water chilling method will be a promising candidate. Further study is required for feasibility verification of the proposed method in the clinical scenario in the future.

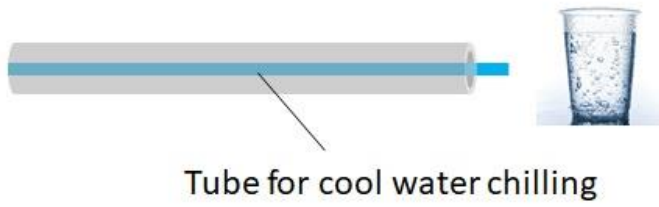


(a)

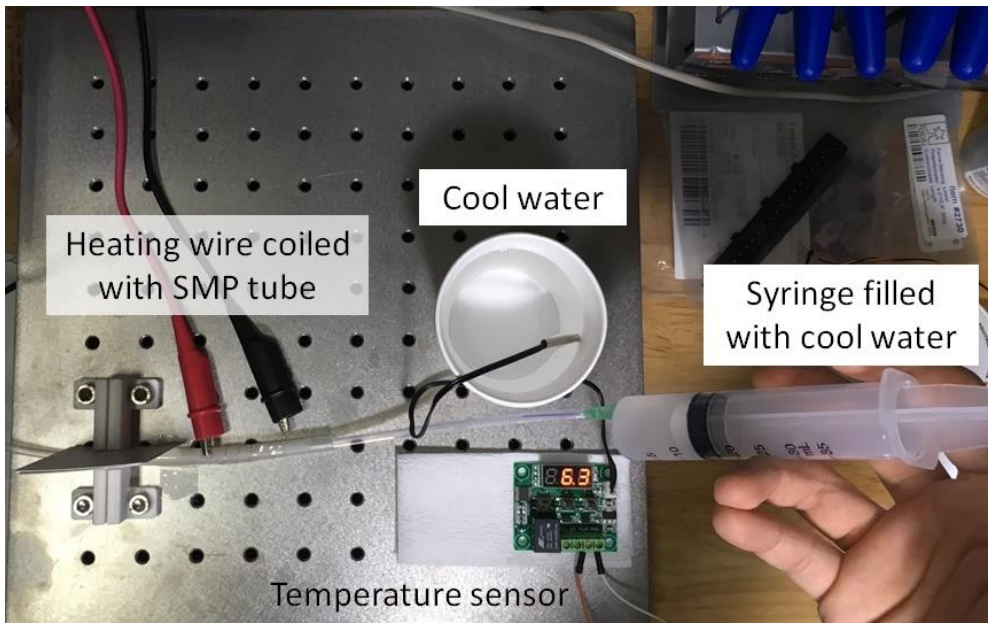


(b)

Figure 4.10: Chilling method with cool water. (a) Water cooling scheme (b) Thermoelectric test cooling using Peltier module

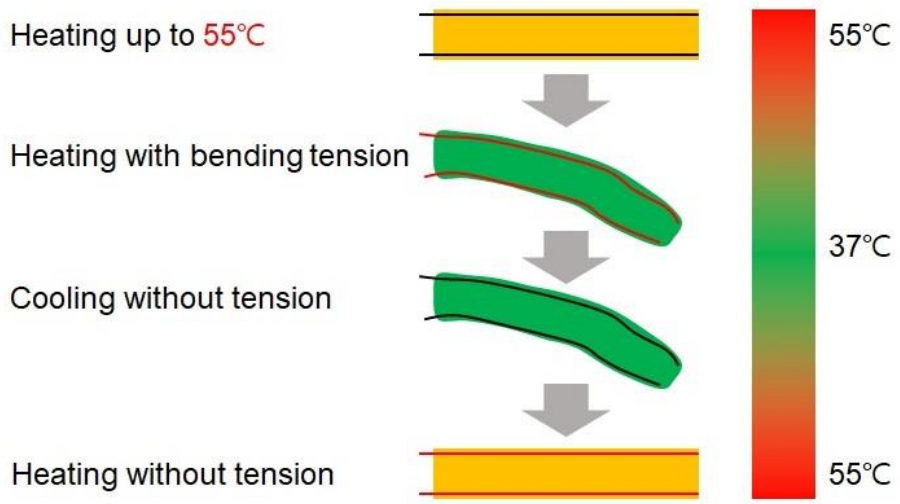


Figure 4.11: Thermoelctric heating and water cooling of SMP joint

As shown in Figure 4.11, the heating and cooling strategy to control a stiffness of the SMP joint was established. First, the SMP joint is coiled with a heating wire. To insert a whole structure, SMP joint should be heated during the insertion. The flexibility of the SMP joint is increased by a thermoelectric heating, then, the shape-locking function will be activated by the cooling down of the SMP joint

## 4.3 SMP in Steering Joint

### 4.3.1 Steerable Catheter with SMP Joint

A steerable catheter with the SMP joint was designed and assembled as shown in Figure 4.12(b). Figure 4.12(a) shows a design of backbone rings to suppress a lateral deflection of the SMP tube in bending motion. Two additional grooves exist for the heating wire that passes through the entire structure. Moreover, the backbone rings are used to be a steering wire path and coiling path of the heating wire. Four slits which are aligned in the perpendicular to the each direction were designed for the steering wire path, and other

two slits were designed for a closed loop formation of the heating wire from the proximal to the distal side. **Figure 4.12(b)** shows steerable joint assembly with a silicone joint in the distal tip. Due to the backbone rings, the lateral deflection is suppressed during a bending motion. The bending angle of the 1st joint was realized up to **180°** without a tube kinking. This is because of the force transmission from the proximal side is maintained by the stiffened SMP joints. The payload was tested using the 1st joint in the curved configuration (see **Figure 4.12(d)**).

In clinical situation, the GI intervention using the proposed steerable catheter with a variable stiffness is illustrated in **Figure 4.13**. The new device for GI intervention can be used without any conflict because the device can play a role as an overtube like other interventional devices such as an endoscope or a guiding sheath. Firstly, the soft guidewire is inserted into the stomach (see **Figure 4.13(a)**). The steerable catheter in rubbery state is overlapped over inserted guidewire (see **Figure 4.13(b)**). Shape-locking of the SMP joint is activated by structure cooling (see **Figure 4.13(c)**). A guidewire is inserted into the distal side (see **Figure 4.13(d)**). In this case, the SMP joint plays a role as a supporting structure. The guidewire is steered by the steerable catheter (see **Figure 4.13(e)**). Finally, the stent is placed by clinician (see **Figure 4.13(f)**).

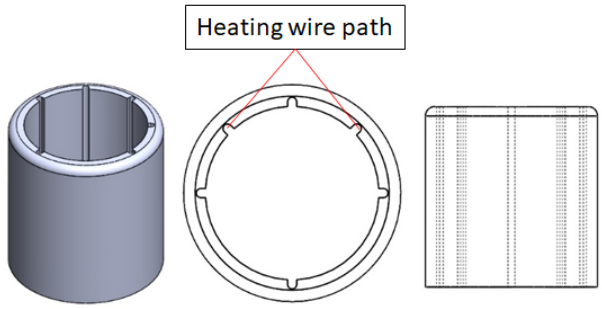


(a)

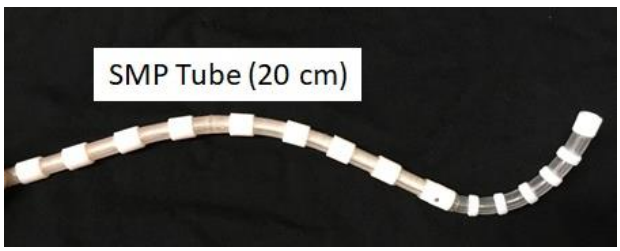


(b)

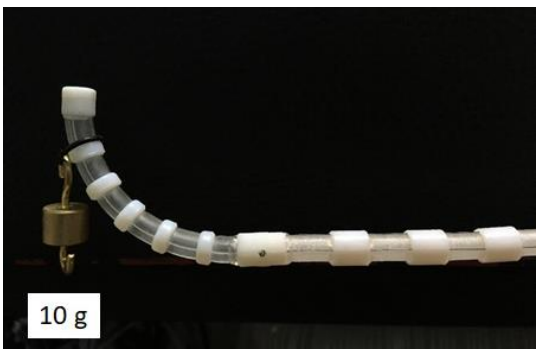


(c) (d)

Figure 4.12: Steerable catheter with SMP joint. (a) Backbone ring for SMP tube (Left:Isometric view, Center:Front view, Right:Side view) (b) Steerable catheter with SMP joint

(c) Bending test of the 1st joint (d) Payload test of the 1st joint

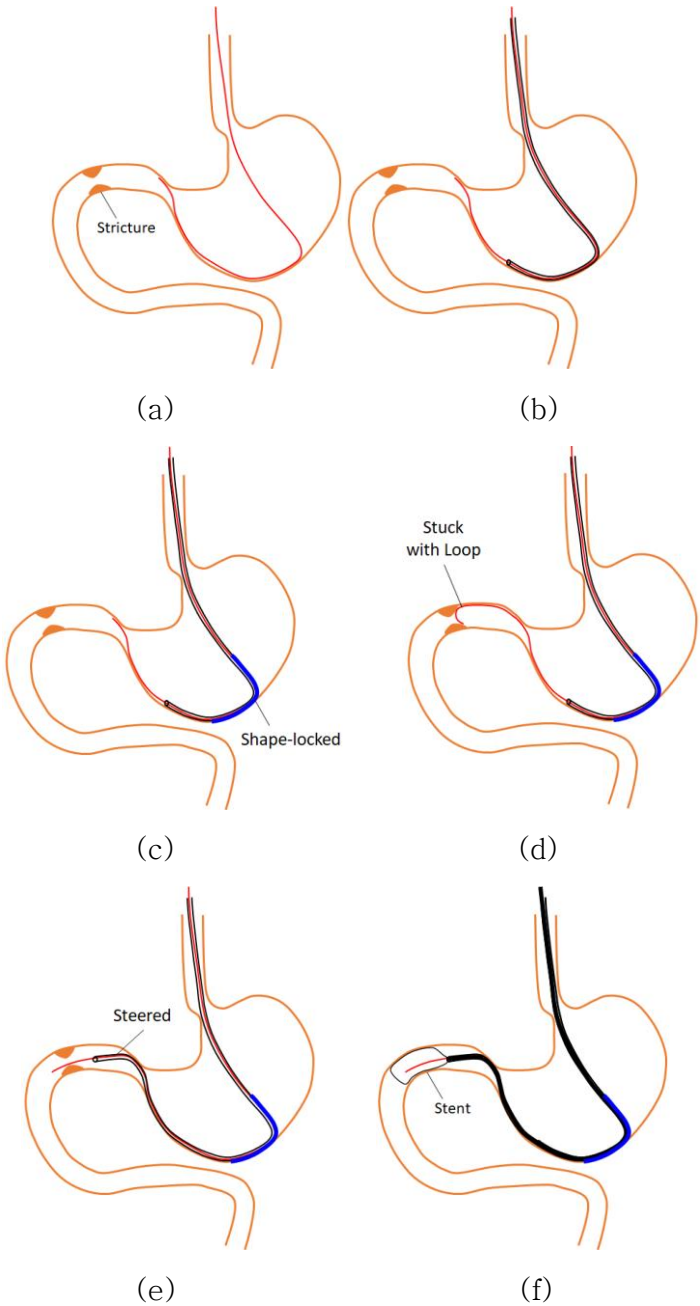


Figure 4.13: New method using steerable catheter.

(a) Soft guidewire is inserted into stomach (b) Steerable catheter is overlapped over inserted guidewire (c) Shape-locking is activated by structure cooling (d) Guidewire is inserted into distal side (e) Guidewire is steered by steerable catheter (f) Stent is placed by clinician

The stenting test process is shown in **Figure 4.14**. The steerable catheter is heated and the phase is shifted to the rubbery state (see **Figure 4.14(a)**). The curved steerable catheter straightens by stent introducer passing through inner lumen (see **Figure 4.14(b)**). The shape of the curved steerable catheter is locked by cooling down (see **Figure 4.14(c)**). The stent introducer is completely passes through the curved steerable catheter lumen without configuration change (see **Figure 4.14(d)**). The stent is pushed out from steerable catheter in the curved configuration (see **Figure 4.14(e)**).

Through the three-point bending test on SMP tube in two states, the bending stiffness was obtained as $EI_{SMP\_G} = 34{,}408\ \mathrm{Nmm^2}$ (glassy) and $EI_{SMP\_R} = 119\ \mathrm{Nmm^2}$ (rubbery). The conformability space of the SMP manipulator was calculated (see **Figure 4.15**). The conformability was maintained by more than 40 in both situations: insertion into the stomach and stent introducer passing through the SMP manipulator lumen. Consequently, the conformability was dramatically increased in any effective length and radius of curvature using the proposed SMP manipulator.

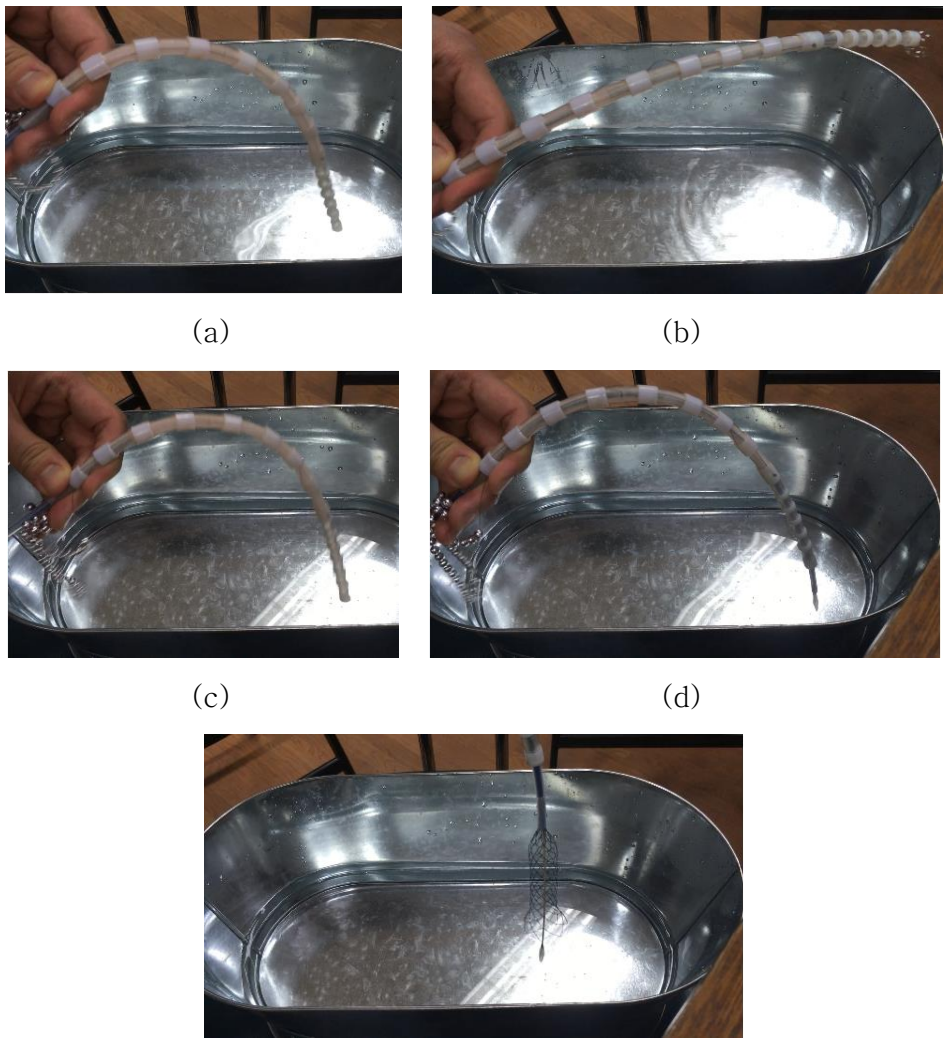

Figure 4.14: Stent placement test using manipulator with variable stiffness.

(a) Steerable catheter in rubbery state (b) Curved steerable catheter straightens by stent introducer passing through inner lumen (c) Shape of curved steerable catheter is locked by cooling (d) Stent introducer passes through curved steerable catheter without configuration change (e) Stent is pushed out from steerable catheter in curved configuration

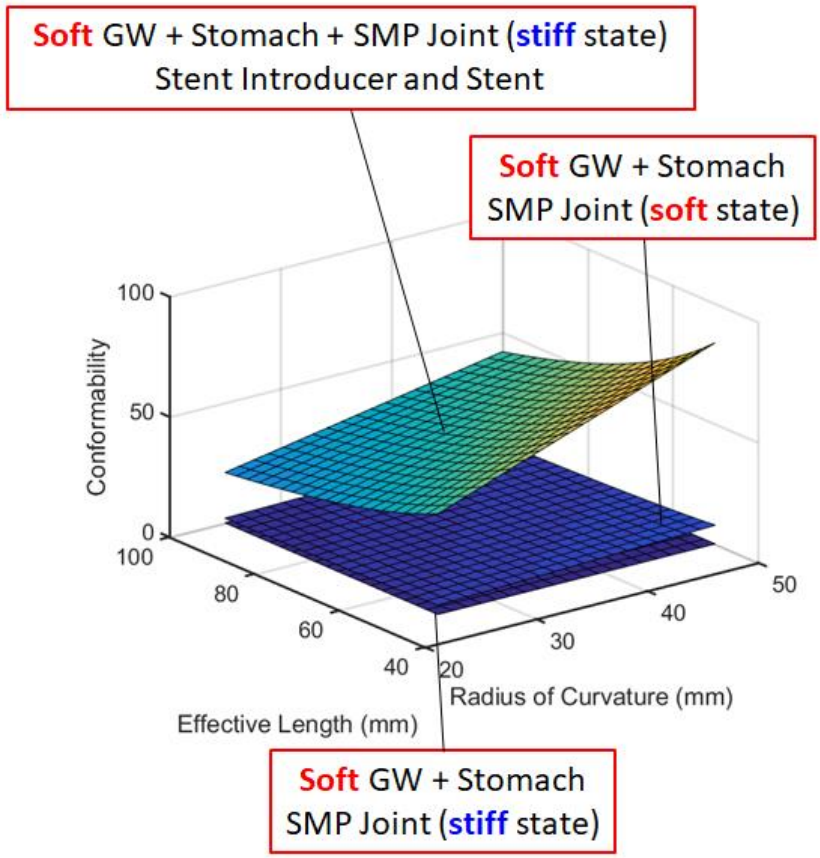


Figure 4.15: Conformability space of the SMP tube during stent introducer passing

# Chapter 5. Experiments

## 5.1 In-vitro Test

In-vitro test for GI tract is difficult to realize a texture and complex geometry. A few researchers have been developed (see Figure 5.1) [108 – 110]. However, the actual size of the test bed for GI intervention have not been developed even in the commercial product.

### 5.1.1 Simple Phantom for GI Tract

A simple phantom was designed that consists of the acrylic plates, the acrylic pipe, and the translucent rubber tubes. The total length and space were designed on the basis on the measured size in several literatures. The length of the esophagus was set to be 30 cm, the distance from the EG junction to the greater curvature is 10 cm, the length from the $1^{st}$ portion of the duodenum to the $4^{th}$ portion of the duodenum was set to be 25 cm. Each portion through the entire structure was set to be 5, 8, 3, 10 cm. The diameter of the acrylic pipe is 2 cm as shown in Figure 5.2(a). Using the prototyped phantom, guiding sheath which is the most large diameter interventional device was tested. In the insertion test, the guiding sheath was lubricated by a medical lubricant. However, the guiding sheath was kinked at the acute angle nearby the duodenal bulb. As described in the previous chapter, the kinked lumen cannot make the stent introducer pass through. In an actual clinical field, the stomach wall is lubricated and distended by the $CO_2$ gas insertion. For this reason, the tissue distension of the soft tissue should be concerned in the in-vitro study. Moreover, the flexible material should be used to realize a tissue distension, and the dimensions should be set to be based on an actual

organ size in terms of the realistic scenario.

(a) (b)


(c)

Figure 5.1: Phantom for GI tract.

(a) Dynamic GI tract phantom [108] (b) Stomach phantom by molding process [109] (c) Full-size phantom of GI tract [110]

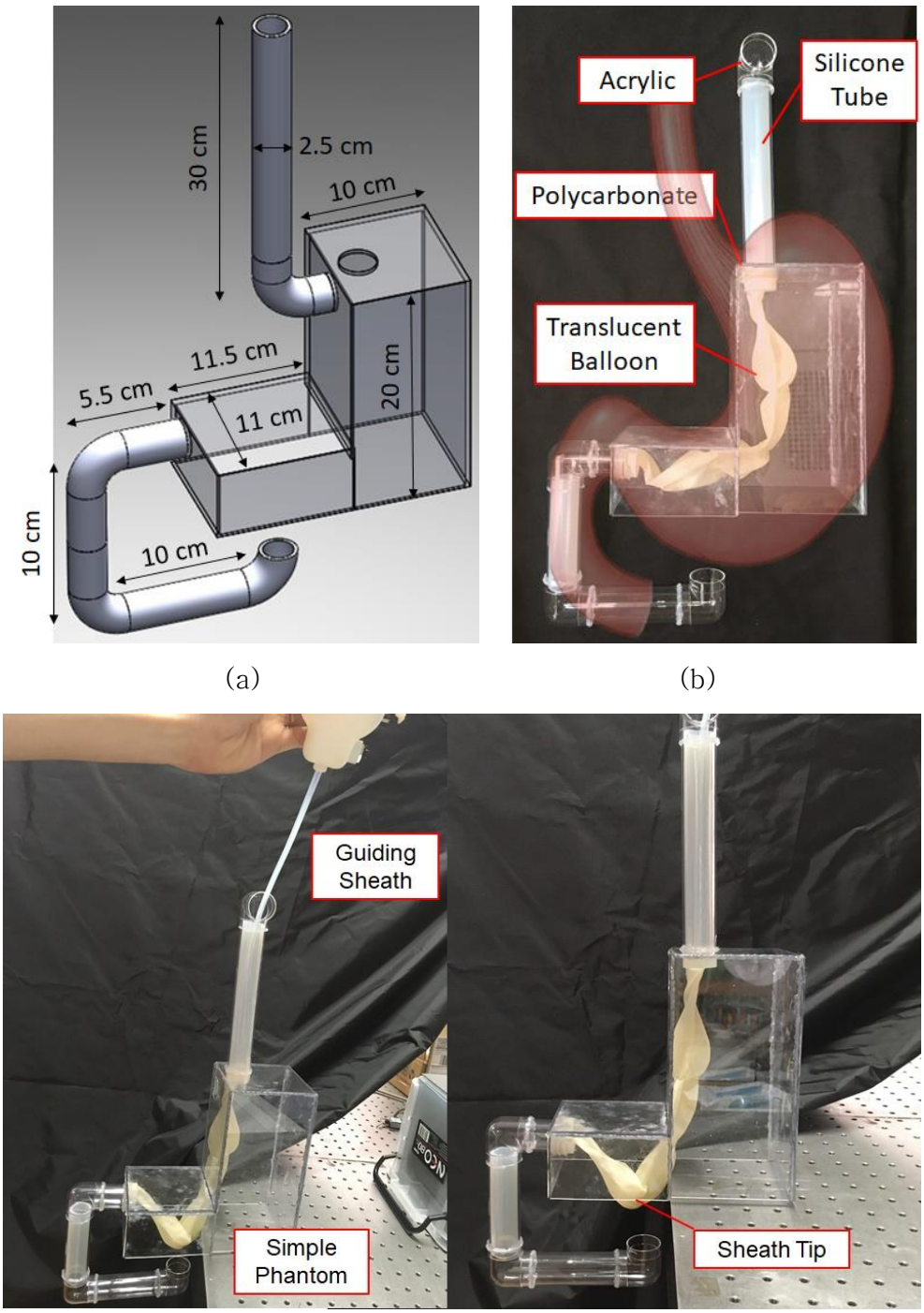


(a) (b)

(c)

Figure 5.2: Simple phantom of GI tract. (a) Simple phantom design (b) Prototyped simple phantom (c) Interventional device insertion

### 5.1.2 Patient-derived Phantom

To consider the realistic scenario in the in-vitro study, the patient-derived CT image was obtained with a cooperation of the department of internal medicine and radiology at Asan Medical Center. The data was obtained from the patient who swallowed a foaming agent. Owing to this, the 3D model was slightly inflated (see Figure 5.3(b)). However, the distal side of the small intestine was not fully realized. Hence, the artificial duodeno-jejunal region was designed on the basis of the anatomic observation of the duodenum [29, 42]. Figure 5.4 shows steerable catheter insertion test procedure with a guidewire using a patient-derived GI phantom. First, the steerable catheter is inserted through the mouth part (see Figure 5.4(a)). The distal tip of the steerable catheter is placed in the stomach region (see Figure 5.4(b)). The distal tip of the steerable catheter is placed in the duodenum part by steering (see Figure 5.4(c)). A guidewire is inserted into the stomach alone (see Figure 5.4(d)). The steerable catheter is overlapped on the inserted guidewire (see Figure 5.4(e)). Approaching the duodenum part is achieved by tip steering of the steerable catheter (see Figure 5.4(f)).

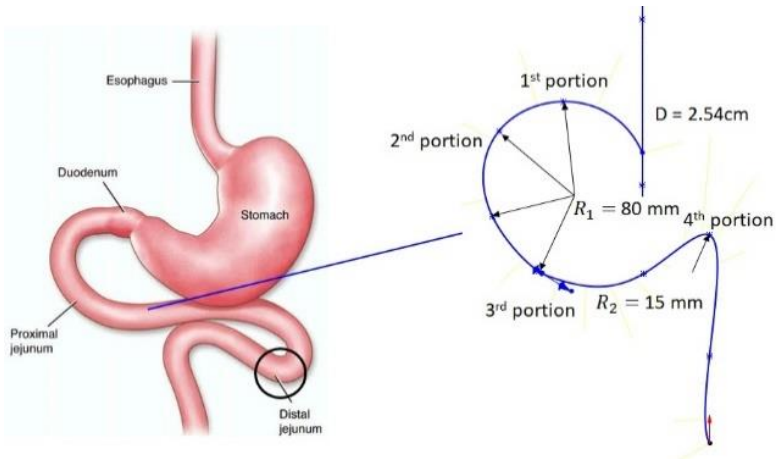


(a)

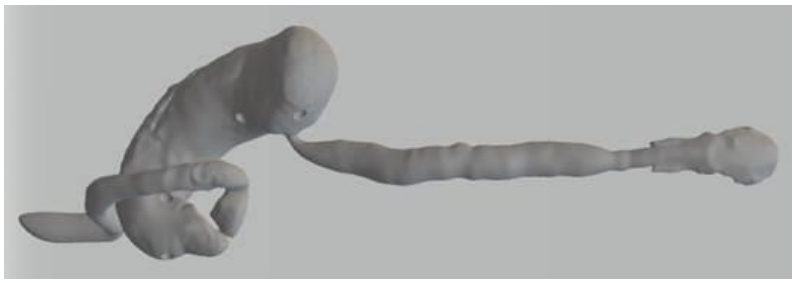

(b)

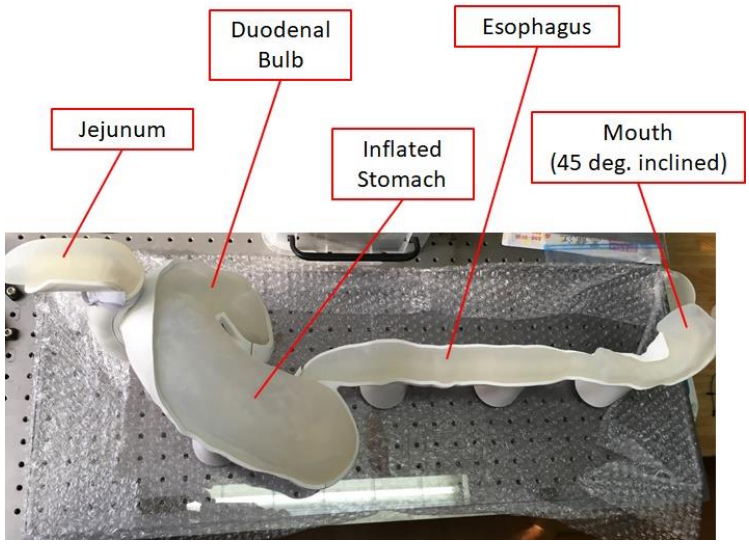


(c)

Figure 5.3: Patient-derived phantom. (a) Duodeno-jejunal region trajectory model (c) Patient-derived phantom model (d) Patient-derived phantom with artificial duodeno-jejunal region

In-vitro test using the patient-derived full-size phantom was conducted with the 1st steerable catheter.

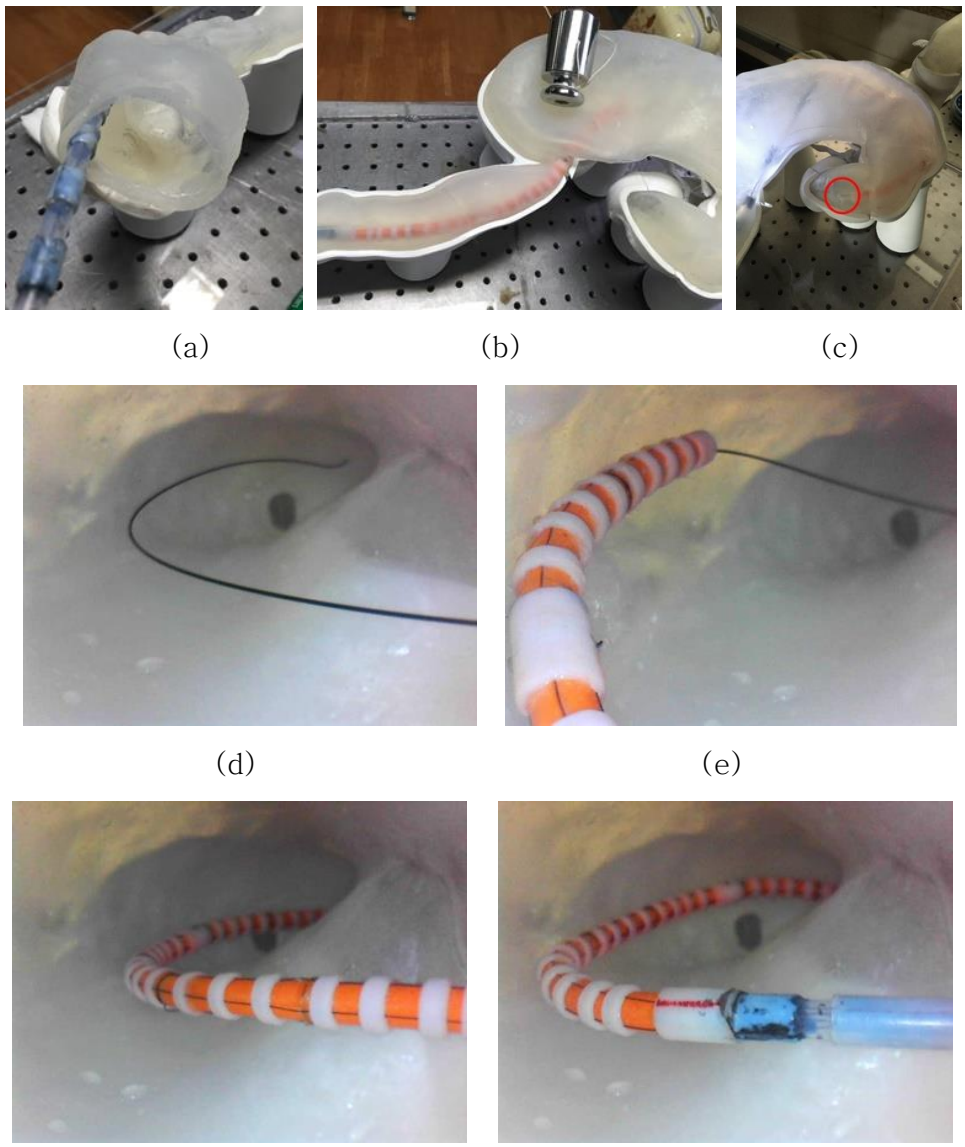

(a) (b) (c)

(d) (e)

(f)

Figure 5.4: Steerable catheter test using the full-size phantom.
(a) Steerable catheter insertion through the mouth part
(b) Distal tip in stomach (c) Distal tip in duodenum
(d) Guidewire in stomach (e) Overlapped catheter on guidewire
(f) Approaching duodenum with tip steering

## 5.2 In-vivo Test

To obtain an actual stiffness data and bending profile in the live stomach, the in-vivo test was conducted using originally designed measuring device as shown in Figure 5.5(b). The one-way bending structure was designed as a distal tip (see Figure 5.5(a)). A load cell (333FB, KTOYO, Korea) and a flex bend sensor(SEN-10264, Sparkfun, U.S.) were embedded in the flexible structure. The load cell can measure the 500 g in maximum. As the flex sensor is flexed, the resistance across the sensor increases. All signals from these sensors are acquired and processed using a microprocessor (Arduino Leonardo, Arduino.cc, Multinational). Figure 5.6 shows the experimental scenes. The experimental results (see Figure 5.7) show the different curve by each trial. This may be caused by the food left in the animal's stomach even though the NPO (Nothing by mouth) was done on the object animal. Nevertheless, the data shows a similar tendency that the bending angle is ranged $5-10^{\circ}$ where the measured force is in $1-3$ N. The results will be a clue for the further study in the future.

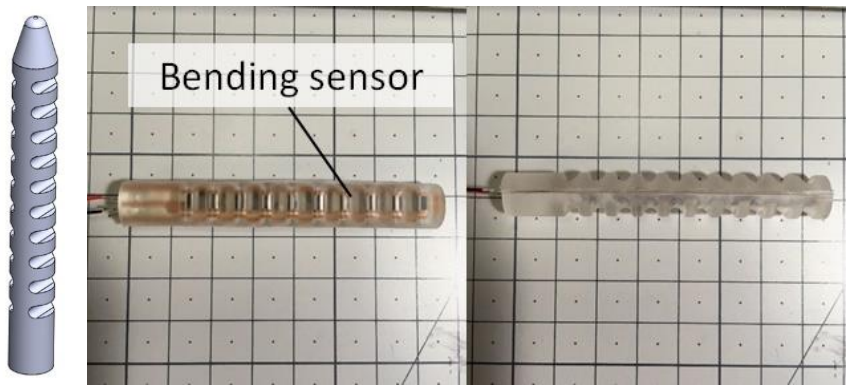


(a)

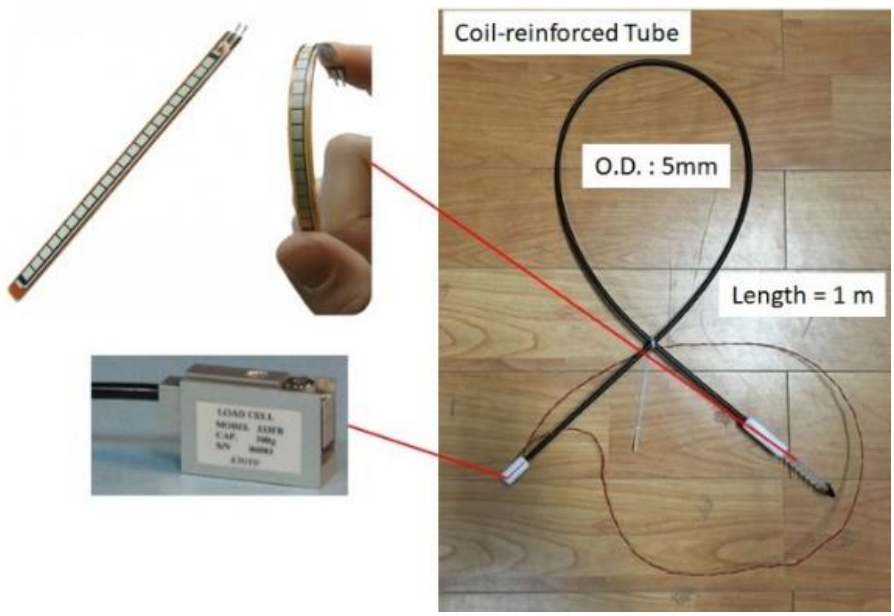


(b)

Figure 5.5: Stiffness and bending profile test device.
(a) Fabricated bending structure by silicone molding (b) Sensors and embedded device for stiffness and bending profile test

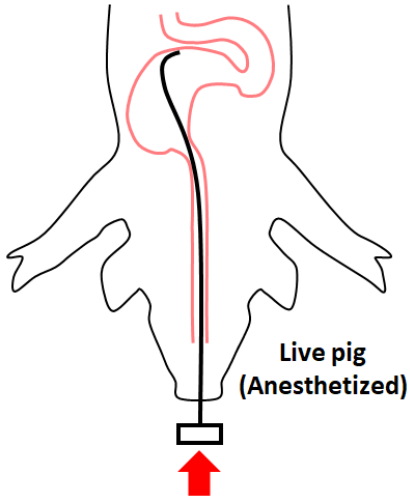


(a)

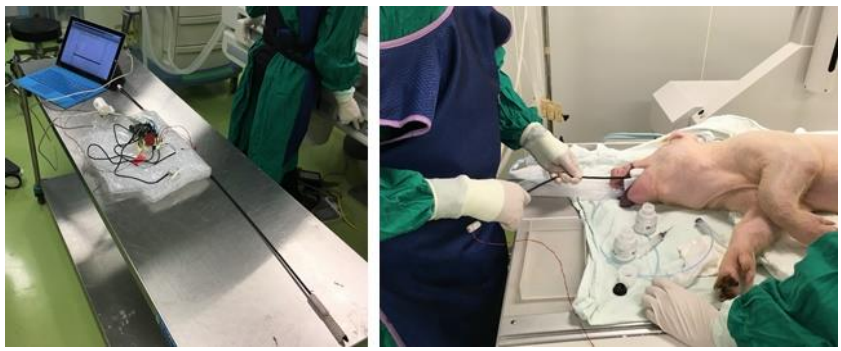

(b)

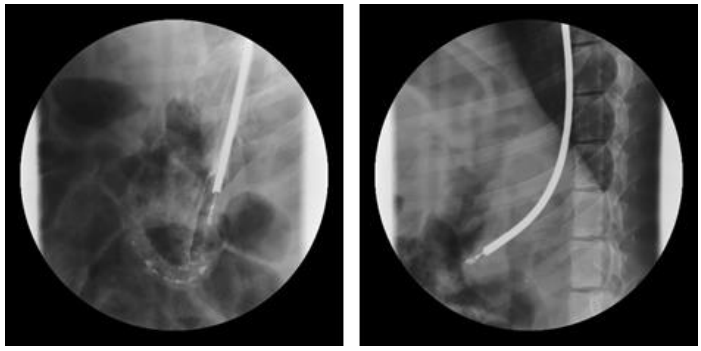

(c)

Figure 5.6: Stiffness and bending profile test. (a) Schematic of stiffness and bending profile test setup (b) Experimental setup in porcine model (c) Fluoroscopic images in stiffness and bending profile test

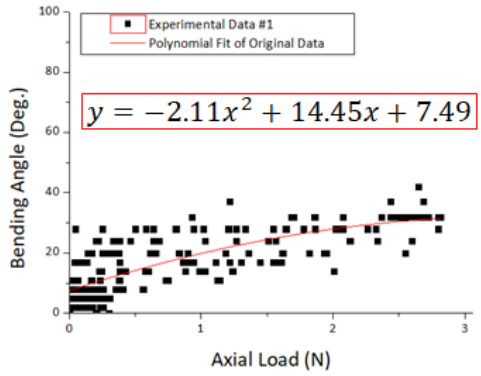


(a)

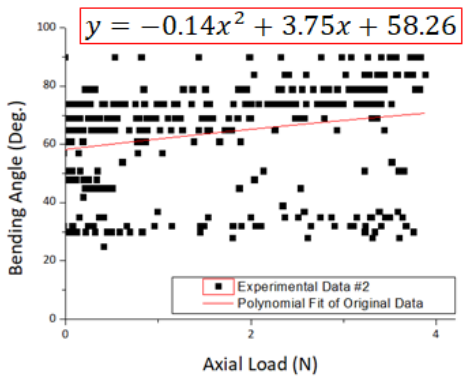


(b)

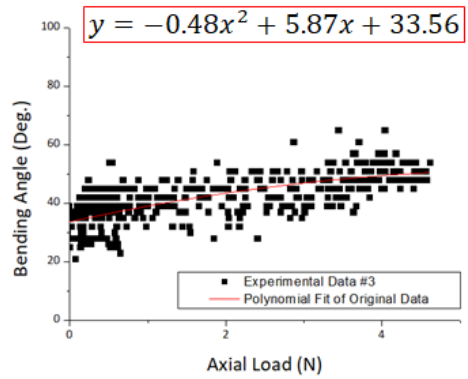


(c)

Figure 5.7: Experimental result from in-vivo test.

(a) Experimental result (trial 1)

(b) Experimental result (trial 2) (c) Experimental result (trial 3)

# Chapter 6. Conclusion

## 6.1 Conclusion

In this study, a new design principle of interventional devices which is based on the conformability model was proposed. The proposed model was built in order to extract the essence of the interactions between the soft tissue and the medical tubes during the GI intervention. In the proposed conformability model, the complexity of multi-body contact behavior between the soft tissue and the medical tube was simplified to the variables: flexural rigidity, curvature, and effective length of the curved space. Conformability in various combinations of conventional GI interventional devices was evaluated in order to design an optimized tube that can be used in GI stenting procedure. As a result, a soft manipulator with variable stiffness was designed and fabricated on the basis of consideration of those conformabilities. The soft manipulator can play a role as an overtube which can maintain a high conformability during GI intervention.

## 6.2 Future Works

The future works are considered as follows:

- Verification of the conformability model in three-dimensional space
- Verification of the conformability model for multi-curvature
- Prediction of a loop formation of the curved tube using the conformability factor
- Stent placement test using the steerable catheter in porcine or dog model
- Optimization of the SMP joint using an extrusion method on

the basis of consideration of medical use

- To decrease an outer diameter of the entire structure, backbone rings mechanism must be embedded in the tubular structure in the limited form factor
- Exploration of a new heating and cooling method for SMP structure
- Decoupling of the steering motion by the motion compensation using a semi-automated actuation by actuators and sensors

# Bibliography


1. Home Care Article, (2015). "What is an Interventional Procedure", Retrieved from https://jfkmc.org/ (accessed Jan. 22, 2019)

2. Health, Center for Devices and Radiological, (2018). "Cerebral Spinal Fluid (CSF) Shunt Systems", Retrieved from http://www.fda.gov/ (accessed Jan. 22, 2019)

3. DG Adler et al., (2013). "Esophageal Stents: Placement, Complications, Tips, and Tricks", Video Journal and Encyclopedia of GI Endoscopy, 1(1), pp. 66-68.

4. Parswa Ansari, (2017). "Intestinal Obstruction", MSD Manual, Retrieved from https://www.msdmanuals.com, (accessed Jan. 22, 2019)

5. Article, (2017). "Cardiac Catheterization", Healthline, Retrieved from https://www.healthline.com/health/cardiac-catheterization/ (accessed Jan. 22, 2019)

6. Miguel De Gregorio et al., (2004). "Colon Stenting: A Review", Seminars in Interventional Radiology, 21(3), pp. 205-216.

7. Arif Emre et al., (2018). "Self-expandable metallic stent application for the management of upper gastrointestinal tract disease", Turkish Journal of Surgery, 34(2), pp. 101-105.

8. Gaidos JK and Draganov PV, (2009). "Treatment of malignant gastric outlet obstruction with endoscopically placed self-expandable metal stents", World J Gastroenterol., 15(35), pp. 4365-4371.

9. Ly J, O'Grady G, Mittal A, et al., (2010). "A systematic review of methods to palliate malignant gastric outlet obstruction", Surg Endosc., 24(2), pp. 290-297.

10. Mittal A, Windsor J, Woodfield J, et al. (2004). "Matched study of three methods for palliation of malignant pyloroduodenal obstruction", Br J Surg., 91(2), pp. 205-209.

11. Costamagna G, Tringali A, Spicak J, et al., (2012). "Treatment of malignant gastroduodenal obstruction with a nitinol self-expanding metal stent: an international prospective multicentre registry", Dig Liver Dis., 44(1), pp. 37-43.

12. Mendelsohn RB, Gerdes H, Markowitz AJ, et al., (2011). "Carcinomatosis is not a contraindication to enteral stenting in selected patients with malignant gastric outlet obstruction", Gastrointest Endosc., 73(6), pp. 1135-1140.

13. Lee EY, Bourke MJ, Williams SJ, et al., (2011). "Severity of initial stent angulation predicts reintervention after successful palliative enteral stenting for malignant luminal obstruction", J Gastroenterol Hepatol., 26(3), pp. 484-491.

14. van Hooft JE, van Montfoort ML, Jeurnink SM, et al., (2011). "Safety and efficacy of a new non-foreshortening nitinol stent in malignant gastric outlet obstruction (DUONITI study): a prospective, multicenter study", Endoscopy, 43(8), pp. 671-675.

15. Vitale G, Davis B and Tran T. (2005). "The advancing art and science of endoscopy", Am J Surg., 190(2), pp. 228-233.

16. Dormann A, Meisner S, Verin N, et al., (2004). "Self-expanding metal stents for gastroduodenal malignancies: systematic review of their clinical effectiveness", Endoscopy, 36(6), pp. 543-550.

17. Johnsson E, Thune A and Liedman B, (2004). "Palliation of malignant gastroduodenal obstruction with open surgical bypass or endoscopic stenting: clinical outcome and health economic evaluation", World J Surg., 28(8), pp. 812-817.

18. Park KB, Do YS, Kang WK, et al., (2001). "Malignant obstruction of gastric outlet and duodenum: palliation with flexible covered metallic stents", Radiology, 219(3), pp. 679-683.

19. Yates MR 3rd, Morgan DE, Baron TH, (1998). "Palliation of malignant gastric and small intestinal strictures with self-expandable metal stents", Endoscopy, 30(3), pp. 266-272.

20. He X, Shin JH, Kim HC, et al., (2005). "Balloon sheaths for gastrointestinal guidance and access: a preliminary phantom study", Korean J. of Radiology, 6(3), pp. 167-172.

21. Mauro MA, Koehler RE, Baron TH, (2000). "Advances in gastrointestinal intervention: the treatment of gastroduodenal and colorectal obstructions with metallic stents", Radiology, 215(3), pp. 659-669.

22. Bae JI, Shin JH, Song HY, et al., (2005). "Use of guiding sheaths in peroral fluoroscopic gastroduodenal stent placement", Eur Radiol., 15(11), pp. 2354-2358.

23. Lee JM, Han YM, Kim CS, et al., (2001). "Fluoroscopic-guided covered metallic stent placement for gastric outlet obstruction and post-operative gastroenterostomy anastomotic stricture", Clin Radiol., 56(7), pp. 560-567.

24. Jung-Hoon Park et al., (2013). "Usefulness of a guiding sheath for

fluoroscopic stent placement in patients with malignant gastroduodenal obstruction", Acta Radiologica., 54(3), pp. 267-271.

25. Braden Kuo and Daniela Urma, (2006). "Esophagus - anatomy and development", GI Motility online. doi:10.1038/gimo6 (accessed Jan. 22, 2019)

26. Richard K. Freeman el al., (2012). "Analysis of Unsuccessful Esophageal Stent Placements for Esophageal Perforation, Fistula, or Anastomotic Leak", Ann Thorac Surg., 94(3), pp. 959-965.

27. Simon P. DiMaio, (2003). "Modelling, simulation and planning of needle motion in soft tissues (Ph.D)", THE UNIVERSITY OF BRITISH COLUMBIA, CANADA.

28. Hoeg et al., (2000). "Biomechanical modeling of the small intestine as required for the design and operation of a robotic endoscope", Int. Conf. on Robotics & Automation 2000, pp. 1599-1606.

29. Maria J.Ferrua et al., (2011). "Understanding the fluid dynamics of gastric digestion using computational modeling", Procedia Food Science, 1, pp. 1465-1472.

30. E.J. Chen et al., (1996). "Young's modulus measurements of soft tissues with application to elasticity imaging", IEEE Transactions on Ultrasonics, Ferroelectrics, and Frequency Control, 43(1), pp. 191-194.

31. Zhang M etl al., (1997). "Estimating the effective Young's modulus of soft tissues from indentation tests—nonlinear finite element analysis of effects of friction and large deformation", Medical Engineering & Physics, 19(6), pp. 512-517.

32. Kato, K, (1915). "Mathematical Investigation on the Mechanical Problems of Transmission Line", Journal of the Japan Society of Mechanical Engineers, 19(41), pp. 72-78.

33. Drake, Richard L.; Vogl, Wayne; Tibbitts, Adam W.M. Mitchell; illustrations by Richard; Richardson, Paul (2005). Gray's anatomy for students, Philadelphia: Elsevier/Churchill Livingstone. ISBN 978-0-8089-2306-0.

34. N. Okamura, (2017). "Gastroptosis", Healthcare, Retrieved from https://kenko-pita.com/gastroptosis-symptom/ (accessed Jan. 22, 2019)

35. Robert Hutchison, (1910). The Principles Of Treatment In Gastroptosis, The British Medical Journal, 1(2575), pp. 1102-1104.

36. Ogden, R. W., (1984). Non-Linear Elastic Deformations, Courier Corporation, ISBN 978-0-486-31871-4.

37. Mir Hamid Reza Ghoreishy, (2012). "Determination of the parameters of the Prony series in hyper-viscoelastic material models using the finite element method", Materials and Design, 35, pp. 791-797.

38. Andrei B. Karpiouk et al., (2009). "Assessment of Shear Modulus of Tissue Using Ultrasound Radiation Force Acting on a Spherical Acoustic Inhomogeneity", IEEE Transactions on Ultrasonics, Ferroelectrics, and Frequency Control 2009, 56(11), pp. 2380-2387.

39. Article, "Human digestive system, Gastric Mucosa", ENCYCLOPEDIA BRITANICA, Retrieved from https://www.britannica.com/science/human-digestive-system/Gastric-mucosa (accessed Jan. 22, 2019), pp. 7-8.

40. C.X.Lin et al., (2017). "Friction behavior between endoscopy and esophageal internal surface", Wear, 376-377, Part A, pp. 272-280.

41. Røn, Troels et al., (2017). "Gastric mucus and mucuslike hydrogels: Thin film lubricating properties at soft interfaces", Biointerphases. 2017 Dec 5;12(5):051001. doi: 10.1116/1.5003708

42. Jens Brøndum Frøkjær el al., (2006). "Ultrasound-Determined Geometric and Biomechanical Properties of the Human Duodenum", Dig Dis Sci., 51(9), pp. 1662-1669, DOI 10.1007/s10620-005-9015-y

43. Lucía C. Fry et al., (2002). "Use of a super-stiff Amplatz guidewire to intubate the duodenum with a duodenoscope", Gastrointestinal Endoscopy, 56(5), pp.773-774.

44. Fluorotherm Materials Overview, (2018). "PTFE Properties", Retrieved from https://www.fluorotherm.com/technical-information/materials-overview/ptfe-properties/ (accessed Jan. 22, 2019)

45. Diggery, Robert, (2012). Catheters: Types, applications and potential complications (medical devices and equipment, Nova Science. ISBN 1621006301.

46. Minou Kouh Soltani et al., (2017). "A Soft Robotics Nonlinear Hybrid Position/Force Control for Tendon Driven Catheters", Int. J. of Control, Automation and Systems, 15(1), pp. 54-63.

47. Laasch Hu et al., (2003). "Comparison of standard and steerable catheters for bile duct cannulation in ERCP", Endoscopy, 35(8), pp.

669-674.

48. Fu, Y., Liu, H., Huang, W., Wang, S., and Liang Z., (2009). "Steerable catheters in minimally invasive vascular surgery", Int J Med Robot Comp., 5(4), pp. 381-391.

49. Yoon, W. J., Reinhall, P. G. and Seibel, E. J., (2007). "Analysis of electro-active polymer bending: A component in a low cost ultra thin scanning endoscope", Sensor Actuat A-Phys., 133(2), pp. 506-517.

50. Faddis, M. N., Blume, W., Finney, J., Hall, A., Rauch, J., Sell, J., Bae, K. T., Talcott, M. and Lindsay, B., "Novel, Magnetically Guided Catheter for Endocardial Mapping and Radiofrequency Catheter Ablation", Circulation, 106(23), pp. 2980-2985.

51. Suzumori, K., Iikura, S. and Tanaka, H., (1991). "Development of flexible microactuator and its applications to robotic mechanisms", IEEE ICRA, pp. 1622-1627.

52. Guo, S., Fukunda, T., Kosuge, K., Arai, F., Oguro, K. and Negoro, M., (1995). "Micro Catheter System with Active Guide Wire", IEEE ICRA, pp. 79-84.

53. Onishia, K., Sewa, S., Asaka, K., Fujiwara, N. and Oguro, K., (2000). "Bending Response of Polymer Electrolyte Actuator", Proc. SPIE 3989, Smart Structures and Materials 2000, pp. 121-128.

54. Yoon, W. J., Reinhall, P. G. and Seibel, E. J., (2007). "Analysis of electro-active polymer bending: A component in a low cost ultra thin scanning endoscope", Sensor Actuat A-Phys., 133(2), pp. 506-517.

55. Product Brochure, "ORBITER ST", Boston Scientific, Retrieved from http://www.bostonscientific.com/en-US/products/catheters--diagnostic/orbiter-st.html (accessed Jan. 22, 2019)

56. Kelly, M. and Fiorella D., (2009). "Traumatic Ophthalmic Artery Pseudoaneurysm Coiled with a Steerable Microcatheter", Can J Neurol Sci., 36(4), pp. 496-499.

57. Geir Arne Tangen et al., (2018). "Manually Steerable Catheter With Improved Agility", Clinical Medicine Insights: Cardiology, 12, pp. 1-4.

58. Product Brochure, "Guiding Sheaths", OSCOR, Retrieved from http://www.oscor.com/guiding-sheaths/ (accessed Jan. 22, 2019)

59. Awaz Ali et al., (2016). "Steerable Catheters in Cardiology: Classifying Steerability and Assessing Future Challenges", IEEE TRANS. ON BIOMEDICAL ENGINEERING, 63(4), pp. 679-693.

60. Shigeo Hirose, Takashi Kado, and Yoji Umetani, (1983). "Tensor actuated elastic manipulator", In 6th IFToMM World Congress, pp. 978-981.

61. Shigeo Hirose, (1993). Biologically Inspired Robots: Serpentile Locomotors and Manipulators, Oxford University Press

62. I.A. Gravagne and I.D. Walker, (2002). "Manipulability, force, and compliance anlysis for planar continuum manipulators", Robotics and Automation, IEEE Transactions on, 18(3), pp. 263-273.

63. I.A. Gravagne, C.D. Rahn, and I.D. Walker, (2003). "Large deflection dynamics and control for planar continuum robots", Mechatronics, IEEE/ASME Transactions on, 8(2), pp. 299-307.

64. P. Breedveld and S. Hirose, (2001). "Development of the endo-periscope for improvement of depth perception in laparoscopic surgery", In ASME Eng. Technical Conf. Computers and Info., Pittsburgh, PA, USA

65. P. Breedveld, J.S. SHeltes, E.M. Blom, and J.E.I. Verheij, (2005). "A new, easily miniaturized steerable endoscope", Eng. in Medicine and Biology Magazine, IEEE, 24(6), pp. 40-47.

66. J. Arata, Y. Saito, and H. Fujimoto, (2010). "Outer shell type 2 dof bending manipulator using spring-link mechanism for medical applications", In Robotics and Automation(ICRA), 2010 IEEE Int. Conf. on, pp. 1041-1046.

67. K. Ikuta, M. Tsukamoto, and S. Hirose, (1988). "Shape memory alloy servo actuator system with electric resistance feedback and application for active endoscope", In Robotics and Automation, 1988. Proceedings., 1988 IEEE Int. Conf. on, 1, pp. 427-430.

68. P. Dario, C. Paggetti, N. Troisfontaine, E. Papa, T. Ciucci, MC Carrozza, and M. Marcacci, "A miniature steerable end-effector for application in an integrated system for computer-assisted arthroscopy", In Robotics and Automation, 1997. Proceedings., 1997 IEEE Int. Conf on, Vol 2, pp.1573-1579, IEEE, 1997.

69. A. Degani, H. Choset, A. Wolf, and M.A. Zenati, (2006). "Highly articulated robotic probe for minimally invasive surgery", In robotics and Automation, 2006. ICRA 2006 Proceedings 2006 IEEE Int. Conf. on, pp. 4167-4172.

70. Akihiko Yagi, Kiyoshi Matsumiya, Ken Masamune, Hongen Liao, and Takeyoshi Dohi, "Rigid-flexible outer sheath model using slider linkage locking mechanism and air pressure for endoscopic surgery",

In Rasmus Larsen, Mads Nielsen, and Jon Sporring, editors, Medical Image Computing and Computer-Assisted Intervention(MICCAI) 2006, Vol. 4190, of Lecture Notes in Computer Science, pp.503-510. Spring Berlin / Heidelberg, 2006

71. A. Moers, M. De Volder, and D. Reynaerts, (2012). "Integrated high pressure microhydraulic actuation and control for surgical instruments", Biomedical Microdevices, p. published online, doi: 10.1007s10544-012-9650-y.

72. P.E. Dupont, J. Lock, B. Itkowitz, and E. Butler, (2010). "Design and control of concentric tube robots", Robotics, IEEE Transactions on, 26(2), pp.209-225.

73. N. Simaan, (2005). "Snake-like units using flexible backbones and actuation redundancy for enhanced miniaturization", In Robotics and Automation, 2005. ICRA 2005. Proceedings of the 2005 IEEE Int. Conf. on, pp. 3012-3017.

74. J. Peirs, H. Van Brussel, D. Reynaerts, and G. De Gersem, (2002). "A flexible distal tip with two degress of freedom for enhanced dexterity in endoscopic robot surgery", In Proceedings of the 13th micromechanics europe workshop, pp. 271-274.

75. Nguyen, B. L., Merino, J. L. and Gang, E. S., (2010). "Remote Navigation for Ablation Procedures - A New Step Forward in the Treatment of Cardiac Arrhythmias", European Cardiology, 6(3), pp. 50-56.

76. Product Brochure, "Sensei-X System", Hansen Medical, Retrieved from https://www.aurishealth.com/hansen-medical/ (accessed Jan. 22, 2019)

77. M.P. Groover, (2002). Automation, Production Systems and Computer-Integrated Manufacturing, Sigma Press

78. Li S, Shen J, Yan Y, Chen D., (2013). "Overview of the vascular interventional surgery robot", Zhongguo Yi Liao Qi Xie Za Zhi, 37(2), pp. 119-122.

79. Ganji Y, Janabi-Sharifi F, Cheema AN., (2009). "Robot-assisted catheter manipulation for intracardiac navigation", Int J Comput Assist Radiol Surg., 4(4), pp. 307-315.

80. Meng C, Zhang J, Liu D, Liu B, Zhou F., (2013). "A remote-controlled vascular interventional robot: system structure and image guidance", Int J Med Robot 2013, 9, pp. 230-239.

81. Saliba W, Cummings JE, Oh S, Zhang Y, Mazgalev TN, Schweikert

RA, et al., (2006). "Novel robotic catheter remote control system: feasibility and safety of transseptal puncture and endocardial catheter navigation", J Cardiovasc Electrophysiol., 17(10), pp. 1102-1105.

82. Thomas Dauteuille et al., (2013). "Development of a real catheter-based force feedback system", ICME 2013, pp.319-322.

83. Christopher J. Payne et al., (2012). "A Force Feedback System for Endovascular Catheterisation", 2012 IEEE/RSJ Int. Conf. on Intelligent Robots and Systems, pp.1298-1304.

84. Ho-Young Song et al., (2004). "Use of a Newly Designed Multifunctional Coil Catheter for Stent Placement in the Upper Gastrointestinal Tract", J Vasc Interv Radiol., 15(4), pp. 369-373.

85. Park KB, Do YS, Kang WK, et al., (2001). "Malignant obstruction of gastric outlet and duodenum: palliation with flexible covered metallic stents", Radiology, 219(3), pp. 679-683.

86. Yates MR 3rd, Morgan DE, Baron TH., (1998). "Palliation of malignant gastric and small intestinal strictures with self-expandable metal stents", Endoscopy, 30(3), pp. 266-272.

87. Meike M. C. Hirdes et al., (2013). "In vitro evaluation of the radial and axial force of self-expanding esophageal stents", Endoscopy, 45(12), pp. 997-1005, DOI 10.1055/s-0033-1344985

88. Evgenia Nikolsky et al., (2003). "Stent Deployment Failure: Reasons, Implications, and Short- and Long-Term Outcomes", Catheterization and Cardiovascular Interventions, 59(3), pp. 324-328.

89. Dan Sanchez, (2017). How to make kink-resistant tubing work in smaller medical devices, Meical Design

90. Technical Datasheet, "PERMABOND POP", Permabond, Retrieved from https://www.permabond.com/wp-content/uploads/2016/04/POP_TDS.pdf, Permabond, Datasheet/ (accessed Jan. 22, 2019)

91. Shiva A, Stilli A, Noh Y, Faragasso A, De Falco I, Gerboni G, Cianchetti M, Menciassi A, Althoefer K, Wurdemann HA, (2016). "Tendon-based stiffening for a pneumatically actuated soft manipulator", IEEE Robot Autom Lett., 1(2), pp. 632-637.

92. Suzumori K,Wakimoto S, Miyoshi K, Iwata K, (2013). "Long bending rubber mechanism combined contracting and extending fluidic actuators", In: IEEE/RSJ international conference on intelligent

robots and systems (IROS), pp 4454-4459.

93. Hassan T, Cianchetti M, Mazzolai B, Laschi C, Dario P, (2017). "Active-braid, a bioinspired continuum manipulator", IEEE Robot Autom Lett., 2(4), pp. 2104-2110.

94. Sturges RH Jr, Laowattana S, (1993). "A flexible, tendon-controlled device for endoscopy", Int J Robot Res., 12(2), pp.121-131.

95. Kim YJ, Cheng S, Kim S, Iagnemma K, (2014). "A Stiffness-Adjustable Hyperredundant Manipulator Using a Variable Neutralline Mechanism for Minimally Invasive Surgery", IEEE Trans Robot 30(2), pp. 382-395.

96. Yagi A, Matsumiya K,Masamune K, Liao H, Dohi T, (2006). "Rigid-flexible outer sheathmodel using slider linkage locking mechanism and air pressure for endoscopic surgery", International conference on medical image computing and computer-assisted intervention (MICCAI). Springer, Berlin, Heidelberg, pp. 503-510.

97. Lendlein A, Kelch S, (2002). Shape-memory polymers, Angew Chem Int. 41(12), pp. 2034-2057.

98. Yang Y, Chen Y, Li Y, Chen MZ, (2016). "3D printing of variable stiffness hyper-redundant robotic arm", In: IEEE international conference on robotics and automation (ICRA), pp 3871-3877.

99. Yang Y, Chen Y, Li Y, Chen MZ,Wei Y, (2017). "Bioinspired robotic fingers based on pneumatic actuator and 3d printing of smart material", Soft Robot, 4(2), pp. 147-162.

100. Yang Y, Chen Y, Li Y, Wang Z, Li Y, (2017). "Novel variable stiffness robotic fingers with built-in position feedback", Soft Robot, 4(4), pp.338-352.

101. Firouzeh A, Salerno M, Paik J, (2017). "Stiffness control with shape memory polymer in underactuated robotic origamis", IEEE Trans Robot, 33(4), pp. 765-777.

102. Yuen MC, Bilodeau RA, Kramer RK, (2016). "Active variable stiffness fibers for multifunctional robotic fabrics", IEEE Robot Autom Lett., 1(2), pp. 708-715.

103. Shaw JA, Kyriakides S, (1995). "Thermomechanical aspects of NiTi", J Mech Phys Solids, 43(8), pp. 1243-1281.

104. Mavroidis C, (2002). "Development of advanced actuators using shape memory alloys and electrorheological fluids", J Res Nondestruct Eval., 14(1), pp.1-32.

105. Schubert BE, Floreano D, (2013). "Variable stiffness material based on rigid low-melting-point-alloy microstructures embedded in soft poly (dimethylsiloxane) (PDMS)", RSC Adv., 3(46) pp. 24671-24679.

106. Laschi C, Mazzolai B, Cianchetti M, (2016). "Soft robotics: technologies and systems pushing the boundaries of robot abilities", Sci Robot, 1(1) eaah3690.

107. Lendlein, A., Kelch, S. (2002). "Shape-memory polymers", Angew. Chem. Int. Ed., 41(12), pp. 2034-2057, doi:10.1002/1521-3773(20020617)41:12<2034::AID-ANIE2034>3.0.CO;2-M.

108. Taylor Cannon et al., (2016). "Developing Dynamic Gastrointestinal Phantoms for Testing Endoscopy and Colonoscopy Devices", Oral Presentation #6 at Vanderbilt Univ.

109. F. J. Chen et al., (2014). "Soft Actuator Mimicking Human Esophageal Peristalsis for a Swallowing Robot", IEEE/ASME TRANSACTIONS ON MECHATRONICS, 19(4), pp.1300-1308.

110. Product Brochure, "Gastrointestinal Phnatom", Buyamag Inc., Retrieved from https://www.buyamag.com/ (accessed Jan. 22, 2019)

## 국문 초록

# 비혈관 중재시술을 위한 연속체 로봇

비혈관 중재 시술은 양성 및 악성 종양 (암)의 표적 치료, 배액, 관 삽입 임플란트, 협착 된 기관에서의 스텐트 삽입 및 고주파 열 치료와 같은 다양한 시술에 사용되고 있다. 최근 위장관에서의 스텐트 삽입은 빠른 병증 완화 효과, 비침습성, 국소 마취 등의 장점 때문에 장 폐쇄 질환의 효과적인 치료법으로 대두되고 있다. 스텐트는 주로 양성 종양 또는 암 수술의 합병증에 의해 좁아진 관상 장기에 삽입되어 이를 영구적으로 확장시키기 위한 목적으로 사용된다.

비혈관 장기에 대한 스텐트 거치는 중재 시술을 통해 수행된다. 위장관 중재 시술에서 스텐트 전달용 튜브는 자연 개구부 (입과 항문)를 통해 삽입되며, 연조직은 삽입 된 튜브에 의해 쉽게 변형된다. 따라서 위장관 중재 시술 시 삽입되는 튜브의 루프 형성, 복통, 궤양 또는 경미한 출혈과 같은 문제를 발생시킨다. 이러한 임상적 난제는 연조직과 삽입되는 튜브 사이의 굴곡 강성 차이에 의해 발생한다. 따라서 중재 시술 기구의 굴곡 강성은 위장관의 강성에 비해 너무 높거나 낮게 설계되어서는 안된다. 현재 비혈관 중재 시술에서는 의료용 튜브와 연조직 사이의 굽힘 강성 차이 제한을 극복하기 위해 다양한 강성을 가진 추가적인 튜브를 시행 착오를 통해 삽입한다. 그러나 중재 시술에서 여러 개의 튜브를 사용하면 시술 시간이 증가한다. 시술 시간의 증가는 형광 투시 장치가 사용되는 중재 시술의 특성상 시술자의 피로감 증대 뿐 아니라 시술자와 환자 양측에 대한 방사선 피폭량 또한 증가시킨다는 문제가 있다. 따라서 시술 시간 단축은 환자와 임상의 모두에게 중요하다. 그러나 위장관 중재 시술 기구의 기계적 및 기능적

특성에 대한 요구 사항은 아직 정량적으로 분석된 바가 없기 때문에 중재 장치의 설계 원리 및 적절하 기구의 선택은 시술자 개개인의 경험에 의존해왔다.

본 연구에서는 순응도 모델을 기반으로 하는 위장관 중재 시술 기구의 새로운 설계 원리를 제안하였다. 제안하는 모델은 위장관 중재 시술 시 연조직과 의료용 튜브 사이의 상호 작용의 본질을 추출하기 위해 정의하였다. 제안하는 순응도 모델에서 연조직과 의료용 튜브 사이의 다중 물체 접촉 거동의 복잡성은 굴곡부에서의 휨 강성, 곡률 및 유효 길이라는 변수로 단순화 되었다. 위장관 스텐트 시술에 최적화 된 튜브를 설계하기 위해 기존의 위장관 중재 기구들의 조합을 순응도 측면에서 평가하였다. 결과적으로 가변 강성 특성을 보유한 소프트 매니퓰레이터를 순응도 모델에 기반하여 설계 및 제작하였다. 소프트 매니퓰레이터는 위장관 중재 시술 중 높은 순응도를 유지할 수 있는 오버 튜브로서의 역할을 수행한다.

제안하는 순응도 모델을 통해 안전한 위장관 중재 시술을 위한 위장관 스텐트 전달 장치에 대한 요구 사항을 정량적으로 정의하였다. 이를 통해 제작한 소프트 매니퓰레이터는 기존의 의료 튜브의 크기와 강성 및 상부 위장관의 해부학을 고려하여 장기를 안전하게 통과 할 수 있는 크기의 유연 재료로 제작하였다. 제안하는 소프트 매니퓰레이터는 얇은 두께를 가진 튜브형 연속체 구조에서 2 자유도 조향을 달성하기 위해 와이어를 이용한 길항 구동 방식을 채택하였다. 소프트 매니퓰레이터는 위장관으로 삽입될 때 높은 순응도를 유지하지만 조향력만으로는 스텐트 삽입기가 본 구조물을 통과할 때 발생하는 힘을 억제하기 어려워 이를 해결하고자 일부 구조를 형상 기억 고분자 재료로 대체하였다. 개선된 소프트 매니퓰레이터는 형상 기억 고분자의 상전이를 통한 강성 변화 특성을 이용할 수 있기 때문에 크기 변화가 없으면서 굴곡된 형상을 유지할 수 있어 스텐트 삽입기가 원하는 궤적을 따라 삽입될 수 있었다. 소프트 매니퓰레이터의 사용성을 높이기 위해 조향 핸들을 제작하였으며, 환자의 상부 위장관의 CT 데이터에

기반하여 유연 재료로 된 시뮬레이터를 제작하여 검증 실험을 진행하였다. 또한, in-vivo 환경에서 위장관의 강성을 측정하기 위한 장치를 개발하여 동물 실험을 진행하였다.

본 연구에서 도출한 순응도 모델은 비혈관 중개 시술 뿐 아니라 혈관을 포함한 다양한 시술에서도 의료 기구와 연조직 사이의 상호작용을 예측하고 평가하기 위한 지표가 될 것으로 기대한다.

**주요어: 비혈관 중재 시술, 스텐트 시술, 순응도 모델, 소프트 매니퓰레이터, 가변 강성, 위장관**
**학번: 2014-31041**

# 감사의 글

박사과정으로 연구실에 들어와 어느덧 4년이 지났습니다. 그렇게 긴 시간은 아닐 텐데 그 시간 속에 응집된 많은 것들로 인해 무겁게 느껴지는 4년이었습니다. 지금 심정은 드디어 박사가 되었다는 성취감이 반이라면 앞으로 잘 할 수 있을까 하는 걱정이 나머지 반을 채우고 있습니다. 학위 논문에 넣을 감사의 글은 학부 졸업 때나 석사 졸업 때도 빼놓지 않고 부지런히도 썼는데 지금은 다소 떨리는 마음으로 이 글을 쓰고 있습니다.

연구실에 들어와 한 동안은 다시 마음껏 배울 수 있다는 것이 마냥 좋았지만 박사 학위는 그저 배움을 증진시키면 주어지는 것이 아니라는 것을 깨닫기까지 긴 시간이 필요했습니다. 박사는 어느 한 부분에서 인류를 통틀어 미답의 영역의 최전방에 서는 것이라고 했는데 과연 제 자신이 그런 사람이 될 수 있는지 확신이 없었습니다.

교수님께서는 항상 저에게 제 연구의 문제 정의가 무엇인지 수많은 질문을 던지셨고, 그것은 내내 고통이었습니다. 스스로도 자신의 연구에서 궁금한 것이 별로 없었기 때문일 것입니다. 누가 봐도 당연하고 자명한 문제를 다루고 있다는 착각에서 비롯된 것이라 생각합니다. 그런데, 그런 수많은 질문을 받으면서 어느새 다른 사람들의 연구가 조금씩 궁금해졌습니다. 각자의 연구에서 문제를 관통하는 핵심을 어떻게 관찰하고 설명할 수 있는지 궁금했습니다. 그런 궁금증이 생기고 나서 다시 자신의 연구로 눈을 돌려 보니 문제는 결코 자명하지 않았습니다. 당연하다고 믿었던 것을 한 번 의심해보는 용기가 생겨난 것이라 생각합니다. 이것이 박사가 되기 위해 필요한 과정이라면, 이렇게 껍질을 깨고 나올 수 있었던 것은 수많은 질문을 통해 담금질 해주신 교수님과 항상 저에게 좋은 자극을 주었던 연구실의 선후배님들 덕분입니다. 모든 분들께 이 글을 통해 진심으로 감사의 마음을 표합니다.

서울아산병원의 송호영 교수님, 저에게 많은 기회와 기대를 주셨고 또 좋은 문제를 발굴할 수 있게 이끌어 주셔서 감사드립니다. 또, 타 분야에 대해 벽을 두지 않고 함께 연구를 진행하고 많은 가르침을 주신 서울아산병원의 교수님들과 연구원 분들께 진심으로 감사드립니다.

어머니, 아버지. 어느 때나 저를 위해 최선을 다 해 주시고 든든하게 밀어 주셔서 진심으로 감사드립니다. 장인어른, 장모님. 항상 믿어주시고 물심양면으로 많이 도와주셔서 감사합니다.

마지막으로, 언제나 제 편에서 응원해주고 힘겨운 시간을 이겨내 준 아내에게 무한한 고마움과 사랑을 담아 이 논문을 바칩니다.

2019년 1월 24일 최준명 드림